# CANADIAN THESES ON MICROFICHE

# THÈSES CANADIENNES SUR MICROFICHE

National Library of Canada
Collections Development Branch

Canadian Theses on
Microfiche Service

Ottawa, Canada
K1A 0N4

Bibliothèque nationale du Canada
Direction du développement des collections

Service des thèses canadiennes
sur microfiche

## NOTICE

The quality of this microfiche is heavily dependent upon the quality of the original thesis submitted for microfilming. Every effort has been made to ensure the highest quality of reproduction possible.

If pages are missing, contact the university which granted the degree.

Some pages may have indistinct print especially if the original pages were typed with a poor typewriter ribbon or if the university sent us an inferior photocopy.

Previously copyrighted materials (journal articles, published tests, etc.) are not filmed.

Reproduction in full or in part of this film is governed by the Canadian Copyright Act, R.S.C. 1970, c. C-30. Please read the authorization forms which accompany this thesis.

## AVIS

La qualité de cette microfiche dépend grandement de la qualité de la thèse soumise au microfilmage. Nous avons tout fait pour assurer une qualité supérieure de reproduction.

S'il manque des pages, veuillez communiquer avec l'université qui a conféré le grade.

La qualité d'impression de certaines pages peut laisser à désirer, surtout si les pages originales ont été dactylographiées à l'aide d'un ruban usé ou si l'université nous a fait parvenir une photocopie de qualité inférieure.

Les documents qui font déjà l'objet d'un droit d'auteur (articles de revue, examens publiés, etc.) ne sont pas microfilmés.

La reproduction, même partielle, de ce microfilm est soumise à la Loi canadienne sur le droit d'auteur, SRC 1970, c. C-30. Veuillez prendre connaissance des formules d'autorisation qui accompagnent cette thèse.

THIS DISSERTATION
HAS BEEN MICROFILMED
EXACTLY AS RECEIVED

LA THÈSE A ÉTÉ
MICROFILMÉE TELLE QUE
NOUS L'AVONS REÇUE

Canada

NL 339 (r. 85/09)

# GENESIS OF GOLD DEPOSITS

# RENABIE AREA, SUDBURY DISTRICT, ONTARIO

by

Stephanos Kilias

A thesis submitted to the School of Graduate Studies in partial fulfillment of the requirements for the degreee of M.Sc. in Geology.

University of Ottawa

Ottawa, Canada

1984

UNIVERSITÉ D'OTTAWA
UNIVERSITY OF OTTAWA

The University of Ottawa requires the signatures of all persons using or photocopying this thesis. Please sign below, and give address and date.

## ABSTRACT

The Renabie area, located 80 km northeast of Wawa, Ontario, is underlain by Archean mafic and felsic metavolcanic rocks of the northeastern end of the Wawa greenstone belt. The metavolcanic rocks are intruded on the east by the Missinaibi Lake Batholith, an Archean trondhjemite and tonalite body. The greenstone sequence experienced metamorphism to the lower amphibolite facies, perhaps coeval with the emplacement of the batholith. This was followed by partial retrogression of the batholith and the adjacent amphibolites to the greenschist facies during subsequent regional metamorphism, involving a carbon-dioxide hydrothermal fluid.

The Renabie Mine and the adjacent Braminco properties have gold-, sulphide-, telluride-bearing quartz-muscovite-carbonate veins in the marginal phase of the batholith and in the adjacent greenstones, within 500 m of the intrusive contact. Wallrocks to these veins are modified (retrograded) by reactions with the gold-bearing hydrothermal fluids involving addition of K, $H_2O$, $CO_2$, Rb, Ba, and leaching of Na, resulting in pervasive development of muscovite and carbonate at the expense of sodic plagioclase.

Wallrock alteration mineral assemblages are indistinguishable from those produced by regional greenschist (retrogressive) metamorphism.

Wallrock alteration and vein filling were concomitant with gold concentration under conditions of greenschist metamorphism at temperatures of T=300°C to 470°C and maximum pressures of P=2-3 kb, at depths of 8-10 km.

Hydrothermal solutions forming the Renabie deposit and the adjacent gold-bearing veins were high temperature ascending aqueous fluids of metamorphic origin, possessing overall low salinities, probably low pH, high initial K/Na ratios, and containing significant quantitites of $CO_2$, along with molecular hydrogen ($H_2$).

An almost pure carbon dioxide fluid with little water was trapped in type II inclusions in the vein quartz, representing an early fluid phase which was probably later depleted in $CO_2$ through its fixation in altered wallrock and vein-filling carbonates, giving rise to $CO_2$-$H_2O$ solutions with approximately 20 vol.% $CO_2$ and corresponding to those trapped in type I inclusions.

A drop in the temperature of the mineralising fluid and wallrock reactions, involving fixation of hydrothermal $CO_2$ in alteration carbonates was important in the concentration of gold in the quartz-muscovite-carbonate veins of the Renabie Mine area.

## TABLE OF CONTENTS

## LIST OF PLATES

## LIST OF TABLES

## LIST OF ILLUSTRATIONS





a: In pocket at back of report.

# CHAPTER 1

## 1. INTRODUCTION

### 1.1 General Statement

The Renabie area of northern Ontario is underlain by mafic and minor felsic volcanic rocks of Archean age that form the northeastern end of the Wawa greenstone belt (Goodwin, 1962) in the Superior Province of the Canadian Shield. The volcanic rocks are intruded on the east by an Archean trondhjemite and tonalite batholith. The deposits at the Renabie mine, and adjoining properties, are gold-telluride-pyrite quartz veins, pods and lenses transecting the marginal phase of the batholith and the metavolcanic rocks.

The objectives of this study are:

1) to discuss the nature of the hydrothermal fluids responsible for formation of gold-bearing quartz veins and for alteration of adjacent wall rocks, in the Renabie mine area;

2) to describe the mineralization and hydrothermal alteration conditions;

3) to propose a mechanism for gold deposition in the Renabie mine area.

Many of the gold deposits in greenstone belts of the Canadian Shield occur within or near felsic intrusive bodies of Archean age (Colvine and Marmont, 1981; Kerrich et al., 1980; Studemeister, 1983). The Renabie area gold deposits offer a good opportunity to study this type of precious metal occurrence.

## 1.2 Location and Access

The Renabie mine is located about 220 km north of Sault Ste. Marie and 80 km northeast of Wawa, in Leeson Township, District of Sudbury, Ontario; the adjacent Braminco prospects, to the south, include claims straddling boundary lines between Leeson, Rennie, Stover and Brackin Townships and boundaries between the Sudbury and Algoma Districts (Figure 1). Access is by paved road from Wawa, 65 km east on highway 651 to Missanabie, then 20 km east on a gravel road.

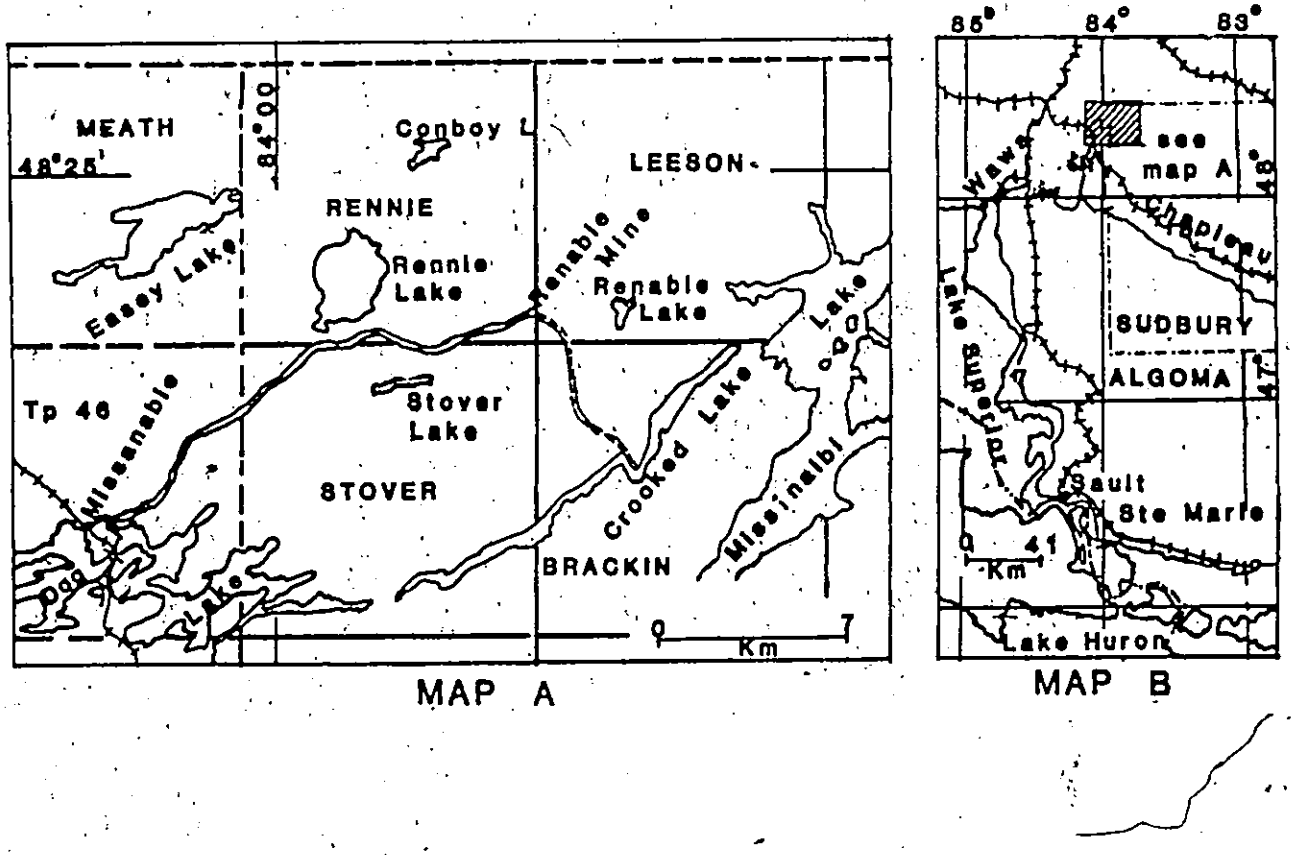


Figure 1 : Location and access routes to the Renabie Mine, Leeson Township, District of Sudbury, Ontario.

## 1.3 Economic History

A gold-bearing quartz vein that was discovered in August 1939 near the Missanabie Station developed into the Renabie Mine (Bruce, 1944). In 1940, Macassa Mines Limited conducted a diamond drilling programme on the original discovery (Ferguson, 1968a).

Renabie Mines Limited, a subsidiary of Macassa Mines Limited, was incorporated in 1941 to undertake further development. Operations were suspended in the spring of 1942 because of wartime conditions and production was resumed in 1946 with the construction of the Renabie No. 2 shaft. The mine was in continuous production, under the ownership of Willroy Mines Limited, from July 1947 to July 1970. Between 1941 and 1970 the property was developed by two shafts, the deepest of which (No. 2) was sunk to 1039 m (3,465 ft) with 20 levels. The mine produced 23,730 kg of gold and 788.8 kg of silver. between 1947 and 1970, the average grade of milled ore was 5.93 g/t gold (Ferguson, 1968a).

The upsurge in the price of gold in the 1970s renewed interest by the new owner, Rengold Mines, and the company financed the reopening of the mine (Northern Miner, 1978). Rengold Mines went bankrupt in 1978 and in July 1979, the

succeeding owner, Sungate Resources, through subsidiary Renabie Mines (1981), estimated a cost of $3.5 million to bring the property into production (Northern Miner, 1979). In 1980-81 the mine was dewatered and rehabilitated, and production was resumed at 550 tonnes per day by April 1982 (Canadian Mines Handbook, 1983-84, p. 327).

In early 1983, Renabie Mines (1981) conducted an underground diamond drilling program. On the basis of this program (Northern Miner, 1983), the company estimated about 1,621,065 tonnes of ore averaging 5.6 g/t gold, representing a 60% improvement in reserves since the end of 1982. Because of this expansion of reserves, changes to the milling plant were planned to enable production of some 1060 kg of gold in 1983. At present, the Renabie Mines (1981) operate under the ownership of Campbell Resources Incorporated.

Braminco Mines Limited, which was incorporated in 1946, owns a block of 20 claims adjoining the Renabie property to the south, including the Braminco 21, the Campbell, and three other gold-bearing veins. The company reported 100,000 tonnes of ore averaging 4.2 g/t gold in the No. 21 vein and 23,400 tonnes averaging 3.64 g/t gold in the No. 7 vein (Canadian Mines Handbook, 1948, p. 32). In late 1983, the company planned to bring the Braminco gold properties

into full-scale production (Northern Miner, 1983).

## 1.4 Previous Work

Burwash in 1934 made a general geological survey at the east end of the Wawa belt and published a compilation map of the "Lochalsh-Missinaibi" area (Burwash, 1937), that included the first geologic description of three Townships east of Renabie. In 1941, Bruce (1944) described the Renabie and adjoining properties in his geological report on the Rennie-Leeson area. A summary of this same first description of the Renabie mine was later published in the CIM's "Structural Geology of Canadian Ore Deposits" (Bruce, 1948).

The gold deposits of the Renabie area were subsequently described by Frohberg (1948), who added more data to Bruce's pioneer work. A geologic description of the Renabie mine and the surrounding properties can be found in the marginal notes on O.D.M. Map No. P. 492 (Ferguson, 1968a).

The general geology immediately east and south of the Renabie area has been described by the Ontario Geological Survey (Riley, 1971; Bennett, 1978).

## 1.5 Methods of Research

Field work was carried out in May 1981 and 1982. In total, four weeks were spent in general geological reconnaissance and sample collecting from the Renabie Mine at the surface ("C" zone) and underground (914 m (3,100 ft), 458 m (1250 ft) levels); from the Braminco 21 and the Campbell gold quartz veins; and from an area of approximately 3km$^2$ that crosses the "granite" - greenstone contact.

Grab samples were collected from the dumps at the Renabie No. 2 shaft and the abandoned Dulama shaft. The O.D.M. Preliminary Geological Map No. P. 452 (Ferguson, 1968a), as well as mine development level plans, were used as basemaps during sample collecting. A total of 130 samples were collected from country rocks, alteration halos and gold-bearing and barren quartz veins for petrological, chemical, and ore investigations. Samples near veins were collected along traverses perpendicular to the veins. Sample location maps may be found in Appendix 1.

One hundred thin sections and fifteen polished thin sections were cut from selected samples to be investigated with petrographic and reflecting microscopes. Fifty of these samples were selected for whole rock X-ray diffraction study. The relative abundance of primary

minerals and their alteration products was determined by measuring peak intensities on X-ray diffraction charts. The telluride mineralogy of three specimens was investigated by electron microprobe, at the Geological Survey of Canada, by Dr. D.C. Harris.

Whole rock chemical analyses (Appendix 2,3) for major and minor elements were done by X-ray fluorescence spectroscopy, on 85 fresh, fist-size representative specimens. Sample location for all analyses listed in Appendices 2 and 3 with the prefix RN can be found in Appendix 1. Determinations of the major and minor element composition of a specimen involved preparing a fusion disk containing 1.5 gms of rock powder, 4.5 gms of $Li_2B_4O_7$ and 0.5 gms of $Li_2CO_3$, and analyzing the disk with an automated Phillips 1410 XRF spectrometer using a Cr tube. The raw analytical data was processed by computer, adopting alpha coefficients of De Jongh (1973). The major element composition is reported as oxides.

Based on replicate determinations and the results on the international rock standard SY-2 (Abbey, 1977), the precision of analytical results is as follows: $SiO_2$, $Al_2O_3$, $Fe_2O_3$ (total), $K_2O$: $\pm$ 2%; $TiO_2$ : $\pm$ 3% $Na_2O$, MgO, CaO : $\pm$ 4%; $P_2O_5$, MnO, : $\pm$ 10%; Ba, Sr : $\pm$ (concentration range of $\geqslant$ 40ppm); Zr : $\pm$ 15% (range of 50

to 500 ppm); Rb, Zn : ± 50% (range of 20 to 40 ppm); Cr, Ni: ± 100% (range of ⩽30 ppm); Y : ± 100 (range of ⩽20 ppm). Loss on ignition (L.O.I.) determinations were conducted on separate aliquots from XRF fusions and they represent volatiles (wt%) lost on ignition at 1000°C uncorrected for oxidation of iron ($Fe^{+2}$) as well as $S^{2-}$ and $Mn^{2+}$.

Fluid inclusion studies were conducted using a commercially available LINKAM TH 600 microthermometric system (Shepard, 1981) (Appendix 4). The redox state of iron for twenty samples were determined using the modified Wilson (1955) method (Reichen and Fahey, 1962) (Appendix 5). For rocks, analyzed as to the redox state of their contained iron and bearing more than 5% pyrite, total iron was determined by Atomic Absorption Spectroscopy. The oxygen isotope composition of seven vein quartz separates were determined by Geochron Laboratories.

## 1.6 Acknowledgements

The author wishes to thank Dr. G.A. Armbrust for initiation and supervising the thesis in the introductory stages, for instruction on the use of the fluid inclusion apparatus, and for his critical reading of the manuscript.

Grateful acknowledgement goes to Dr. D.D. Hogarth for his help during the research and for his constructive reading of the thesis.

The writer is grateful to Dr. P.A. Studemeister for helpful suggestions and invaluable discussions during the course of investigation.

Thanks also go to Dr. R.I. Thorpe of the Geological Survey of Canada for providing geochronological data and commenting on the manuscript.

Thanks are also due to Dr. D.C. Harris of the Geological Survey of Canada for determining the telluride mineralogy of specimens by electron microprobe.

Permission to visit the Renabie mine was provided by Renabie Mines (1981) Ltd.

The author is also indebted to Dr. K. Hattori for commenting on the manuscript.

The writer also wishes to thank the following persons for their contribution to this thesis:

Mr. Ron Hartree for guidance in the analyses of rocks by XRF and XRD;

Mr. Edward Hearn for helping with microphotography;

Mr. Bob Taylor for preparation of thin and polished sections;

Ms Evelyn Mourelatos for typing the thesis;

My parents for being the source of encouragement throughout the project.

# CHAPTER 2

## 2. GEOLOGY OF THE RENABIE AREA

### 2.1 General Statement

The Renabie area is at the easternmost end of the Wawa Greenstone belt (Goodwin, 1962). The Wawa belt, an east-west trending succession of three volcanic cycles (Goodwin, 1962; Attoh, 1980), is located in the Lake Superior region of Ontario (Figure 2). The lowermost cycle is composed of mafic to intermediate flows which grade upwards into felsic pyroclastic rocks and is conformably capped by Algoma-type iron-formation. The middle cycle, composed of mafic and felsic pyroclactic flows is uncomformably overlain by clastic metasedimentary rocks of the Dore group. The uppermost cycle consists of mafic to intermediate flows with minor pyroclastic rocks. The volcanic rocks are of the basalt-andesite-rhyolite association and the clastic metasedimentary rocks are predominantly conglomerates, graywackes and argillites. Complex granitic bodies border and intrude the Archean succession. Late Precambrian diabase and lamprophyre cut the aforementioned rocks. According to Wanless et al. (1966) there are, on the basis of K-Ar data, at least three

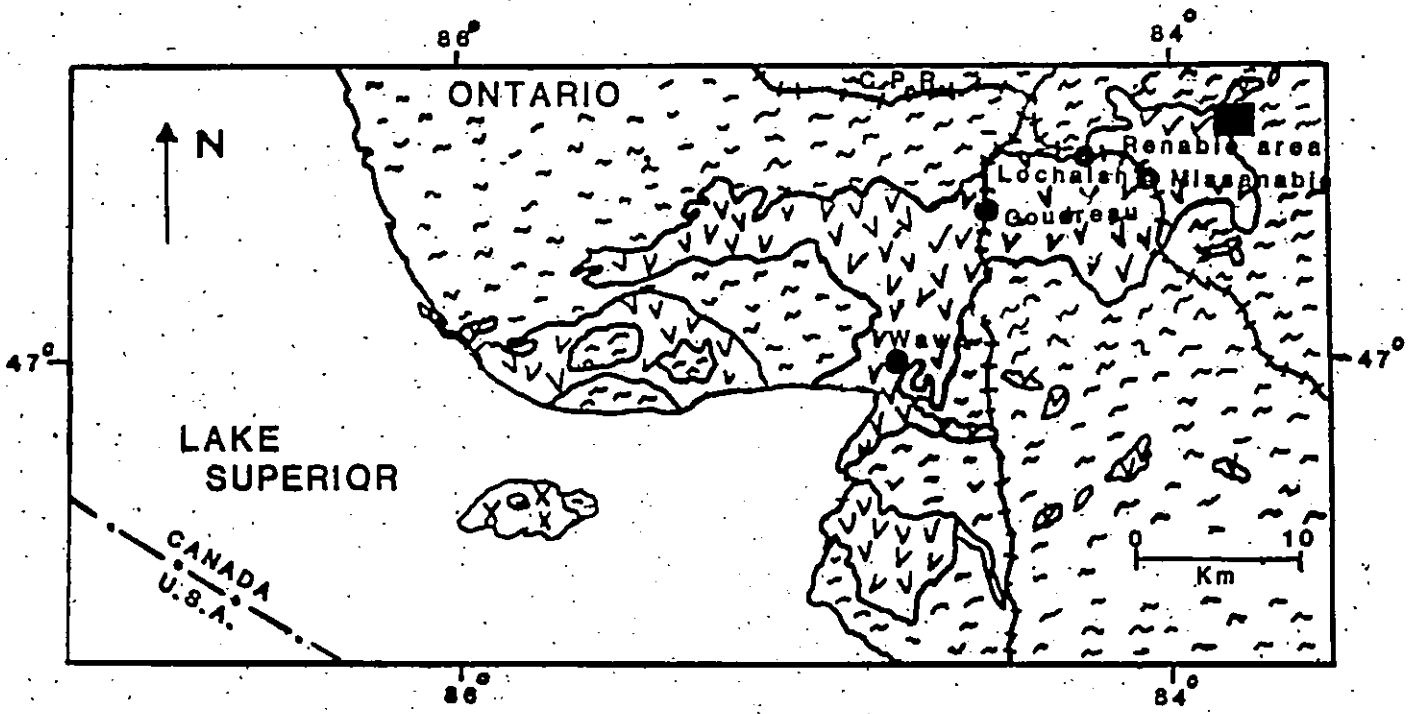


PROTEROZOIC

VOLCANIC AND SEDIMENTARY ROCKS

ARCHEAN

METASEDIMENTARY AND METAVOLCANIC ROCKS

INTRUSIVE IGNEOUS AND HIGH GRADE METAMORPHIC ROCKS

Renable area

Figure 2 : Regional geology of the Wawa Greenstone Belt, District of Algoma, Ontario. ( O.G.S. Map No. 2241 ).

distinct ages of diabase dikes in the area, extending three townships to the west from the Renabie Mine, ranging from 2,155 165 to 1,495 125 M.a. Figure 3 summarizes data on geochronology in relation to the stratigraphic succession of the Wawa belt.

The Wawa greenstone belt has been folded about three east-west trending cylindrical axes, which were in turn overlapped by NW trending folds. Wave-like patterns, in the longitudinal section, have resulted. Younger, prominent, N to NW striking and steeply dipping transverse faults cross-cut the Archean stratigraphy and disrupt the primary fold patterns (Goodwin, 1962).

The entire Wawa sucession was metamorphosed, probably during a deformation and metamorphic event at 2700 to 2685 Ma (Percival and Krogh, 1983). The metamorphic grade is greenschist facies on a regional scale and locally to amphibolite facies in the vicinity of felsic intrusions.

Gold-bearing quartz-carbonate veins, in granite intrusions or flanking metavolcanic rocks, have yielded about 50% of the gold produced in the Wawa District between 1900 and 1950 (Goodwin, 1961). The close spatial association between former gold producers and granitic intrusive rocks is exemplified by the Parkhill, Grace, Minto, Jubilee,

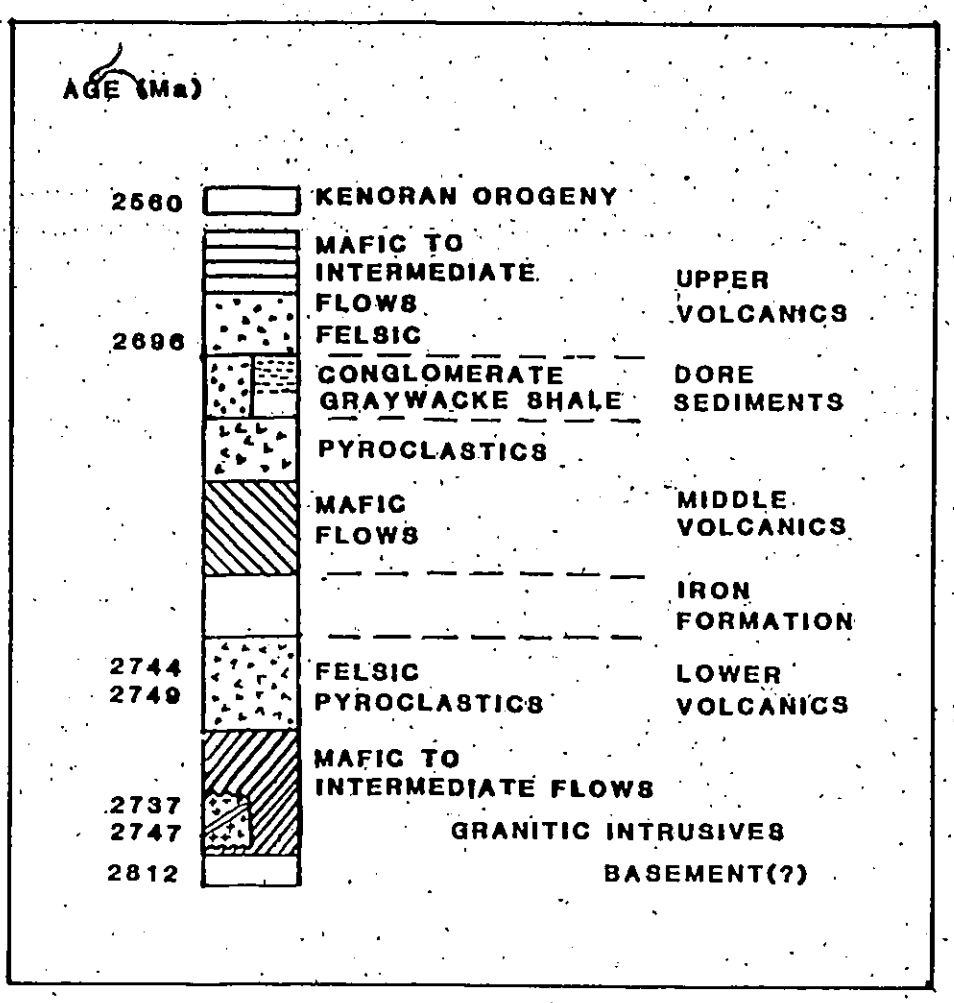


Figure 3 : Generalized geochronology ( after Turek et al., 1982 ) and stratigraphic column for the Wawa greenstone belt ( based on Goodwin, 1962; Attoh, 1980 ) .

Cooper, Deep Lake, Smith and Cora mines, south of Wawa Lake, and the Cline Lake and Algoma Summit mines near Goudreau. The mines exploited gold-bearing veins transecting the margins of granitic intrusions and/or nearby metavolcanic rocks. In general, native gold coexists with galena, molybdenite, and arsenopyrite in continuous or discontinuous quartz-carbonate lenses or pods (Frohberg, 1935).

## 2.2 Mafic and Felsic Metavolcanic Rocks

The mafic and felsic volcanic rocks in the Renabie mine area are part of the lowermost volcanic cycle of the Wawa greenstone belt (Riley, 1971).

Mafic metavolcanic rocks in the Renabie area, at a distance of less than 1000 m from the intrusive contact (Figure 4), are generally dark green, showing local variation in grain size and texture. They are characterized by a fine-to medium-grained granoblastic or foliated groundmass of essential hornblende, and oligoclase to andesine or albite, accompanied by subordinate chlorite and carbonate, and locally variable amounts of epidote. Assessory minerals include quartz, titanian-magnetite surrounded by titanite, apatite, biotite, and actinolite.

Idioblastic to hypidioblastic hornblende occurs in oriented prisms largely accounting for the foliation present in the rocks. Poikiloblastic hornblende is commonly crowded with inclusions of quartz and mottled and replaced by chlorite and carbonate (Plate 1.1 a). Some carbonate completely surrounds hornblende. The margins of hornblende grains are commonly very irregular against partly surrounding fine grained quartz, carbonate, and chlorite (Plate 1.1 b).

Chlorite flakes characteristically cross-cut hornblende prisms, at an angle to the general foliation, and also occur at the outer fringes of calcite veins cross-cutting epidote-hornblende assemblages (Plate 1.2 a,b).

Porphyroblastic varieties of mafic metavolcanic rocks consist of medium-grained hornblende porphyroblasts, within a granoblastic (or hornfelsic) groundmass of oligoclase to andesine or albite plagioclase, fine-grained amphibole, epidote and quartz. Accessory minerals include carbonate and titanian-magnetite surrounded by titanite. Elongated hornblende porphyroblasts commonly, but not invariably, show a slight preferred planar orientation.

Amphibole porphyroblasts are also zoned with a poikiloblastic interior of hornblende and a rim of actinolite. Replacement is incipient to complete. Zoned

Plate 1.1 a: Poikiloblastic hornblende (H) replaced by chlorite (Chl). Crossed polarizers.

Plate 1.1 b: Poikiloblastic hornblende (H) mottled by chlorite (Chl) and carbonate (Ca), with serrated margins surrounded by quartz (Q), chlorite and carbonate.
Crossed polarizers.

**Plate 1.1 a**

0.1 m m

**Plate 1.1 b**

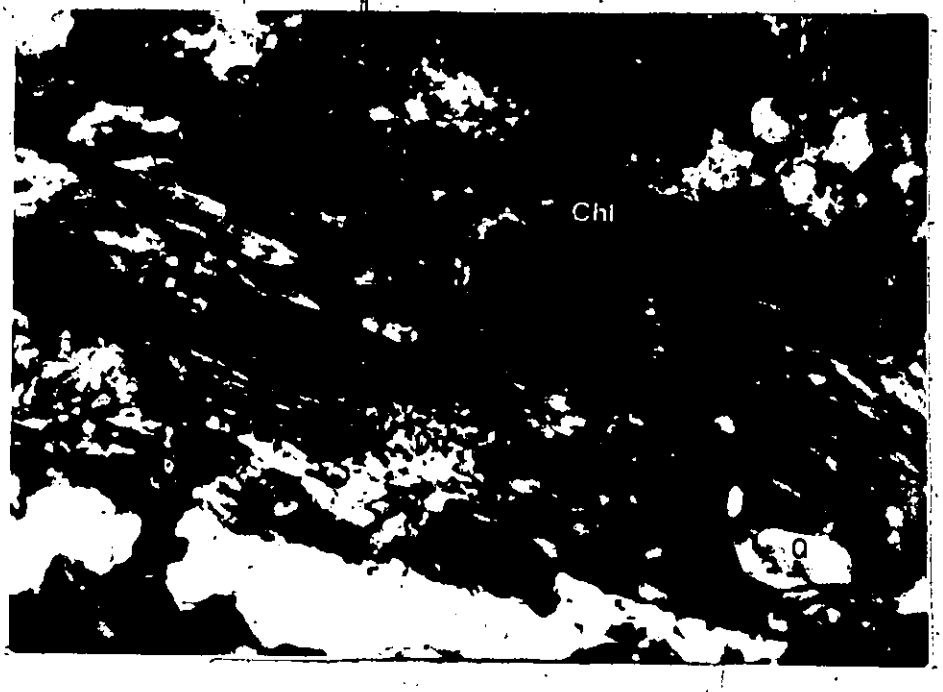


COLOURED PICTURES
Images en couleur

Plate 1.2 a: Chlorite (Chl) flakes cross-cutting hornblende (H) at an angle to the general foliation (Arrow). Fine grained foliated matrix consists of hornblende, quartz, epidote and carbonate. Crossed polarizers.

Plate 1.2 b: Microfracture filled with carbonate (Ca) and chlorite (Chl) cross-cutting epidote-hornblende assemblages. Crossed polarizers.

*Plate 1.2 a*

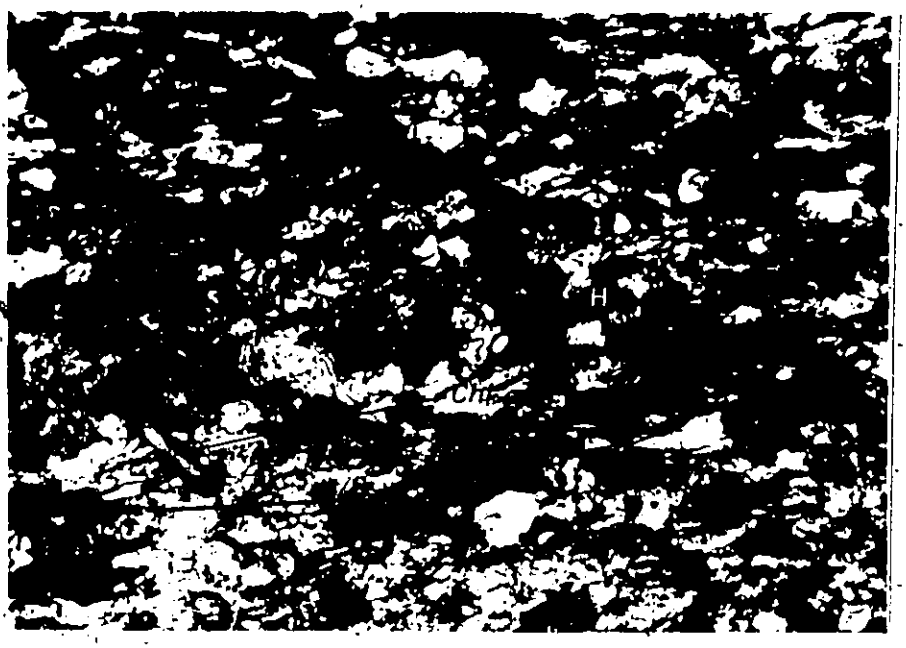


0.1 mm

*Plate 1.2 b*

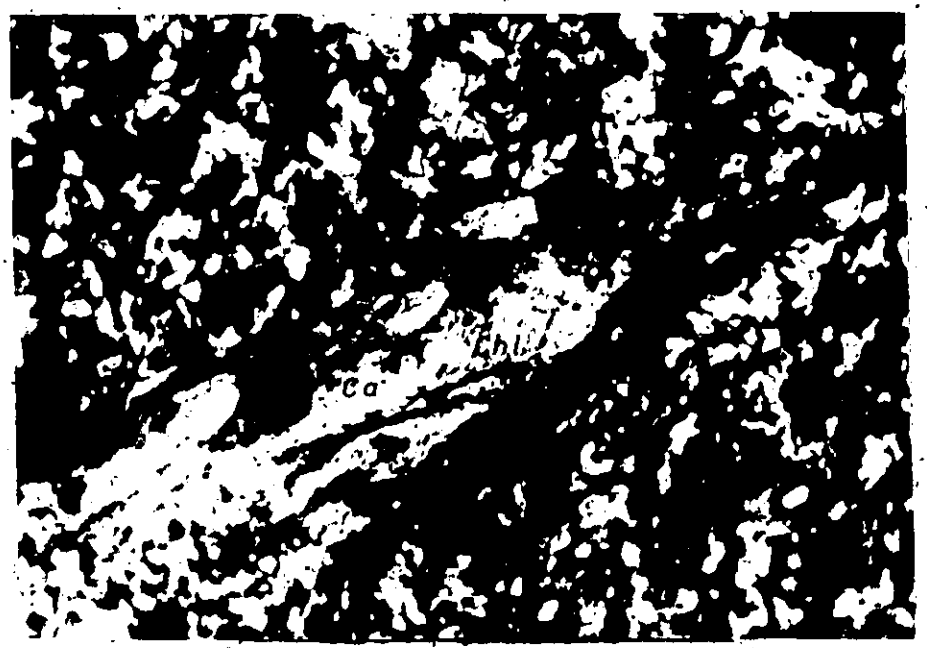


COLOURED PICTURES
Images en couleur

crystals have serrated margins and are enclosed by a halo of chlorite, calcite and quartz (Plate 1.3 a). Hornblende porphyroblasts are also replaced by epidote and carbonate along fractures (Plate 1.3 b).

Felsic metavolcanic rocks presumably overlie the mafic metavolcanics (Ferguson, 1968a). Felsic metavolcanic rocks are light grey-green in color, and are composed of medium grained phenocrysts of quartz and saussuritized albite-oligoclase, surrounded by a fine-grained matrix of chlorite pseudomorphs after biotite, quartz, plagioclase, epidote and muscovite (Plate 1.4). Titanite and pyrite partially altered to hematite are accessory minerals. A well-developed foliation is defined by the alignment of chlorite flakes and small lenses of quartz and plagioclase.

Feldspar and quartz-feldspar porphyry dikes are common within the metabasalt. Mineralogically and texturally they resemble the porphyritic felsic metavolcanic rocks and only their crosscutting relationships allow their distinction.

## 2.3 Felsic Intrusive Rocks

A complex batholith, consisting dominantly of massive to gneissic trondhjemite, with minor weakly foliated to

Plate 1.3 a: Anhedral amphibole with a core of hornblende (dark gray) and a pale rim of actinolite (Ac) surrounded by carbonate (Ca), quartz (Q) and chlorite (Chl). Crossed polarizers.

Plate 1.3 b: Anhedral amphibole with a core of hornblende (dark gray) and a pale rim of actinolite (Ac) is replaced by carbonate along a microfracture. Crossed polarizers.

a

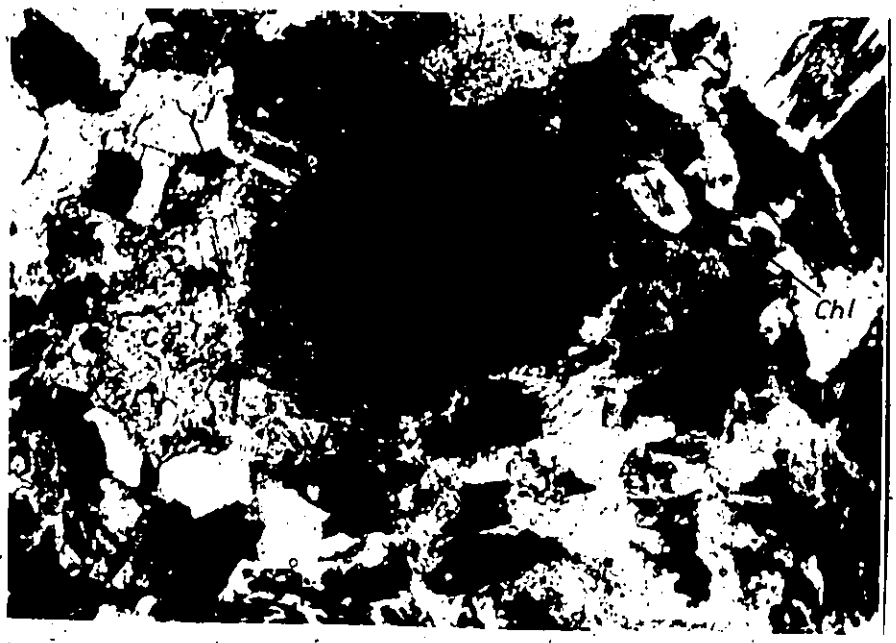


0.1 mm

b

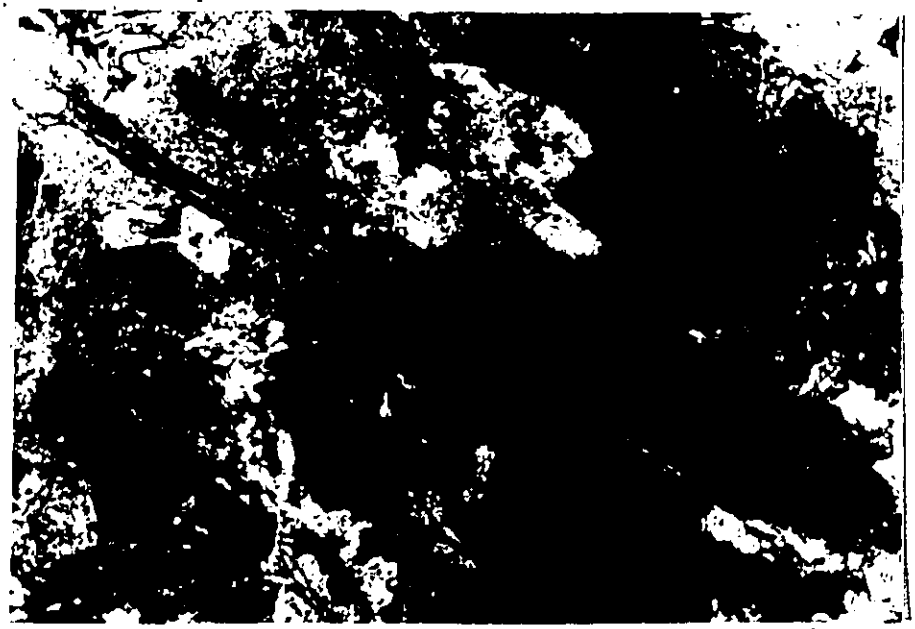

Plate 1.4 : Phenocrysts of altered plagioclase in a fine grained groundmass of chlorite, quartz, carbonate, muscovite and epidote. Crossed polarizers.

COLOURED PICTURES
Images en couleur

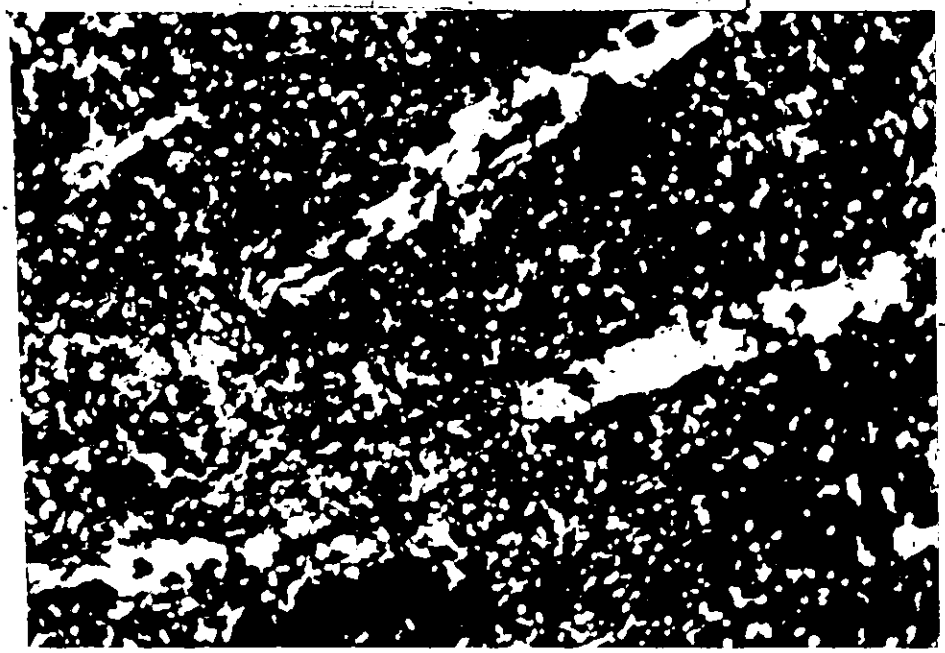

gneissic tonalite, intrudes the metavolcanic rocks on the east (Figure 4).

Gneissic trondhjemite is a light coloured gray-green to pinkish-gray, medium grained rock, with a fine grained granular matrix swirling around medium grained, marginally granulated, quartz and feldspar porphyroclasts (Plate 2.1 a,b). The rock is composed of 25-28% quartz, 35-45% altered oligoclase, 15% muscovite, 8% chlorite and biotite, with accessory carbonate, alkali-feldspar, hematite, pyrite, titanite and apatite. Individual laminae consist of aligned muscovite flakes, chlorite-biotite and epidote aggregates, and quartz-feldspar layers. The eye-shaped quartz and feldspar porphyroclasts are also aligned parallel to the trend of lamination, increasing the impression of the overall kinematic origin of the rock fabric.

Gneissic tonalites are distinct black and white foliated rocks, with a considerably greater proportion of ferromagnesian minerals than the trondhjemitic phases. These rocks are composed of a medium-to fine-grained assemblage of 22-25% quartz, 40% altered andesine, 13% hornblende, 10% biotite, chlorite, epidote and muscovite, and accessory alkali feldspar, titanite, pyrite and magnetite. The foliated texture is a manifestation of the

Plate 2.1 a: Eye-shaped fractured quartz porphyroclast wrapped around by a foliated fine grained matrix of muscovite (Mu), quartz (Q),and chloritized biotite (Bi). Crossed polarizers.

Plate 2.1.b: Eye-shaped fractured altered plagioclase porphyroclast wrapped around by a foliated matrix of fine grained muscovite (Mu), quartz (Q) and chloritized biotite (Bi). Crossed polarizers.

*Plate 2.1a*

COLOURED PICTURES
Images en couleur


0.1mm

*Plate 2.1b*

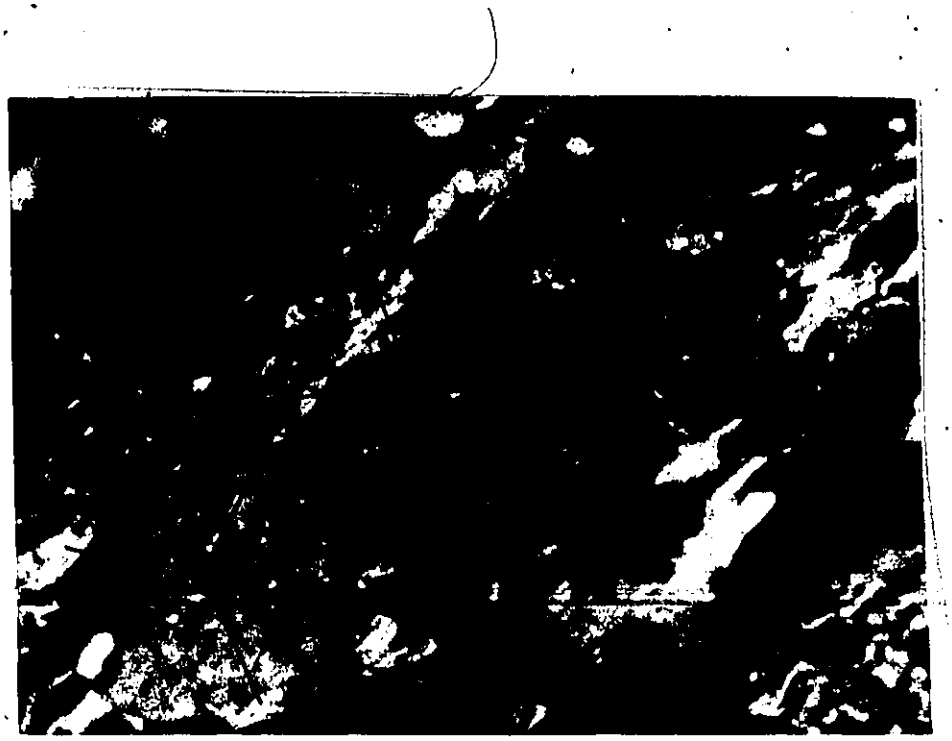

preferred orientation of hornblende crystals, biotite and chlorite flakes, and elongated quartz and feldspar grains, wrapped around elongated feldspar and quartz porphyroclasts. This texture is similar to the laminated texture in the trondhjemites.

The massive-to weakly-foliated intrusive rocks are leucocratic coarse-to medium-grained trondhjemites, and mesocratic medium to fine-grained tonalites. They are characterized by a subhedral granitoid granular texture with a locally overprinted mild foliation and locally granoblastic recrystallized texture (Plate 2.2 ).

Subhedral plagioclase is moderately to intensely mottled with fine-grained sericite, epidote and carbonate (Plate 2.3 a). Compositionally zoned crystals have mottled cores and clear rims of less calcic plagioclase approaching almost pure albite (Plate 2.3 b). Biotite and hornblende are partly replaced by chlorite with or without carbonate and quartz (Plate 2.4 a,b). Hornblende is also replaced by epidote along fractures. Calcite-filled fractures cross-cut trondhjemites and tonalites. Quartz and feldspar porphyroclasts show undulose extinction and may be fractured.

Plate 2.2 : Granitoid assemblage of anhedral quartz and subhedral plagioclase mildly mottled with sericite, fine grained carbonate, and epidote, associated with chloritized hornblende. Crossed polarizers.

COLOURED PICTURES
Images en couleur

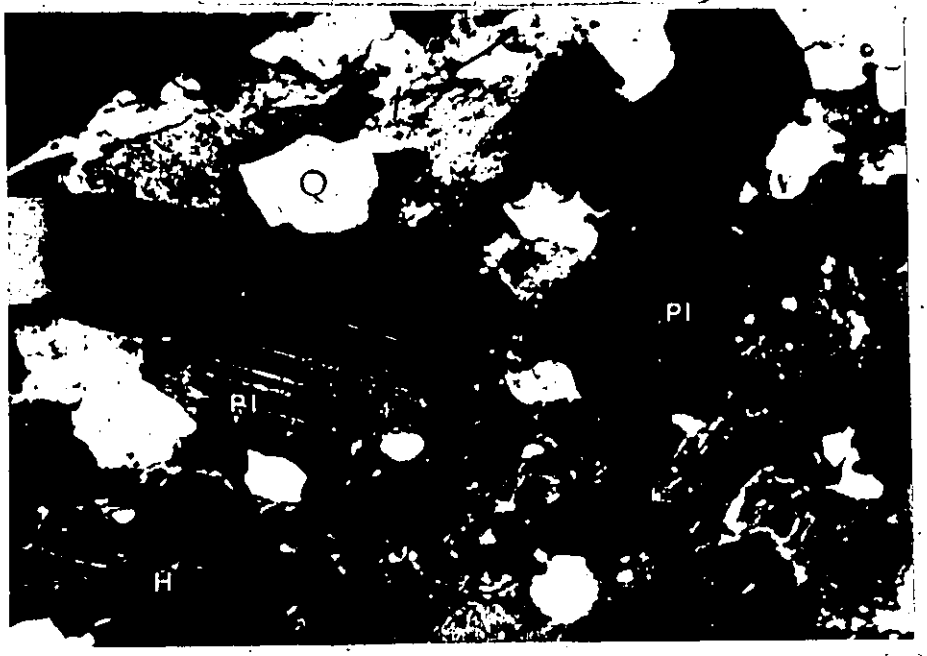

Plate 2,3 a: Subhedral plagioclase intensely mottled with fine grained sericite, carbonate and epidote. Crossed polarizers.

Plate 2.3 b: Compositionally zoned plagioclase lath with mottled core and a clear rim of albite. Crossed polarizers.

COLOURED PICTURES
Images en couleur

a

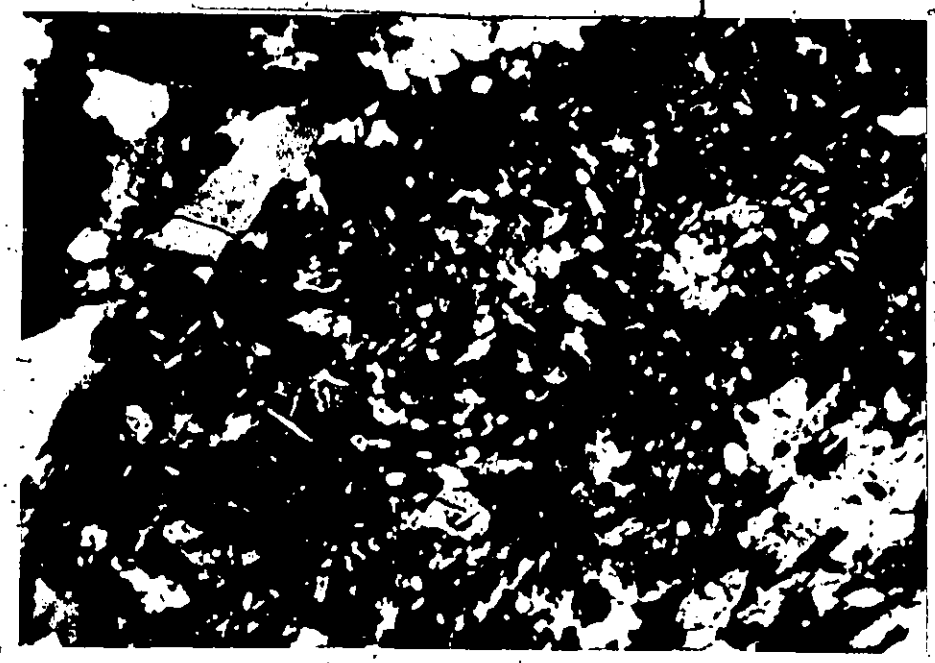

0.1 mm

b

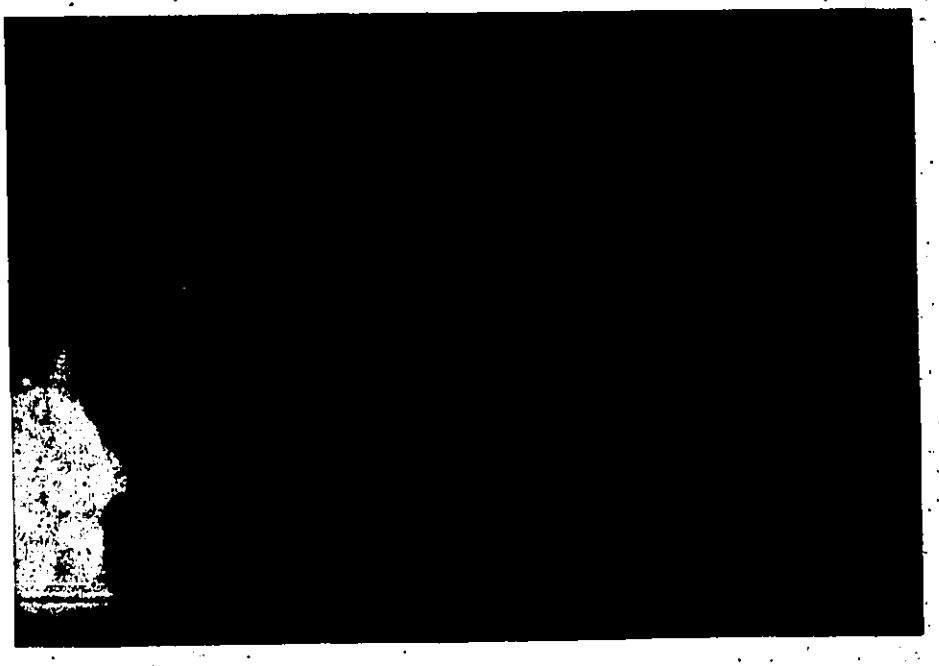

Plate 2.4 a: Biotite (Bi) and poikiloblastic hornblende (H) replaced by chlorite (Chl). Crossed polarizers.

Plate 2.4 b: Biotite (Bi) replaced by chlorite (Chl). Crossed polarizers.

COLOURED PICTURES
Images en couleur

Plate 2.4 a

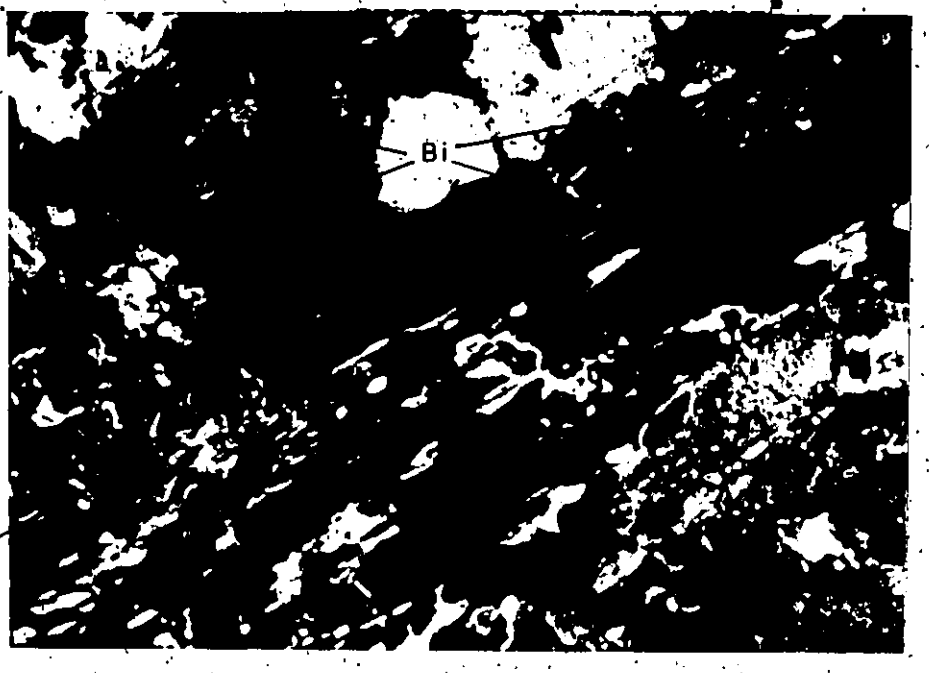


0.1 mm

Plate 2.4 b

Narrow aplite dikes cut the trondhjemitic-tonalitic rocks. Rocks are termed trondhjemites and tonalites in the normative classification of siliceous plutonic rocks after O'Connor (1965), modified by Barker (1979) (Figure 5).

The Renabie area trondhjemite-tonalite is part of the large batholithic terrain, the Missinaibi Lake batholith (MLB) (Percival, 1981) that embays the Wawa greenstone belt at its easternmost end. It is bordered by migmatite and there are minor porphyry, gabbro, and pyroxenite (Percival, 1981; Thurston et al., 1977). The MLB appears to represent an Archean, late synvolcanic and early syntectonic intrusion with a minimum age of 2707 Ma (Percival and Krogh, 1983). It was emplaced at a mesozonal level, detaching and engulfing the lowermost cycle of the Wawa greenstone belt, now represented by amphibolitic zenoliths, and also an older pre-2765 Ma, tonalitic gneiss basement, thought to be a remnant of an ancient sequence.

The batholithic rocks in the Renabie mine area may represent either parts of the gneissic margins of the MLB, or remobilized pre-2765 Ma basement.

Figure 5 : Modal analyses of felsic intrusive rocks from the Renabie area .

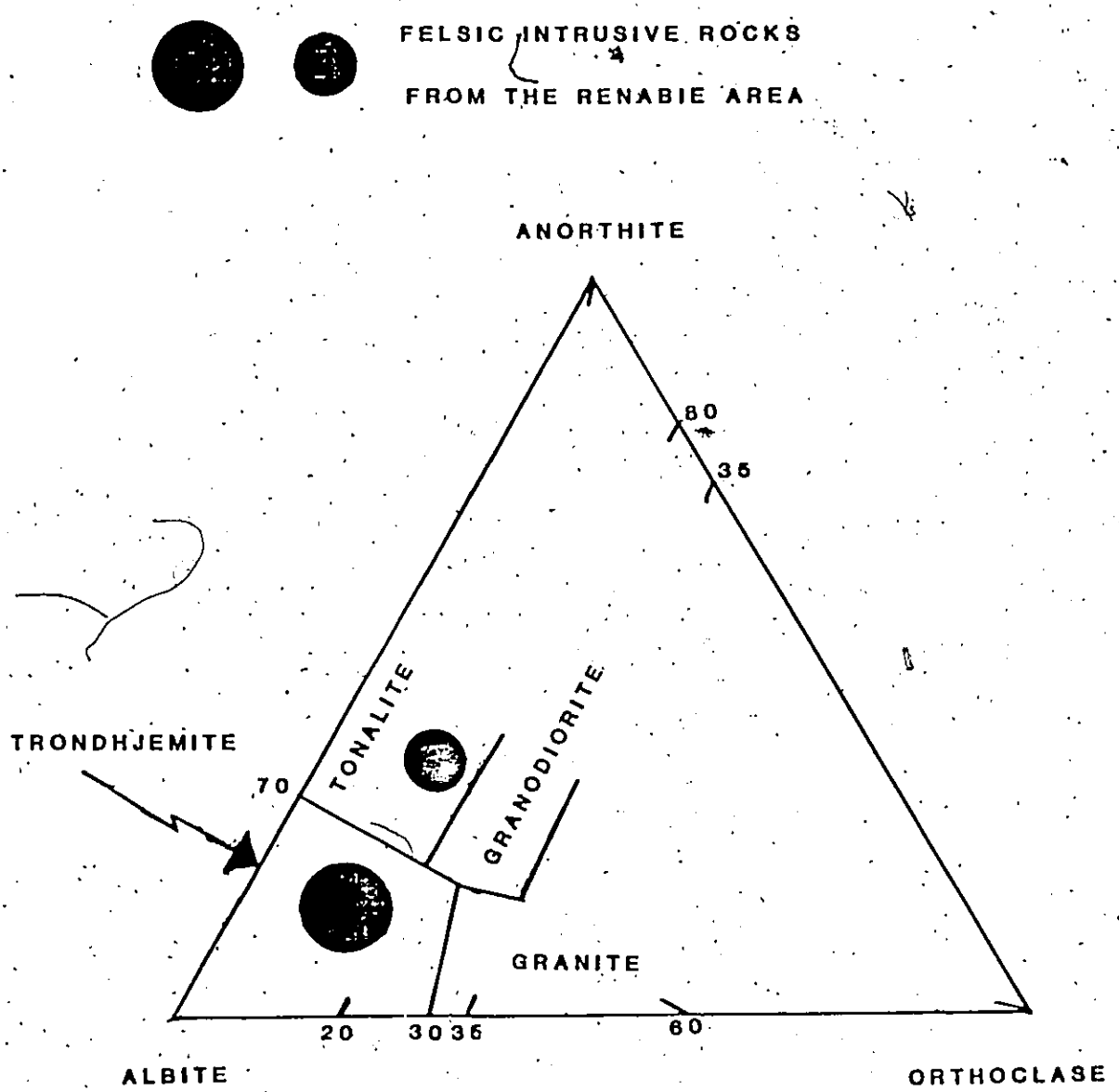


( Compositional fields are after Barker, 1979 )

## 2.4 Mafic Intrusive Rocks

The Renabie mine area is cross-cut by diabase dikes with sinuous outlines which commonly bifurcate and then abruptly pinch out. Their predominant trends vary from northwest to north-northwest. Diabase, croscutting metavolcanics in the map area, is a dark green ophitic textured rock, consisting of subhedral grains of augite rimmed by uralite, set in a matrix of mildly saussuritized labradorite laths. Accessory minerals include quartz, biotite, chlorite and magnetite.

A narrow foliated lamprophyre dike which was encountered, at the 914 m level workings of the Renabie mine, contains fragments of purplish vein quartz, and cuts the foliation of the tronthjemitic wall rock. The lamprophyre is a dark green to black rock consisting of densely packed chloritized biotite containing secondary sphene and ilmenite and saussuritized subhedral to anhedral, andesine laths, with interstitial quartz, carbonate surrounding minor anhydrite, and micrographic intergrowths of quartz and alkali-feldspar.

## 2.5 Structure

The batholithic rocks have an arcuate contact with the greenstone succession, curving from northeast in the northern part (not shown on figure 4) of the area to northwest in the southern part. Drilling has indicated that the intrusive contact has an average dip of 55°W.

The gneissic structure of the batholithic rocks is nearly parallel to the contact and is generally conformable with the foliation within the lavas, dipping westward at about 60 degrees. It appears to be a product of protoclastic cohesive flow under conditions of high shear stress.

There are three main faults in the Renabie mine, namely the West, the Shaft, and the D fault (Figure 6), striking approximately north and dipping 70° to 80° W (Ferguson, 1968b). The Shaft fault displaces the "granite" - greenstone contact 300 m along strike (Figure 4). All the faults intersect both the mineralized zones and the diabase dikes in the mine.

**LEGEND**

LAMPROPHYRE

D// DIABASE

FELSIC META-INTRUSIVE ROCKS

Agd : Granitoid to gneissic trondhjemite

Agd2 : Granitoid to gneissic tonalite

Pf : Feldspar porphyry

FELSIC METAVOLCANIC ROCKS

Vd : Porphyritic metadacite

MAFIC METAVOLCANIC ROCKS

Vbm : Foliated fine to medium grained metabasalt

**GEOLOGICAL SYMBOLS**

Geological boundary, approximate

Fault indicated or assumed

Ore zone

Figure 6 : Geological cross-sections showing the distribution of faults in the Renabie mine, and the relationship of ore zones to the "granite"-greenstone contact. ( after Ferguson, 1968b ). Location shown on Figure 4.

Scale

0 150m

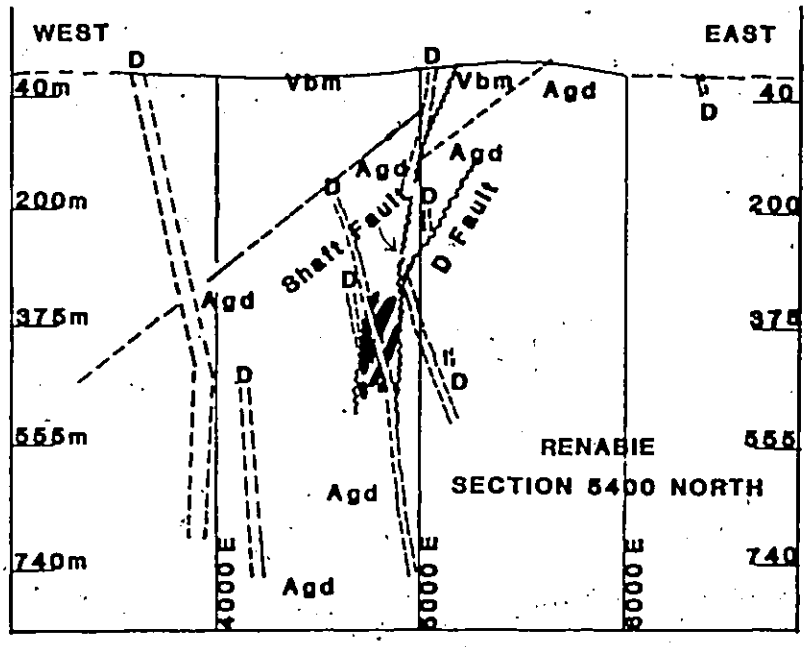
WEST
EAST
40m
200m
375m
555m
740m
Vbm
Agd
D
Shaft Fault
D Fault
RENABIE
SECTION 5400 NORTH
4000 E
5000 E
6000 E

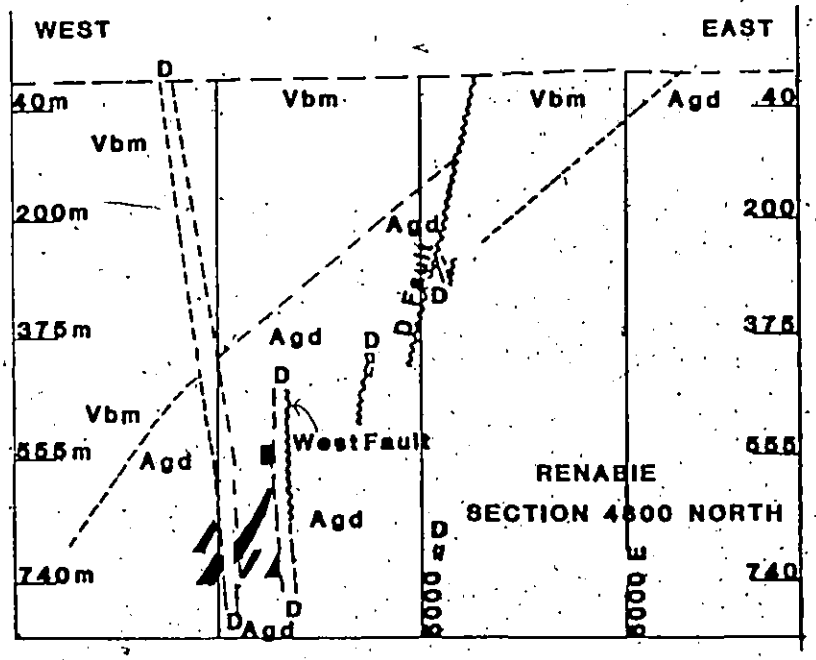
WEST
EAST
40m
200m
375m
555m
740m
Vbm
Agd
D
D Fault
West Fault
RENABIE
SECTION 4800 NORTH
5000 E
6000 E

# CHAPTER 3

## 3. GOLD MINERALIZATION IN THE RENABIE AREA

### 3.1 General Statement

The gold deposits in the Renabie area are gold-, sulphide-, and telluride-bearing quartz veins in the marginal phase of the batholith and in the adjacent greenstones, within 500 m of the intrusive contact. There is a general sympathetic relationship between gold, sulphide, and telluride mineral occurrences in the deposits of the area.

### 3.2 The Renabie Vein

The information on the Renabie Gold Mine is based on data and samples collected during a visit to the Renabie mine, the marginal notes on O.D.M. Map No. P. 492 (Ferguson, 1968a), and the mine description by Bruce (1944).

The Renabie Gold Mine (Plate 3.1) has an 800 m long east-west striking, steeply dipping vein that crosscuts trondhjemite and tonalite at the west margin of the Missinaibi Lake Batholith. Disrupted vein sections form the Renabie ore zones, ranging from 4 to a maximum of 210 m

Plate 3.1 : View of the mine plant, looking west, Renabie mine, Leeson township, Ontario.

COLOURED PICTURES
Images en couleur

in length, and from less than 1 m to 30 m in width. The mineralized zones generally dip to the southwest and are irregular and variable in shape forming lenses, pipes and tabular bodies. Some ore shoots consist of a complex of closely spaced veins or lenses enveloped and separated by altered schistose wallrock. The vertical extend of the vein has been explored to a depth of 950 m.

The eastern-most section of the Renabie vein, known as the "C" zone (Figure 4), cuts gneissic tonalite. The part that is exposed on the surface is an east-west trending 20 m thick quartz vein (Plate 3.2 a) which includes streaks and elongated oval shaped inclusions of schistose wallrock (Plate 3.2 b).

At the 914 m level of the mine workings, sections of the vein exhibit a banded structure parallel to the borders. The most abundant type of banding is brought about by stringers of muscovite-rich host rock and by oval shaped altered wallrock fragments (Plate 3.3 ). A second type is caused by shearing and granulation parallel to the walls.

Plate 3.2 a: The eastern section of the "C" ore zone, looking west along strike, Renabie mine.

Plate 3.2 b: Elongated inclusions of schistose wallrock in the eastern section of the "C" ore zone, Renabie mine.

COLOURED PICTURES
Images en couleur

Plate 3.2 a

Plate 3.2 b

Plate 3.3 : Banded structure of the Renabie vein, 914m (3100ft) level workings, Renabie mine.

COLOURED PICTURES
Images en couleur

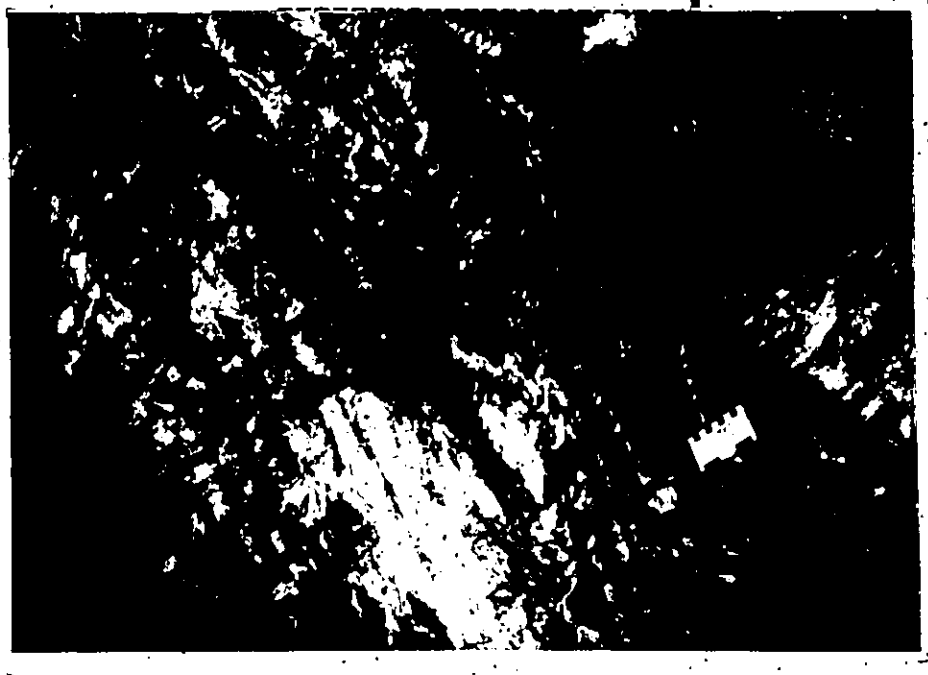

### 3.2.1 Mineralogy

Quartz is by far the most abundant constituent, accounting for about 90% of the vein filling. Most of the quartz is of a massive or granular, milky or dirty gray variety due to minute fluid and solid inclusions. Under the microscope the vein quartz exhibits undulatory extinction, evidence of strain during and after its formation.

Other essential gangue minerals include carbonate and muscovite. They are most abundant along the vein borders. Carbonate forms mineral aggregates with quartz, whereas muscovite is mostly found in monomineralic clusters associated with quartz and carbonate (Plate 3.4a,b).

Accessory tourmaline and chlorite are present in the "C" zone.

Ore grade vein sections of the vein may contain between 5 and 20% sulphides, dominantly pyrite, accompanied by minor galena, chalcopyrite, sphalerite, molydenite and native gold. Telluride minerals, including tellurobismuthite ($Bi_2Te_3$), altaite (PbTe), hessite ($Ag_2Te$), petzite ($Ag_3AuTe_2$), a

Plate 3.4 a: Massive aggregate of carbonate (Ca) with quartz (Q). Microphotograph under crossed polarizers of vein filling, Renabie mine.

Plate 3.4 b: Quartz (Q) associated with carbonate (Ca) and muscovite (Mu). Microphotograph under crossed polarizers of vein filling. Renabie mine.

COLOURED PICTURES
Images en couleur

a

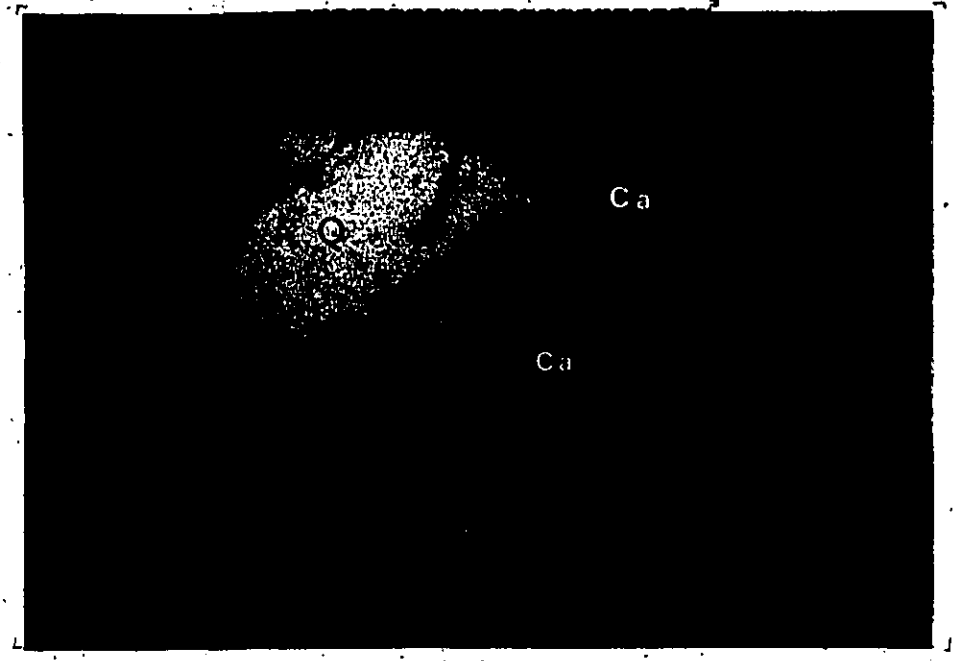


0.1 mm

b

rare Pb-Bi telluride known as rucklidgeite ($(Bi,Pb)_3Te_4$) (Rucklidge, 1969), are also present.

Microscopic subrounded or elongated grains of native gold commonly occur along the boundaries of pyrite and galena grains, (Plate 4.1 a,b) and rarely as inclusions in pyrite with tellurides (e.g. altaite, hessite) (Plate 4.2 ). Gold also occurs in petzite, and can be associated with altaite and tellurobismuthite. Electron-microprobe analyses by Dr. D.C. Harris of the Geological Survey of Canada on five gold grains show that the Au/Ag ratio ranges from 5.7 to 9.6 (Table 1).

Pyrite, the most abundant metallic mineral, forms small cubes and irregular grains. It is typically fractured and replaced by quartz and chalcopyrite, with or without galena and gold.

Galena forms hypidiomorphic crystals characteristically associated with gold (Plate 4.1 b). Galena intergrowths with chalcopyrite fill fractures in vein quartz and also replace pyrite along fractures. The mineral also occurs as isolated grains.

Plate 4.1 a: Gold (Au) associated with pyrite (Py). Microphotograph under reflected light.

Plate 4.1 b: Gold (Au) in association with galena (Gn), pyrite (Py), hessite (Hs) and tellurobismuthite (TEBI). Microphotograph under reflected light.

Plate 4.1 a


1/10mm

Plate 4.1 b

Plate 4.2 : Gold (Au) with altaite (At) and hessite (Hs) as inclusions in pyrite.
Microphotograph under reflected light.

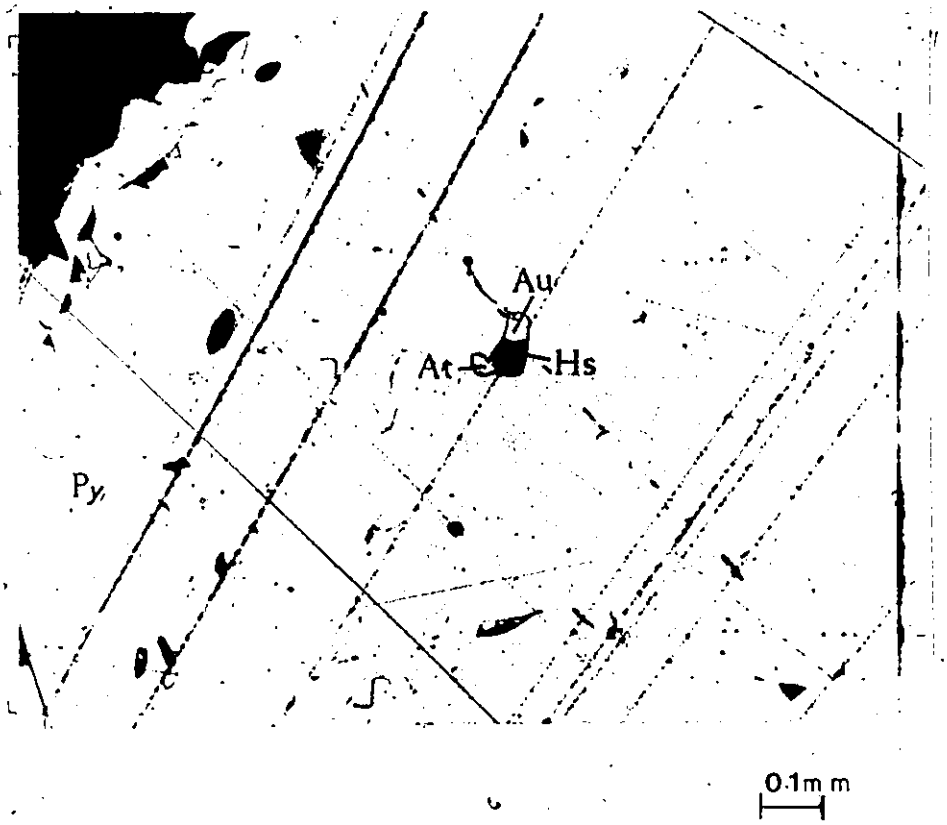
Au
At
Hs
Py
0.1m m

Table 1 : Electron microprobe analyses of gold and tellurides from the Renabie gold-bearing vein.

( Analyst : Dr. D.C. Harris, Geological Survey of Canada )

| | | | | | |
|---|---|---|---|---|---|
| | GOLD | | | | |
| (wt%) | 1 | 2 | 3 | 4 | 5 |
| Ag | 9.4 | 9.2 | 14.5 | 14.9 | 14.2 |
| Au | 88.0 | 88.3 | 83.8 | 85.0 | 84.6 |
| TOTAL | 97.4 | 97.5 | 98.3 | 99.9 | 98.8 |
| Au/Ag | 9.4 | 9.6 | 5.8 | 5.7 | 6.0 |
| | RUCKLIDGEITE | | | | |
| Pb | 17.3 | | | | |
| Bi | 39.2 | | | | |
| Te | 45.3 | | | | |
| TOTAL | 101.8 | | | | |
| | TELLUROBISMUTHITE | | | | |
| Bi | 51.0 | | | | |
| Te | 47.8 | | | | |
| TOTAL | 98.8 | | | | |

Molybdenite, where present, has the same mode of occurrence as do galena and chalcopyrite.

Sphalerite is very minor, occurring as thin films bordering pyrite cubes and also associated with chalcopyrite.

Tellurobismuthite, the most abundant of the telluride minerals, forms lath-shaped crystals associated with galena and gold (Plate 4.3 a) and is also present as isolated prisms in the quartz vein material.

Altaite, the second most common telluride, forms irregular grains commonly occurring interstitially to pyrite cubes or in association with gold (Plate 4.3 b).

Rucklidgeite was first reported as an unidentified Pb-Bi telluride from the Robb-Montbray property in Québec, subsequently from two localities in Russia by Zav'yalov and Begizov (1977), and recently from the Ashley deposit, Ontario (Harris et al., 1983). The mineral occurs as intergrowths with altaite (Plate 4.3 c).

Plate 4.3 a: Tellurobismuthite (TEBI) lath shaped crystals with gold (Au) on galena (Gn).

Plate 4.3 b: Gold (Au) with altaite (At) interstitial to pyrite (Py).

Plate 4.3 c: Rucklidgeite (R) intergrown with altaite (At), associated with pyrite (Py), galena (Gn) and chalcopyrite (Cp).

( Microphotographs under reflected light )

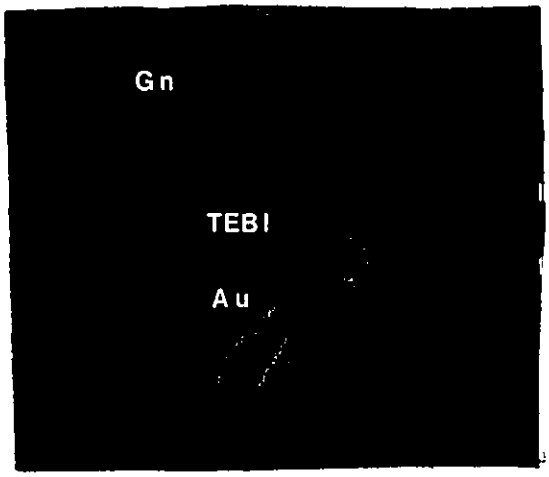


a

0.1 m m

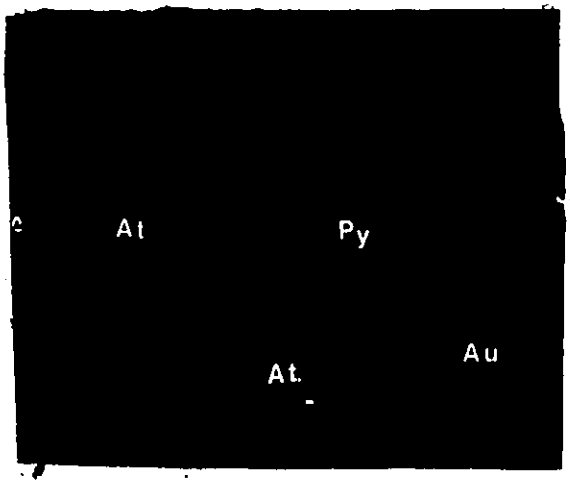


b

0.1 m m

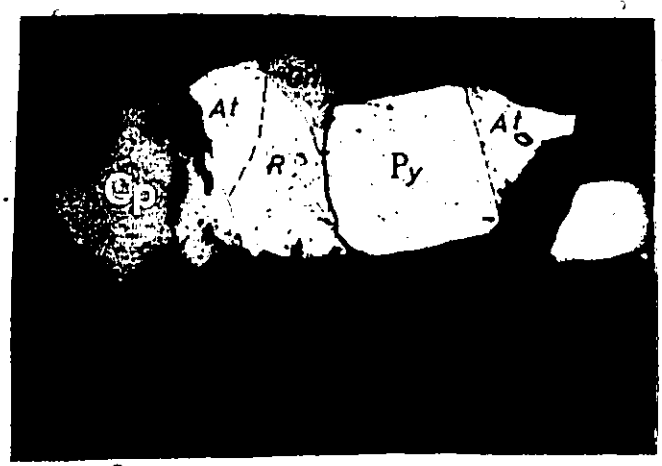


c

0.1 m m

### 3.2.2 Wallrock Alteration

In the immediate vicinity of the Renabie vein, the trondhjemitic and tonalitic wallrocks have been hydrothermally altered during the formation of the vein to a schistose assemblage of muscovite, quartz, carbonate (calcite), chlorite, albite and pyrite. Chlorite is pseudomorphous after biotite and muscovite is pseudomorphous, in part, after plagioclase (Plate 5.1 a,b). These schists are transected by lensoidal quartz stringers immediately adjacent to the vein and grade outward into gneissic trondhjemite or tonalite over a distance of 3 to 4 meters.

Schistose wallrock inclusions in the vein are impregnated with abundant pyrite. These schists carried low gold values according to Frohberg (1948).

The "granitic" wallrocks are mineralogically and texturally changed with decreasing intensity away from the vein for distances up to three meters. The prominent mineralogical (Figures 7 and 8) and textural changes towards the vein are:

1) A change from medium-grained foliated or gneissic rocks into fine-grained fissile rocks;

Plate 5.1 a: Foliated assemblage of muscovite (Mu), carbonate (Ca) and quartz (Q) in altered wallrocks to the Renabie vein.
Crossed polarizers.

Plate 5.1 b: Muscovite (Mu) pseudomorphs after plagioclase and chlorite (Chl) pseudomorphs after biotite in association with carbonate (Ca) and quartz (Q) in altered wallrocks to the Renabie vein.
Crossed polarizers.

COLOURED PICTURES
Images en couleur

*Plate 5.1a*

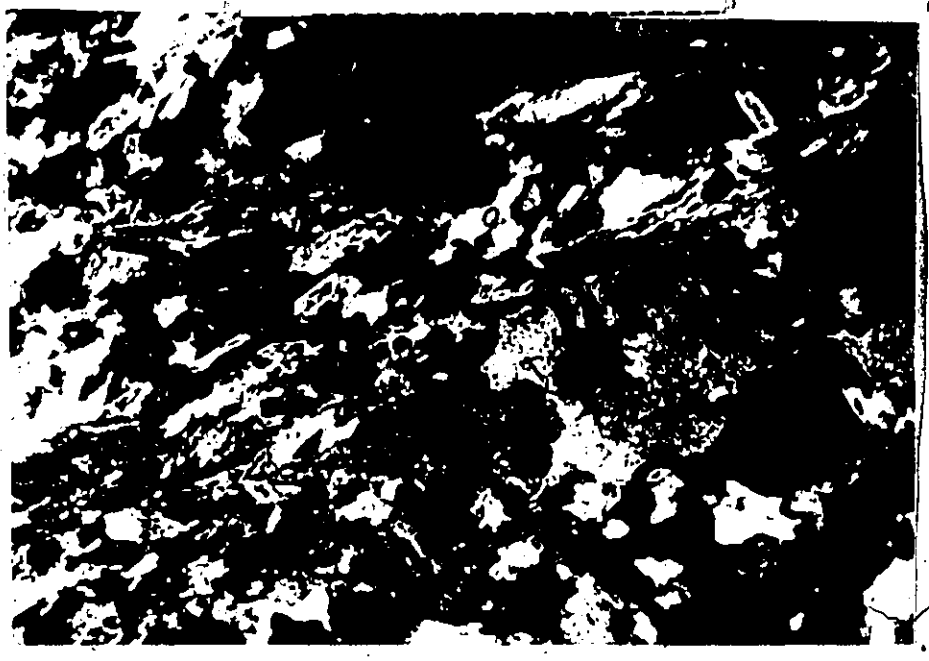

0.1 mm

*Plate 5.1 b*

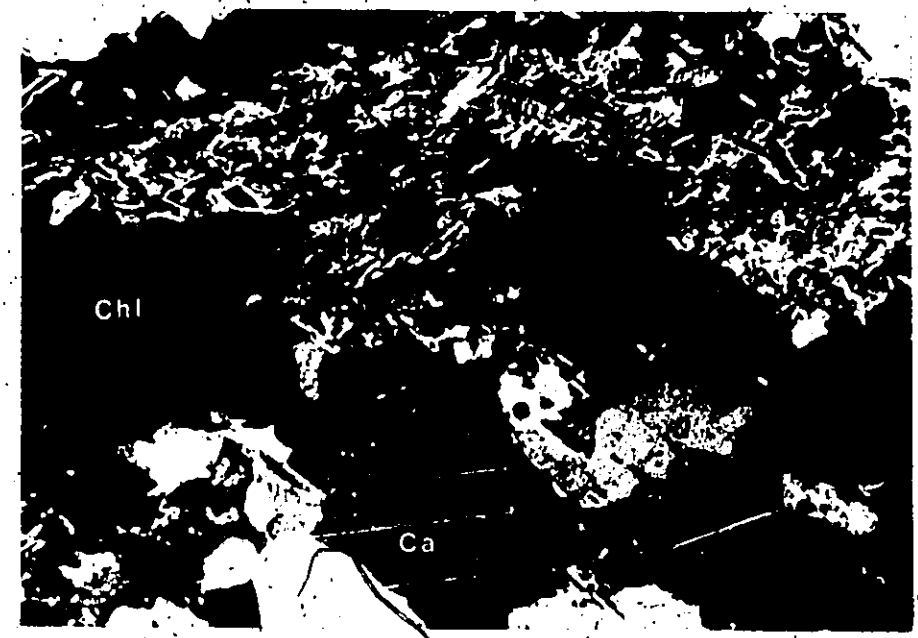

Figure 7 : Mineralogical changes in tonalitic wallrocks about the Renabie gold-bearing quartz-muscovite-carbonate vein in the eastern section of the "C" zone, Renabie mine. ( Traverse suite : 16 → 25 ).

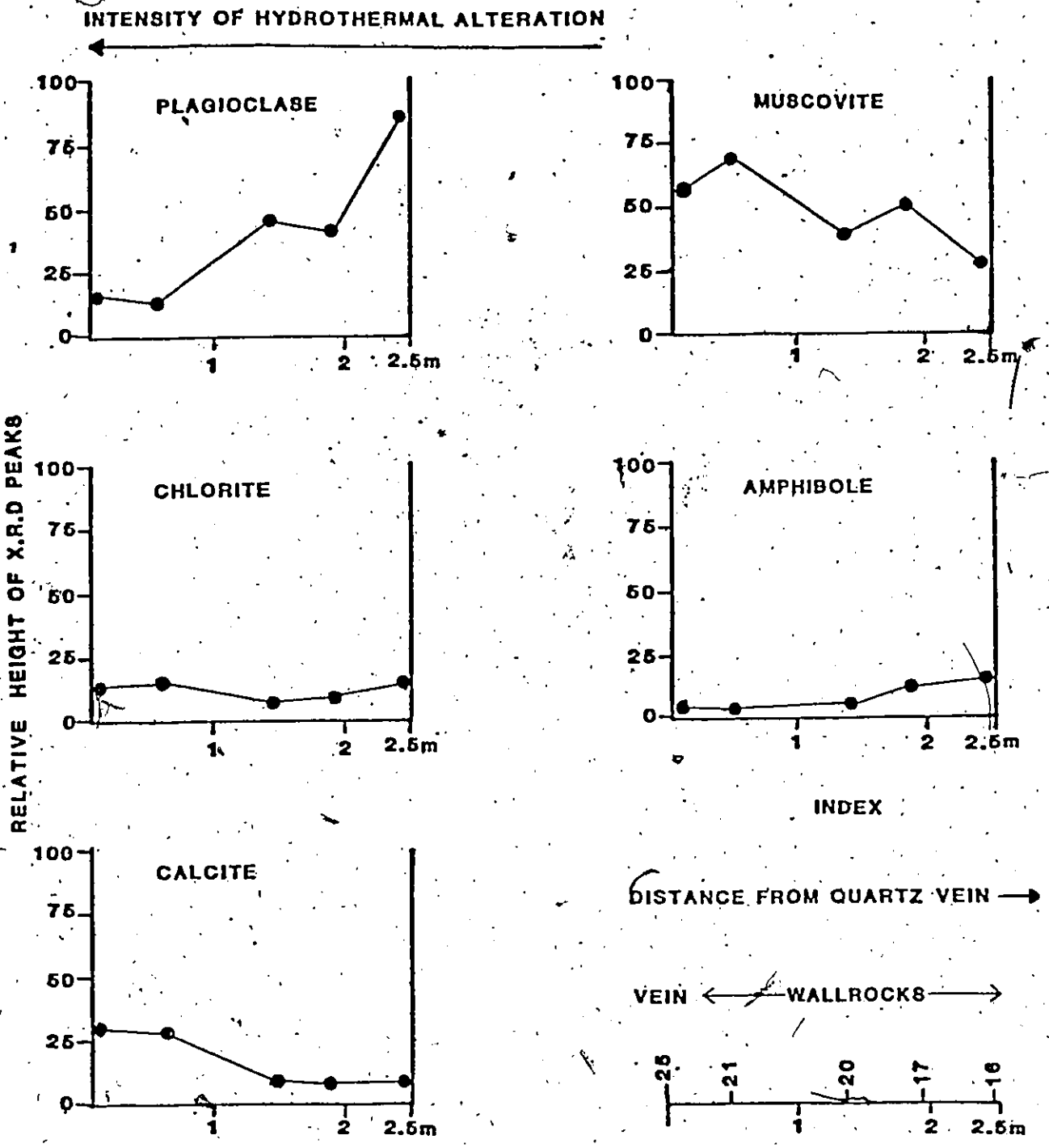

Figure 8 : Mineralogical changes in trondhjemitic wallrocks about the Renabie gold-bearing quartz-muscovite-carbonate vein at the 914m (3100ft) level workings, Renabie mine. ( Traverse suite : 125 → 129 ).

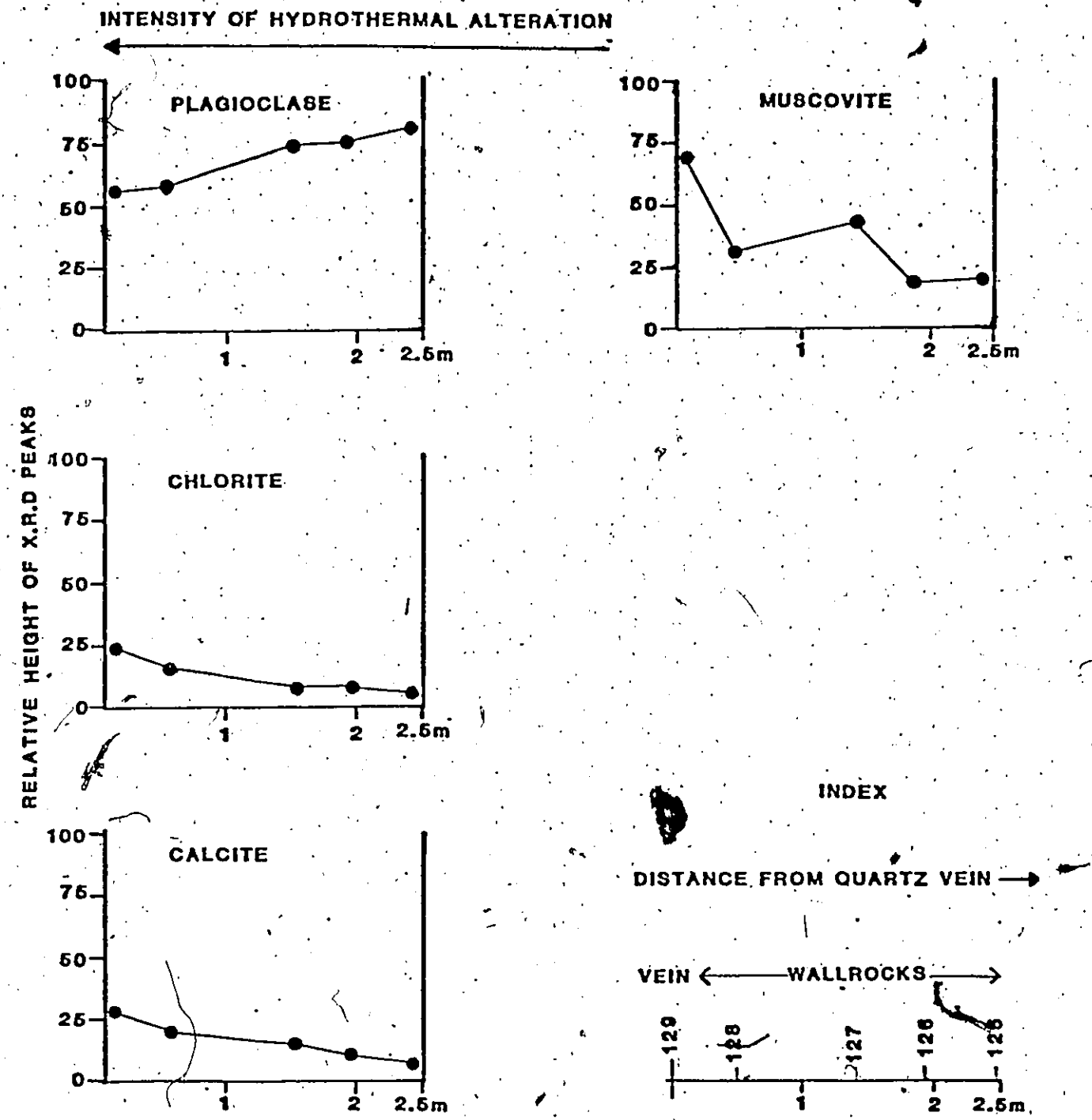

2) Increase in the alteration of individual minerals exemplified by the transformation of saussuritized plagioclase into sericite-carbonate pseudomorphs; or transformation of chloritized biotite and hornblende into chlorite pseudomorphs.

3) Dramatic increase in muscovite (sericite), accompanied by steady increase in carbonate, chlorite and pyrite;

4) Decrease in feldspar, biotite and hornblende.

The relative abundance of wallrock primary minerals and their alteration products was determined by measuring the heights of various peak intensities on X-ray diffraction charts (Figure 7,8). The measured heights do not represent absolute amounts, but are useful to show mineralogical changes that occur during hydrothermal alteration (Armbrust, 1980). The mineralogical changes for biotite and pyrite were deduced from thin section examination. Streaks and fragments of hydrothermally altered wallrock material which are included into the veins are composed of a medium grained fissile assemblage of densely packed chlorite and muscovite flakes, and fine grained carbonate and sericite aggregates, aligned parallel to

the vein's walls. The chlorite is pseudomorphous after biotite and hornblende, and the carbonate-sericite aggregates completely replace plagioclase. Oval-shaped, granulated quartz porphyroclasts are commonly set into the fissile matrix with the longer dimension also aligned parallel to the schistosity. Wallrock fragments are impregnated with abundant pyrite in the "C" zone. The altered wallrock fragments are enveloped by granulated quartz.

### 3.2.3 Deformation

The Renabie ore bodies appear highly contorted, probably by an episode of disharmonic folding as indicated by microfolds developed in the schistose wallrocks. The microfolds plunge about 70° W and their axial planes strike roughly E-W.

The gold-bearing quartz is commonly sheared and fractured and shows late sericite and chlorite on fractures. Gold ore is also cut and offset by mafic dikes and faults (Figure 6). Thus, it is believed that the present ore configuration characterized by a large number of small discontinuous ore shoots, is the result of severe tectonism accompanying vein formation or later during faulting and dike intrusion.

### 3.2.4 Age of the Vein

Lead isotope data indicate formation of the Renabie auriferous veins 2688 Ma ago, according to a new lead evolution model for deposits from the Superior province of the Canadian Shield (Thorpe, 1982, and personal communication). The Stacey-Kramer's (1975) model provides a model age of 2692 Ma for the same sample. These ages plot slightly off the paleoisochron defined by Thorpe (1982) primarily on the basis of data for Superior Province massive sulphide deposits. These dates are in good agreement with a metamorphic and deformation event that affected the Archean, near Lochalsh (Figure 2), and which has been dated at 2700 to 2685 Ma by U-Pb dating of zircons (Percival and Krogh, 1983).

## 3.3 Braminco No. 21 Vein

The Braminco No. 21 Vein, located 1.8 km southeast of the Renabie mine, belongs to the Braminco prospects. The Braminco prospects include six north-northwest trending, steeply dipping (Ferguson, 1968a), quartz-carbonate veins which transect trondhjemite and metabasalt (Figure 4).

The No. 21 vein crosscuts trondhjemite, strikes approximately due north and dips steeply. At its southeast end, where it disappears beneath a swamp, the width of the quartz is 4 m.

### 3.3.1 Mineralogy

The No. 21 vein is a massive quartz-muscovite-carbonate aggregate with up to 30% pyrite, accompanied by less than 5% chalcopyrite, galena, altaite, hessite, tellurobismuthite, sphalerite and native gold.

Textural relationships among metallic minerals are similar to those of the Renabie deposit.

### 3.3.2 Wallrock Alteration

The Braminco No. 21 vein is bordered by a fine grained leucocratic schist consisting of muscovite, carbonate, chlorite, quartz and albite, which grades outwards into weakly foliated to gneissic trondhjemite. Wallrocks, at a distance of 3 m away from the vein, have experienced the same kind of mineralogical (Figure 9), textural, and structural changes as the trondhjemitic wallrocks about the Renabie vein.

Figure 9 : Mineralogical changes in trondhjemitic wallrocks about the Braminco No. 21 gold-bearing quartz-muscovite-carbonate vein, Braminco gold prospects, southeast of the Renabie mine. (Traverse suite:59→69)

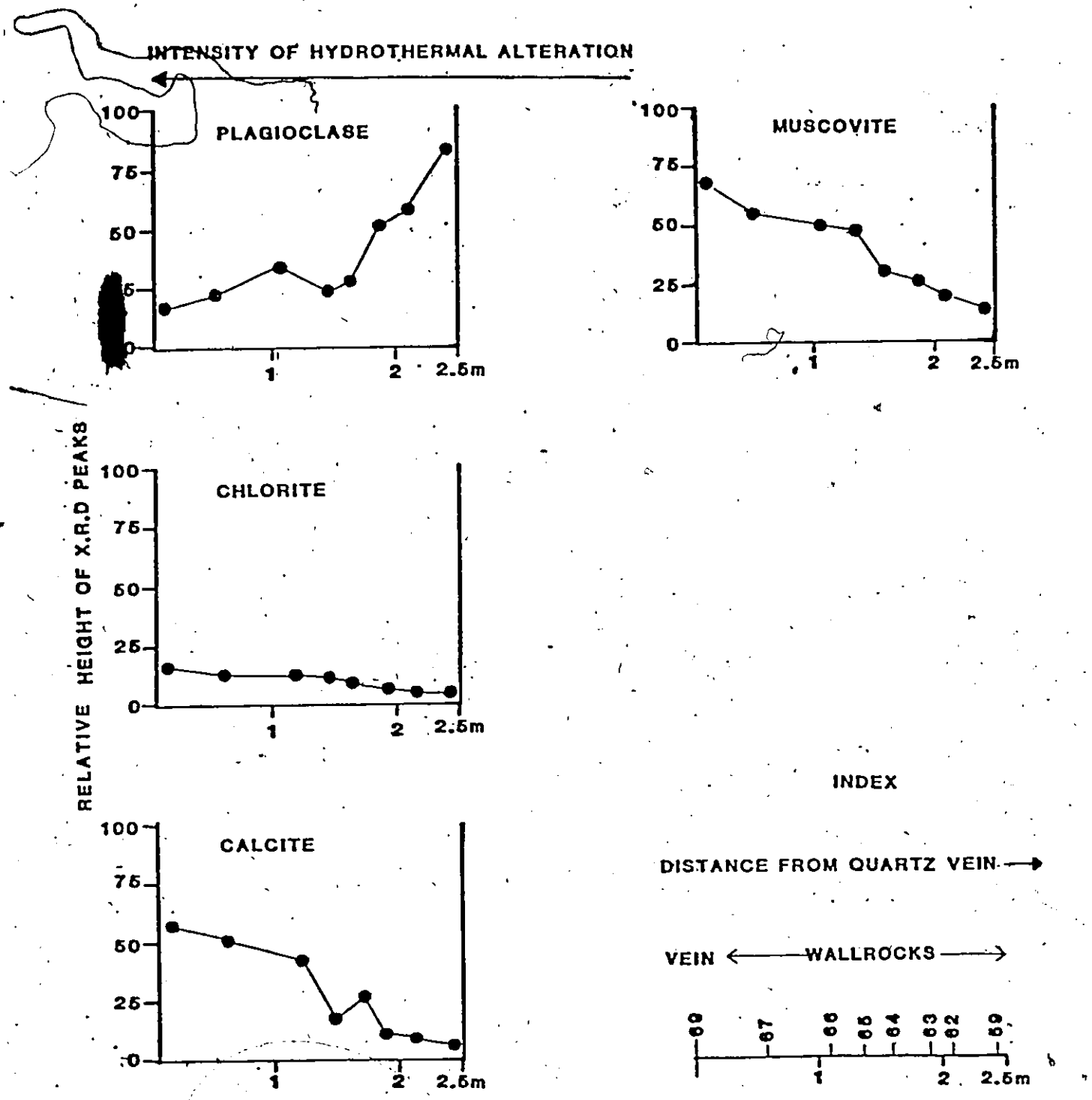

## 3.4 Campbell Vein

The Campbell gold-bearing vein, which belongs to the Braminco Prospects (Figure 4), occurs in metabasalt at a distance of 100 m from the "granite" - greenstone contact. The southernmost extension strikes approximately north. The original find was described by Gardiner and Low (1947) as lenses of quartz up to 13 m in width, rapidly pinching out to the north. The vein consists of massive quartz with carbonate and muscovite, and 10-30% disseminated pyrite. No other metallic mineralization was found in the samples collected.

### 3.4.1 Wallrock Alteration

Metabasalts enveloping the Campbell vein consist of a schistose assemblage of chlorite, epidote, carbonate pseudomorphs after hornblende, albite pseudomporphs after more calcic plagioclase, quartz, muscovite and pyrite.

The prominent mineralogical (Figure 10), textural, and structural changes that are documented in the wallrocks within 4 m of the Campbell gold-bearing vein, and that increase in intensity toward the vein are:

Figure 10 : Mineralogical changes in metabasaltic wallrocks about the Campbell gold-bearing quartz-muscovite-carbonate vein, Braminco gold prospects, southwest of the Renabie mine. ( Traverse suite : 78 → 90 ).

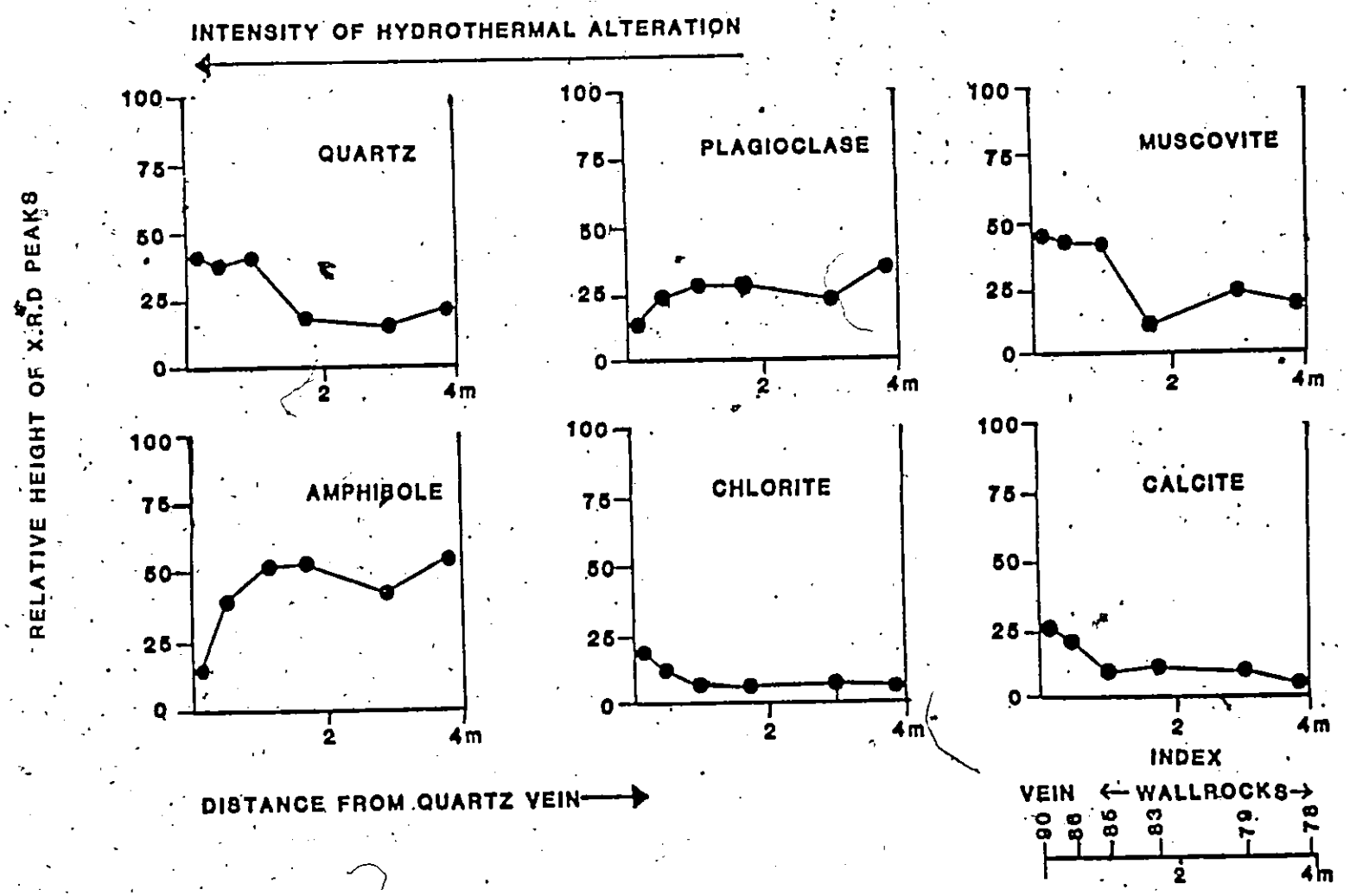

1) Enhancement of a steeply dipping foliation parallel to the vein's general attitude;

2) Medium grained rocks with porphyroblastic textures pass into fine grained schists, followed by the abrupt appearance of pyrite- bearing quartz lenses;

3) Increase in quartz, chlorite, white mica, pyrite, and carbonate minerals;

4) Decrease in hornblende.

Mineralogical changes for pyrite were deduced from thin section examination.

# CHAPTER 4

## 4. GEOCHEMISTRY OF THE WALLROCK ALTERATION

### 4.1 General Statement

This chapter describes the changes in major and minor element abundances during the hydrothermal alteration of wallrocks adjacent to gold-bearing veins in the Renabie mine area, and investigates the redox nature of the fluids ascribed to this alteration. Mass balance calculations express the element distribution, and redox state of iron relationships provide evidence on the nature of the fluids.

### 4.2 Mass Balance Equation

During hydrothermal alteration the absolute abundances of elements change by real gains or losses for mobile elements, by dilution during increasing addition of other chemical components, or, for immobile elements, by concentration through leaching of soluble components. Gresens (1967) derived a general equation that allows calculation of cation gains and losses accompanying metasomatic transformation of a given parent rock to its

alteration product. Specific gravity data are incorporated into this mass balance equation, and so compositional variations are related to volume changes. Simple comparisons of bulk rock compositions (wt.%) of parent rock and alteration product do not satisfactorily account for changes in element abundances, unless possible changes in volume, produced by gain or loss of volatiles, ionic packing and/or deformation, are taken into account.

Gresen's mass balance equation is given as:

$$\Delta xi = a\,(Fv\ xi^{d}\ (\beta^{d}/\beta^{p}) - xi^{p} \qquad (1)$$

where the parameters are:

$\Delta xi$ = Chemical change: the change in abundance of element i.

a = Initial quantity of parent rock prescribed 100 gms.

Fv = The volume factor: ratio between the final and initial volumes of rock masses.

$xi^{p,d}$ = Weight fraction of element i in parent rock and alteration product respectively.

$\beta^{p,d}$ = Specific gravity of parent and alteration product, respectively.

A unique solution to equation (1) is obtained by knowing or inferring:

1. The chemical composition and the specific gravity of the parent and alteration product.

2. The change in volume or the isochemical behaviour of element(s), during the transformation in question.

For any transformation of a given parent rock to its complement alteration product, volume factors may be found by:

1. Estimating the volume change based on independent evidence, such as changes in the shape of crystals.

2. Demonstrating the isochemical behaviour of two or more elements. Two elements probably remained immobile during hydrothermal alteration if they maintain approximately constant ratios to one another in a rock suite bearing variable intensities of alteration (Tables 2,3,4,5). Consistency of the ratios establishes derivation from a common parental rock type, with respect to a set of elements which behaved isochemically.

3. Choosing the value where the component lines, for immobile elements, simultaneously cross the zero mass change axis in a composition-volume diagram, Gresen's

Table 2 : Chemical analyses of wallrocks about the Renabie gold-bearing quartz-muscovite-carbonate vein at the eastern section of the "C" zone, Renabie mine. ( Traverse suite: 16 → 25 )

| Distance from quartz vein. ( m ) | 2.5 | 1.9 | 1.4 | 0.5 | 0 |
|---|---|---|---|---|---|
| Sample number | 16 | 17 | 20 | 21 | 25 |
| (wt%) | | | | | |
| $SiO_2$ | 66.14 | 64.04 | 64.41 | 61.95 | 57.70 |
| $Al_2O_3$ | 16.17 | 14.45 | 15.52 | 14.47 | 15.46 |
| $Fe_2O_3(T)$ | 5.48 | 4.68 | 4.80 | 4.52 | 5.20 |
| MgO | 2.23 | 1.66 | 1.72 | 1.93 | 2.45 |
| CaO | 5.32 | 4.47 | 4.59 | 4.90 | 6.02 |
| $Na_2O$ | 4.12 | 3.36 | 3.38 | 1.02 | 1.71 |
| $K_2O$ | 0.92 | 1.31 | 1.51 | 4.41 | 4.48 |
| $TiO_2$ | 0.52 | 0.45 | 0.48 | 0.52 | 0.49 |
| $P_2O_5$ | 0.06 | 0.08 | 0.10 | 0.09 | 0.07 |
| MnO | 0.09 | 0.07 | 0.07 | 0.10 | 0.01 |
| S | 0.00 | 0.00 | 0.02 | 0.18 | 0.10 |
| L.O.I | 0.80 | 4.80 | 2.71 | 5.70 | 6.00 |
| TOTAL | 100.94 | 99.37 | 99.95 | 100.38 | 99.92 |
| (ppm) | | | | | |
| Ba | 252 | 354 | 422 | 913 | 543 |
| Cr | 35 | 12 | 56 | 2 | 53 |
| Zr | 136 | 139 | 170 | 144 | 133 |
| Sr | 263 | 275 | 364 | 327 | 294 |
| Rb | 7 | 28 | 35 | 127 | 129 |
| Y | 5 | 7 | 10 | 16 | 11 |
| Zn | 54 | 41 | 40 | 102 | 80 |
| Ni | 25 | 17 | 87 | 22 | 33 |
| S.G. | 2.77 | 2.74 | 2.76 | 2.77 | 2.78 |
| $(Al_2O_3/TiO_2)$ | 31.00 | 32.10 | 32.3 | 27.9 | 31.5 |

Table 3 : Chemical analyses of wallrocks about the Renabie gold-bearing quartz-muscovite-carbonate vein at the 914m (3100ft) level workings, Renabie Mine. (Traverse suite 125 → 129)

| Distance from quartz vein. | (m) | 2.5 | 1.9 | 1.4 | 0.5 | 0 |
|---|---|---|---|---|---|---|
| Sample number | | 125 | 126 | 127 | 128 | 129 |
| | (wt%) | | | | | |
| $SiO_2$ | | 70.68 | 69.86 | 71.63 | 68.81 | 71.12 |
| $Al_2O_3$ | | 14.37 | 14.85 | 14.83 | 13.84 | 14.76 |
| $Fe_2O_{3(T)}$ | | 1.95 | 1.96 | 2.03 | 2.14 | 1.69 |
| MgO | | 0.37 | 0.49 | 0.32 | 0.38 | 0.41 |
| CaO | | 2.25 | 2.48 | 2.38 | 2.61 | 0.63 |
| $Na_2O$ | | 4.92 | 4.86 | 4.68 | 3.49 | 3.53 |
| $K_2O$ | | 1.51 | 1.34 | 1.58 | 2.73 | 3.17 |
| $TiO_2$ | | 0.18 | 0.19 | 0.19 | 0.19 | 0.19 |
| $P_2O_5$ | | 0.04 | 0.02 | 0.02 | 0.03 | 0.07 |
| MnO | | 0.04 | 0.03 | 0.04 | 0.04 | 0.01 |
| S | | 0.02 | 0.0 | 0.01 | 0.05 | 0.05 |
| L.O.I | | 3.46 | 3.95 | 3.14 | 4.91 | 5.90 |
| TOTAL | | 99.89 | 100.93 | 100.95 | 99.38 | 101.65 |
| | (ppm) | | | | | |
| Ba | | 350 | 387 | 553 | 451 | 603 |
| Cr | | 23 | 8 | 23 | 25 | 40 |
| Zr | | 85 | 136 | 86 | 88 | 68 |
| Sr | | 341 | 376 | 313 | 217 | 271 |
| Rb | | 41 | 17 | 35 | 77 | 82 |
| Y | | 10 | 11 | 10 | 8 | 6 |
| Zn | | 3 | 16 | 36 | 42 | 39 |
| Ni | | 46 | 1 | 0 | 7 | 6 |
| S.G. | | 2.70 | 2.72 | 2.73 | 2.73 | 2.72 |
| $(Al_2O_3/TiO_2)$ | | 79.80 | 78.10 | 78.00 | 72.80 | 77.70 |

Table 4 : Chemical analyses of wallrocks about the Braminco No. 21 gold-bearing quartz-muscovite-carbonate vein, Braminco gold prospects, southeast of the Renabie mine. ( Traverse suite : 59 ⟶ 69 ).

| Distance from quartz vein. ( m ) | 2.5 | 2.1 | 1.9 | 1.6 | 1.4 | 1.1 | 0.5 | 0 |
|---|---|---|---|---|---|---|---|---|
| Sample number | 59 | 62 | 63 | 64 | 65 | 66 | 67 | 69 |
| (wt%) | | | | | | | | |
| $SiO_2$ | 72.51 | 70.32 | 70.37 | 71.04 | 68.69 | 67.51 | 72.09 | 75.18 |
| $Al_2O_3$ | 15.38 | 14.49 | 15.23 | 14.12 | 14.94 | 16.73 | 15.61 | 14.51 |
| $Fe_2O_{3(T)}$ | 2.27 | 2.42 | 2.37 | 2.17 | 2.50 | 2.90 | 2.50 | 2.56 |
| MgO | 0.58 | 0.63 | 0.60 | 0.62 | 0.58 | 0.54 | 0.62 | 0.40 |
| CaO | 2.50 | 2.49 | 2.46 | 2.64 | 2.88 | 0.92 | 1.22 | 0.77 |
| $Na_2O$ | 5.03 | 3.46 | 2.44 | 1.72 | 2.58 | 0.78 | 1.49 | 0.47 |
| $K_2O$ | 1.50 | 2.74 | 3.62 | 4.20 | 3.61 | 5.41 | 4.56 | 4.69 |
| $TiO_2$ | 0.27 | 0.25 | 0.26 | 0.24 | 0.26 | 0.29 | 0.26 | 0.25 |
| $P_2O_5$ | 0.01 | 0.01 | 0.02 | 0.02 | 0.02 | 0.10 | 0.06 | 0.08 |
| MnO | 0.04 | 0.04 | 0.04 | 0.05 | 0.05 | 0.02 | 0.03 | 0.02 |
| S | 0.00 | 0.07 | 0.18 | 0.25 | 0.03 | 0.03 | 0.07 | 0.05 |
| L.O.I. | 0.91 | 2.62 | 2.97 | 3.34 | 3.49 | 4.00 | 2.50 | 2.61 |
| TOTAL | 100.08 | 99.70 | 100.70 | 100.44 | 99.78 | 99.61 | 101.01 | 100.80 |
| (ppm) | | | | | | | | |
| Ba | 503 | 466 | 459 | 462 | 482 | 656 | 564 | 992 |
| Cr | 5 | 9 | 3 | 0 | 0 | 28 | 10 | 23 |
| Zr | 117 | 113 | 112 | 121 | 120 | 111 | 118 | 97 |
| Sr | 278 | 203 | 259 | 229 | 282 | 200 | 221 | 191 |
| Rb | 28 | 65 | 99 | 109 | 94 | 142 | 125 | 122 |
| Y | 0 | 4 | 6 | 5 | 7 | 9 | 4 | 6 |
| Zn | 29 | 47 | 63 | 52 | 40 | 65 | 50 | 62 |
| Ni | 14 | 13 | 12 | 15 | 2 | 0 | 1 | 0 |
| S.G. | 2.69 | 2.70 | 2.69 | 2.73 | 2.72 | 2.77 | 2.73 | 2.79 |
| $(Al_2O_3/TiO_2)$ | 56.90 | 57.90 | 58.50 | 58.80 | 57.50 | 57.70 | 60.00 | 58.40 |

Table 5 : Chemical analyses of wallrocks about the Campbell gold-bearing quartz-muscovite-carbonate vein, Braminco gold prospects, southeast of the Renabie mine. ( Traverse suite : 78⟶90 ).

| Distance from quartz vein. ( m ) | 4 | 2.5 | 1.8 | 1 | 0.5 | 0 |
|---|---|---|---|---|---|---|
| Sample number | 78 | 79 | 83 | 85 | 86 | 90 |
| (wt%) | | | | | | |
| $SiO_2$ | 54.46 | 38.74 | 55.23 | 59.66 | 54.75 | 50.17 |
| $Al_2O_3$ | 12.86 | 14.56 | 7.20 | 8.95 | 6.72 | 14.77 |
| $Fe_2O_3$(T) | 13.45 | 18.67 | 7.17 | 7.76 | 6.60 | 12.00 |
| MgO | 3.53 | 4.15 | 9.56 | 7.49 | 8.46 | 7.60 |
| CaO | 9.97 | 13.11 | 11.87 | 7.72 | 11.10 | 5.00 |
| $Na_2O$ | 2.68 | 1.93 | 2.41 | 1.93 | 1.95 | 1.49 |
| $K_2O$ | 0.50 | 2.21 | 2.56 | 3.86 | 2.59 | 2.68 |
| $TiO_2$ | 1.75 | 1.98 | 0.37 | 0.39 | 0.36 | 1.26 |
| $P_2O_5$ | 0.12 | 0.00 | 0.00 | 0.00 | 0.00 | 0.10 |
| MnO | 0.27 | 0.30 | 0.16 | 0.14 | 0.16 | 0.20 |
| S | 0.00 | 0.32 | 0.00 | 0.00 | 0.00 | 0.00 |
| L.O.I. | 0.30 | 3.87 | 4.10 | 2.70 | 6.81 | 2.40 |
| TOTAL | 99.89 | 99.84 | 100.63 | 100.60 | 99.86 | 99.87 |
| (ppm) | | | | | | |
| Ba | 57 | 468 | 143 | 284 | 308 | 140 |
| Cr | 42 | 60 | 360 | 183 | 281 | 287 |
| Zr | 154 | 134 | 64 | 284 | 45 | 101 |
| Sr | 330 | 349 | 257 | 258 | 197 | 115 |
| Rb | 0 | 43 | 0 | 13 | 16 | 8 |
| Y | 31 | 45 | 46 | 30 | 26 | 39 |
| Zn | 97 | 205 | 47 | 59 | 45 | 94 |
| Ni | 23 | 20 | 43 | 207 | 53 | 100 |
| S.G. | 3.20 | 2.89 | 2.86 | 2.74 | 2.81 | 2.85 |
| $(Al_2O_3/Y)$ | 0.41 | 0.32 | 0.28 | 0.30 | 0.28 | 0.38 |

equation demonstrates that chemical variations are linearly related to Fv's during metasomatism (Figures 11,12,13,14).

## 4.3 Redox State of Iron

A change in the redox state of iron ($Fe^{2+}/Fe_T$) is a sensitive indicator of fluid flow through rocks. In general, rocks are resistant to shifts in ($Fe^{2+}/Fe_T$) unless large volumes of fluid bearing reducing or oxidizing reactants such as $H_2$ or $O_2$ are present: (Kerrich et al.; 1977; Spooner et al, 1977, Studemeister, 1983).

Fluids originating at depths of up to 15 km are probably hot, reducing and $H_2$-bearing (Hawkes, 1980). The dominant hydrogen-generating reaction at depth is the dissociation of water in the presence of minerals with ferrous iron. According to Eugster and Skippen (1967), the buffer reaction for a basalt in equilibrium with water is as follows:

$$\underset{\text{Fayalite}}{3Fe_2SiO_4} + \underset{\text{Water}}{2H_2O} \longrightarrow \underset{\text{Magnetite}}{2Fe_3O_4} + \underset{\text{Quartz}}{3SiO_2} + \underset{\text{Hydrogen}}{2H_2}$$

The drastic reduction of primary ferric iron in wallrocks, as demonstrated by shifting of ($Fe^{2+}/Fe_T$) to higher values, implies extensive interaction with fluids

Figure 11 : Volume factor versus change in major element abundances for the transformation of gneissic trondhjemite to hydrothermally-altered schistose trondhjemite. ( Rock pair : 125 → 129 ).

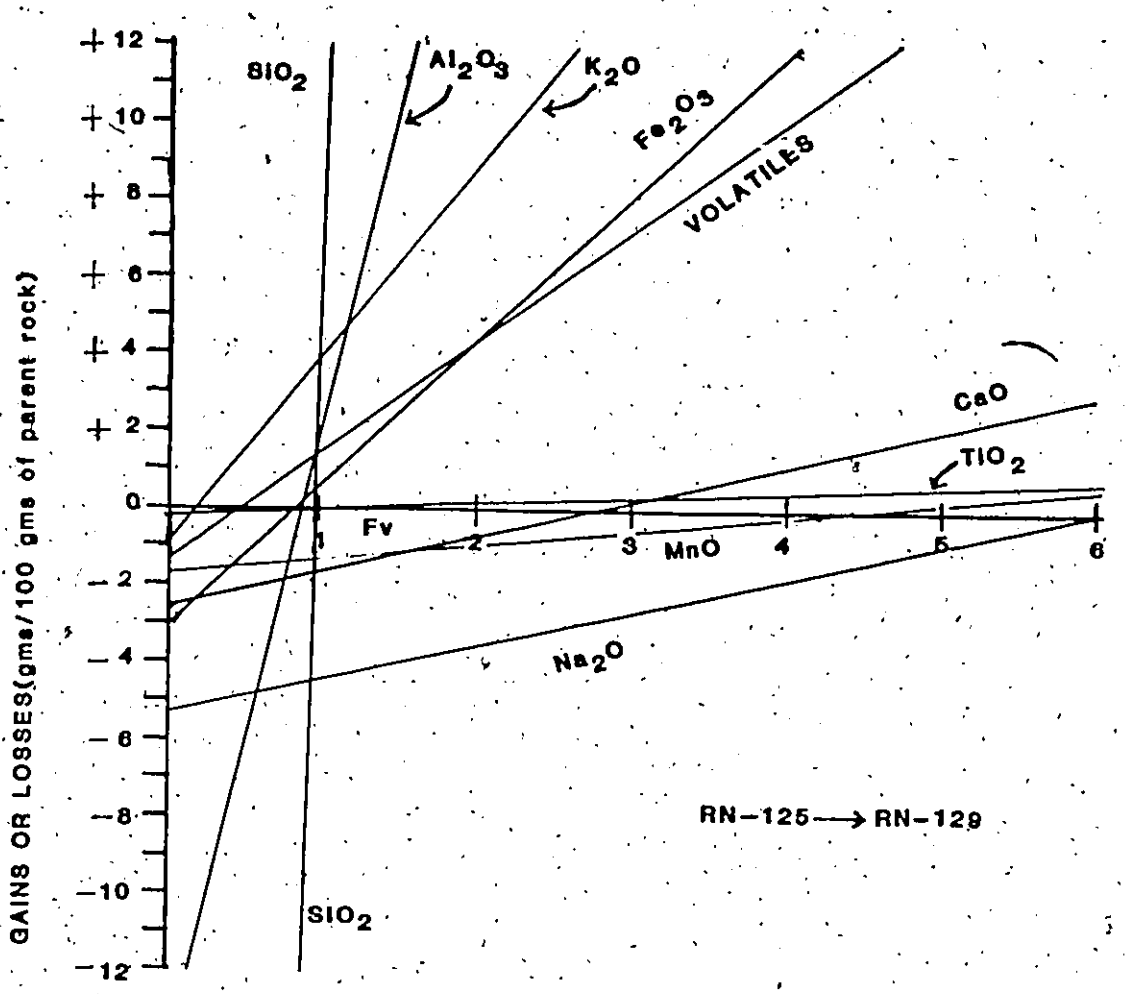

Figure 12 : Volume factor versus change in minor element abundances for the transformation of gneissic trondhjemite in hydrothermally-altered schistose trondhjemite. ( Rock pair : 125⟶129 ).

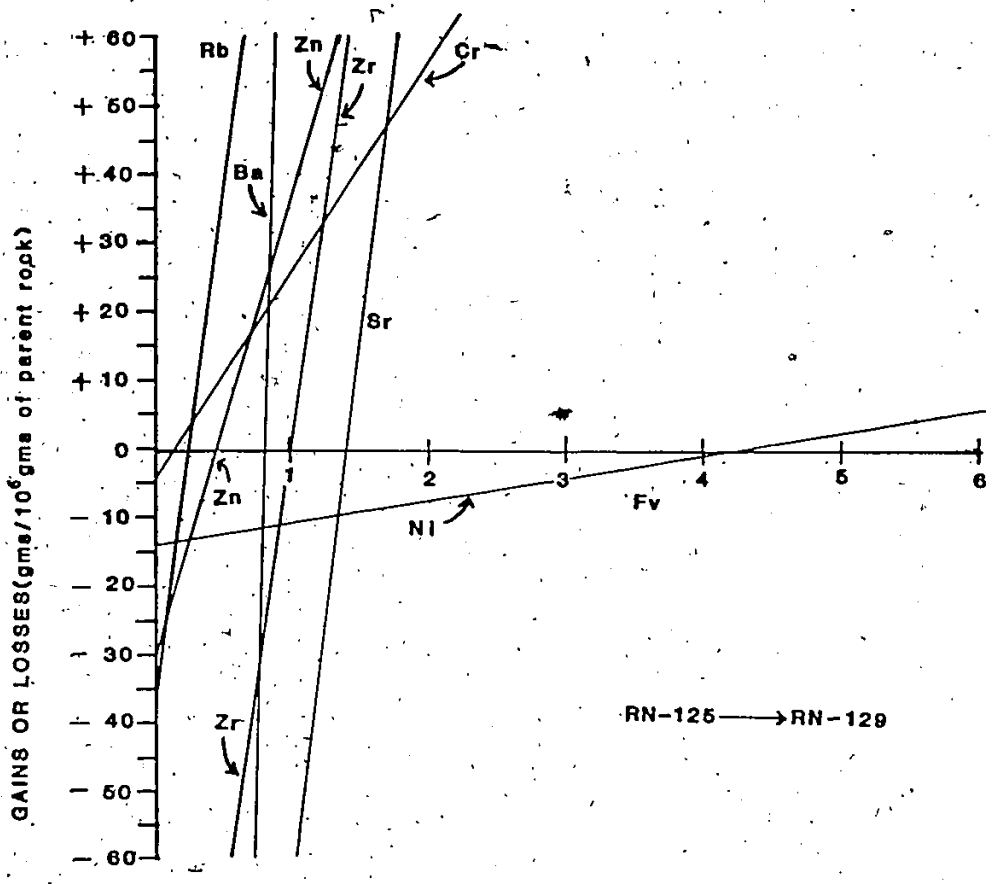

Figure 13 : Volume factor versus change in major element abundances for the transformation of gneissic trondhjemite to hydrothermally-altered schistose trondhjemite. ( Rock pair : 59 → 69 ).

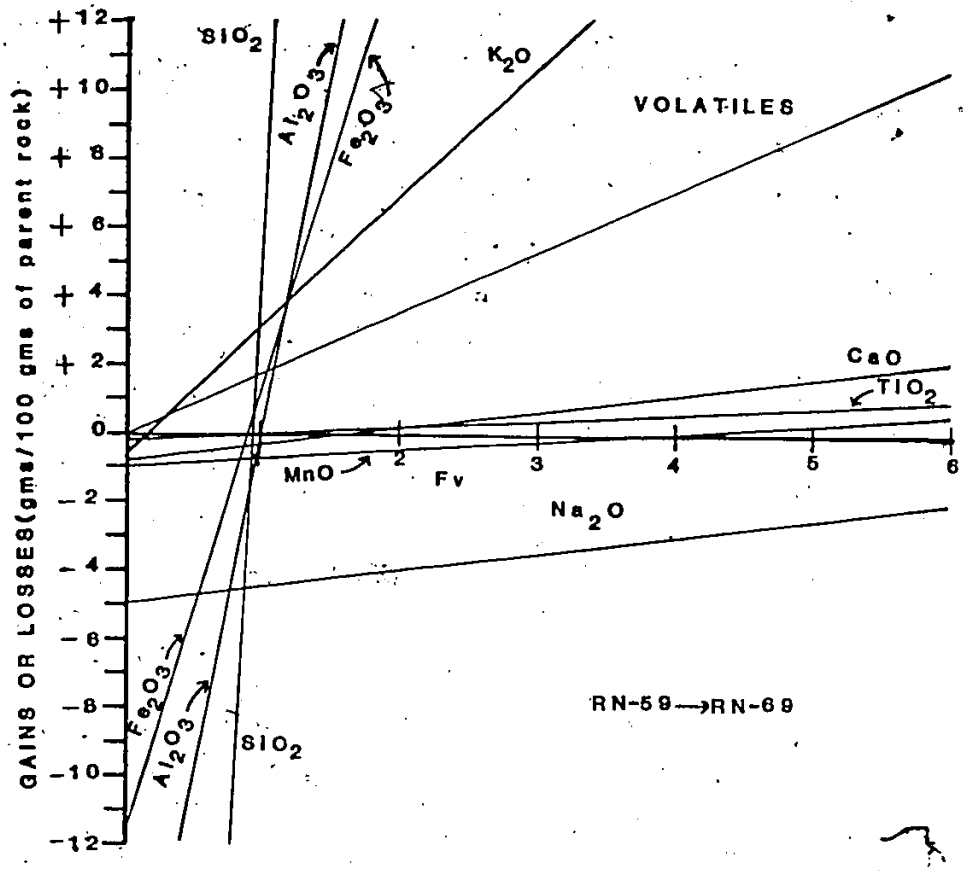

Figure 14 : Volume factor versus change in minor element abundances for the transformation of gneissic trondhjemite to hydrothermally-altered schistose trondhjemite. ( Rock pair : 59 → 69 ).

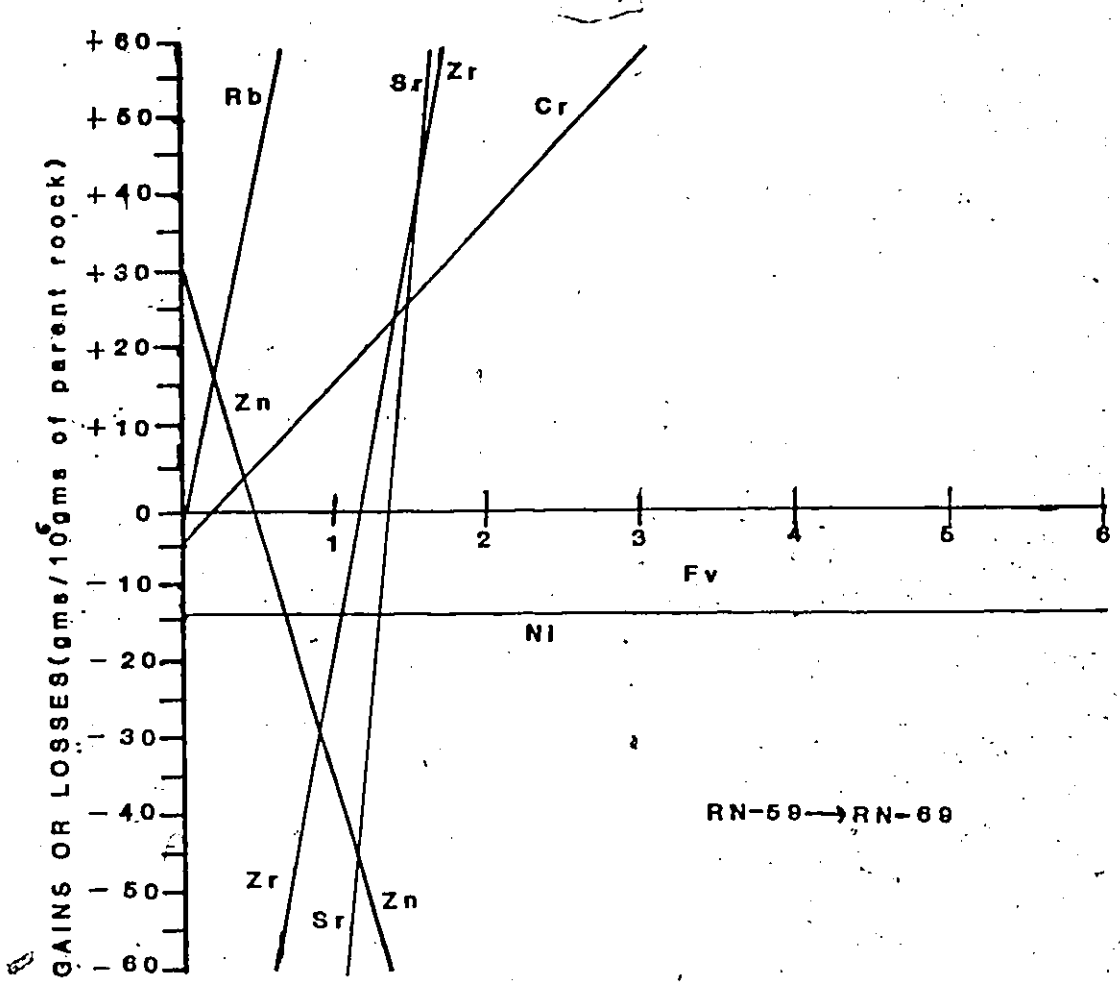

originating under high temperature reducing conditions (Kerrich et al., 1977; Studemeister, 1983). According to the same authors the reduction of ferric iron is due to hydrogen fixation and it can be approximated by the following reaction:

$$\underset{\text{Mineral}}{Fe_2O_3} + \underset{\text{Hydrogen}}{H_2} \longrightarrow \underset{\text{Mineral}}{2FeO} + \underset{\text{Water}}{H_2O}$$

Hydrogen fixation in wallrocks takes place in response to differences in equilibrium $H_2$ pressure at decreasing temperature-pressure states, as the fluids ascend through the crust.

Surface waters of Phanerozoic time in contact with the atmosphere are oxygenic. As these waters percolate or convect through the lithosphere $O_2$ and $SO_4^{-2}$ are consumed by oxidation of rocks. Spooner et al. (1977) attributed a lowering of $(Fe^{2+}/Fe_T)$ in metabasalts of an ophiolite succession to reaction with descending oxygenic seawater during ocean-floor hydrothermal metamorphism.

Thus, in hydrothermal systems, rocks reacting with hot ascending fluids are reduced as the water is cooled, whereas rocks in contact with descending cool fluids are oxidized as the water is heated. The latter conclusion may

not be applicable for Archean times, in light of different atmospheric conditions from those of the Phanerozoic earth.

## 4.4 Results

Gresen's equation of metasomatism was used in order to evaluate the changes in major and minor element distribution in the trondhjemitic (tonalitic) and amphibolitic wallrocks during the quartz - muscovite - carbonate - pyrite - albite - chlorite alteration.

Two sample traverses were in trondhjemitic, one in tonalitic, and one traverse was in amphibolitic wallrocks. Fresh parent rock samples were collected along each traverse at some distance beyond the halo of rocks that were visibly altered by the hydrothermal-mineralizing event.

Specimens from any one traverse in "granitic" rocks have relatively uniform $Al_2O_3/TiO_2$ ratio (Tables 2,3,4,5), suggesting isochemical behaviour for Al and Ti. The two elements are empirically known as immobile elements. In addition, composition volume diagrams have the component lines for Al and Ti crossing the axis of zero chemical change within a very narrow range of values (Figures 11,

13). The volume factor, Fv, used in mass balance calculations of "granitic" wallrocks was therefore an average of volume factors obtained by solving Gresens equation with $\Delta$ XAl = 0 and $\Delta$ XTi = 0 (Tables 6,7,8). For similar calculations carried out for the amphibolitic wallrock traverse, an average of volume factors for Al and Y was used (Table 9).

Results of calculations are plotted as chemical changes versus distance from vein. The gains or losses are expressed in gms/100 gms of parent rock for major elements, and in gms/$10^6$ gms of parent rock for minor elements. Integrating the area between zero chemical change and the extrapolated chemical change curve provides an estimate of the net change in element abundance. Consistent negative or positive net chemical changes for an element indicates, respectively, leaching or addition of the element in question.

The significant chemical changes in the composition of the "granitic" wallrocks (Figures 15,16,17 a,b) include:

1. Major gains in K, Rb, Ba, and volatiles ($H_2O$, $CO_2$, S).

2. Major loss in Na.

Table 6 : Volume factors, $F_v$, for the transformation of gneissic tonalite to hydrothermally-altered schistose tonalite in wallrocks about the Renabie gold-bearing quartz-muscovite-carbonate vein, at the eastern section of the "C" zone, Renabie mine. ( Traverse suite: 16⟶25 )

| ROCK PAIR: | 16⟶17 | 16⟶20 | 16⟶21 | 16⟶25 |
|---|---|---|---|---|
| | | $F_v$ | | |
| $SiO_2$ | 1.08 | 1.03 | 1.06 | 1.14 |
| $Al_2O_3$ | 1.14 | 1.04 | 1.11 | 1.04 |
| $Fe_2O_3$(T) | 1.24 | 1.14 | 1.21 | 1.05 |
| MgO | 1.40 | 1.30 | 1.15 | 0.90 |
| CaO | 1.25 | 1.16 | 1.08 | 0.88 |
| $Na_2O$ | 1.28 | 1.09 | 4.03 | 3.13 |
| $K_2O$ | 0.96 | 0.57 | 0.20 | 0.20 |
| $TiO_2$ | 1.15 | 1.08 | 2.00 | 1.05 |
| $P_2O_5$ | 0.79 | 0.60 | 3.00 | 0.85 |
| MnO | 1.48 | 1.29 | 0.89 | 0.89 |
| L.O.I. | 1.01 | 0.80 | 0.17 | 0.13 |
| Ba | 0.78 | 0.59 | 0.27 | 0.46 |
| Cr | 0.80 | 0.62 | 17.50 | 0.65 |
| Zr | 1.00 | 0.80 | 0.94 | 1.01 |
| Sr | 0.89 | 0.72 | 0.80 | 0.89 |
| Rb | 0.39 | 0.20 | 0.05 | 0.05 |
| Y | 0.55 | 0.50 | 0.31 | 0.45 |
| Zn | 1.51 | 1.35 | 0.52 | 6.72 |
| Ni | 0.45 | 0.28 | 1.13 | 0.75 |
| $\frac{(Al_2O_3+TiO_2)}{2}$ | 1.15 | 1.06 | 1.56 | 1.05 |

Table 7 : Volume factors, $F_v$, for the transformation of gneissic trondhjemite to hydrothermally-altered schistose trondhjemite in wallrocks about the Renabie gold-bearing quartz-muscovite-carbonate vein, at the 914m (3100 ft) level workings, Renabie mine.
( Traverse suite: 125 → 129 )

| ROCK PAIR: | 125 → 126 | 125 → 127 | 125 → 128 | 125 → 129 |
|---|---|---|---|---|
| | | $F_v$ | | |
| $SiO_2$ | 0.99 | 0.97 | 1.01 | 0.98 |
| $Al_2O_3$ | 0.99 | 0.95 | 1.02 | 0.96 |
| $Fe_2O_{3(T)}$ | 0.98 | 0.95 | 0.90 | 1.14 |
| MgO | 1.05 | 0.95 | 0.96 | 0.89 |
| CaO | 1.31 | 0.93 | 0.85 | 3.54 |
| $Na_2O$ | 1.01 | 1.13 | 1.39 | 1.38 |
| $K_2O$ | 0.78 | 0.79 | 0.54 | 0.47 |
| $TiO_2$ | 0.98 | 0.93 | 0.80 | 1.27 |
| $P_2O_5$ | 1.00 | 1.97 | 1.31 | 0.56 |
| MnO | 1.25 | 0.98 | 0.98 | 3.97 |
| L.O.I. | 0.88 | 1.09 | 0.70 | 0.58 |
| Ba | 0.70 | 0.62 | 0.76 | 0.57 |
| Cr | 0.60 | 0.98 | 0.90 | 0.57 |
| Zr | 1.01 | 0.98 | 0.95 | 1.24 |
| Sr | 0.88 | 0.92 | 1.55 | 1.24 |
| Rb | 0.67 | 0.90 | 0.52 | 0.49 |
| Y | 1.01 | 0.98 | 1.23 | 1.65 |
| Zn | 0.89 | 1.26 | 0.98 | 1.17 |
| Ni | 0.50 | 0.58 | 0.42 | 0.49 |
| $\frac{(Al_2O_3+TiO_2)}{2}$ | 0.99 | 0.94 | 0.91 | 1.12 |

Table 8 : Volume factors, Fv, for the transformation of gneissic trondhjemite to hydrothermally-altered schistose trondhjemite in wallrocks about the Braminco gold-bearing quartz-muscovite-carbonate vein, Braminco gold prospects, southeast of the Renabie mine. ( Traverse suite: 59 → 69 )

| ROCK PAIR: | 59→62 | 59→63 | 59→64 | 59→65 | 59→66 | 59→67 | 59→69 |
|---|---|---|---|---|---|---|---|
| | | | | $F_v$ | | | |
| $SiO_2$ | 1.03 | 1.03 | 0.99 | 1.04 | 1.04 | 0.98 | 0.92 |
| $TiO_2$ | 0.84 | 0.84 | 0.83 | 0.78 | 0.74 | 0.86 | 0.88 |
| $Al_2O_3$ | 1.06 | 1.01 | 0.99 | 1.02 | 0.88 | 0.95 | 1.02 |
| $Fe_2O_3$(T) | 0.95 | 0.95 | 0.90 | 0.90 | 0.80 | 0.90 | 0.86 |
| MnO | 0.99 | 1.00 | 0.78 | 1.97 | 1.94 | 1.31 | 1.92 |
| MgO | 0.99 | 0.98 | 0.98 | 0.98 | 0.95 | 0.98 | 1.44 |
| CaO | 0.99 | 0.90 | 0.85 | 0.85 | 2.63 | 1.75 | 3.13 |
| $K_2O$ | 0.55 | 0.41 | 0.35 | 0.41 | 0.26 | 0.32 | 0.30 |
| $Na_2O$ | 1.42 | 2.08 | 2.89 | 1.90 | 6.22 | 3.28 | 10.25 |
| $P_2O_5$ | 0.99 | 0.50 | 0.49 | 0.50 | 0.09 | 0.16 | 0.12 |
| L.O.I | 0.36 | 0.32 | 0.28 | 0.27 | 8.31 | 0.37 | 1.11 |
| Ba | 1.07 | 1.09 | 1.07 | 1.03 | 0.77 | 0.87 | 0.00 |
| Cr | 0.55 | 1.66 | 0.00 | 6.92 | 0.16 | 0.49 | 0.20 |
| Zr | 1.03 | 1.04 | 0.95 | 1.03 | 0.97 | 0.97 | 0.48 |
| Sr | 1.36 | 1.07 | 1.19 | 0.96 | 1.37 | 1.23 | 1.16 |
| Rb | 0.42 | 0.28 | 0.25 | 0.97 | 0.19 | 0.22 | 1.40 |
| Zn | 0.61 | 0.46 | 0.55 | 0.29 | 0.43 | 0.57 | 0.22 |
| Ni | 1.07 | 1.16 | 0.92 | 0.71 | 4.53 | 13.79 | 0.45 |
| $\frac{(Al_2O_3 + TiO_2)}{2}$ | 0.96 | 0.93 | 0.91 | 0.90 | 0.81 | 0.91 | 0.95 |

Table 9 : Volume factors, $F_v$, for the transformation of foliated metabasalt to hydrothermally-altered chloritic schist in wallrocks about the Campbell gold-bearing quartz-carbonate vein, Braminco gold prospects, southwest of the Renabie mine. ( Traverse suite: 78 → 90 ).

| ROCK PAIR: | 78 → 79 | 78 → 83 | 78 → 85 | 78 → 86 | 78 → 90 |
|---|---|---|---|---|---|
| | | | $F_v$ | | |
| $SiO_2$ | 1.55 | 1.10 | 1.05 | 1.13 | 1.16 |
| $Al_2O_3$ | 0.97 | 1.99 | 1.67 | 2.17 | 0.97 |
| $Fe_2O_{3(T)}$ | 0.79 | 2.09 | 2.02 | 2.32 | 1.07 |
| MgO | 0.94 | 0.34 | 0.55 | 0.47 | 0.52 |
| CaO | 0.84 | 0.93 | 1.50 | 0.86 | 2.23 |
| $Na_2O$ | 1.53 | 1.24 | 0.79 | 1.56 | 0.64 |
| $K_2O$ | 0.15 | 0.50 | 0.40 | 0.35 | 0.49 |
| $TiO_2$ | 0.97 | 5.29 | 5.24 | 5.53 | 1.55 |
| $P_2O_5$ | - | - | - | - | 1.34 |
| MnO | 0.99 | 1.88 | 2.25 | 1.92 | 1.51 |
| L.O.I. | 0.09 | 0.27 | 0.13 | 0.05 | 0.46 |
| Ba | 0.13 | 0.44 | 0.23 | 0.21 | 0.45 |
| Cr | 0.77 | 0.13 | 0.26 | 0.17 | 0.16 |
| Zr | 1.27 | 2.69 | 0.63 | 3.89 | 1.71 |
| Sr | 1.04 | 1.44 | 1.49 | 1.90 | 3.22 |
| Rb | 0.00 | 0.00 | 0.00 | 0.00 | 0.00 |
| Y | 0.76 | 1.99 | 1.90 | 1.96 | 1.51 |
| Zn | 0.52 | 2.30 | 1.92 | 2.45 | 1.15 |
| Ni | 1.27 | 0.59 | 0.12 | 0.49 | 0.25 |
| $\frac{(Al_2O_3+Y)}{2}$ | 0.97 | 1.99 | 1.78 | 2.06 | 1.24 |

Figure 15A : Changes in major element abundances in wallrocks about the Renabie gold-bearing quartz-muscovite-carbonate vein in the eastern section of the "C" zone, Renabie mine. ( Traverse suite : 16 25 ).

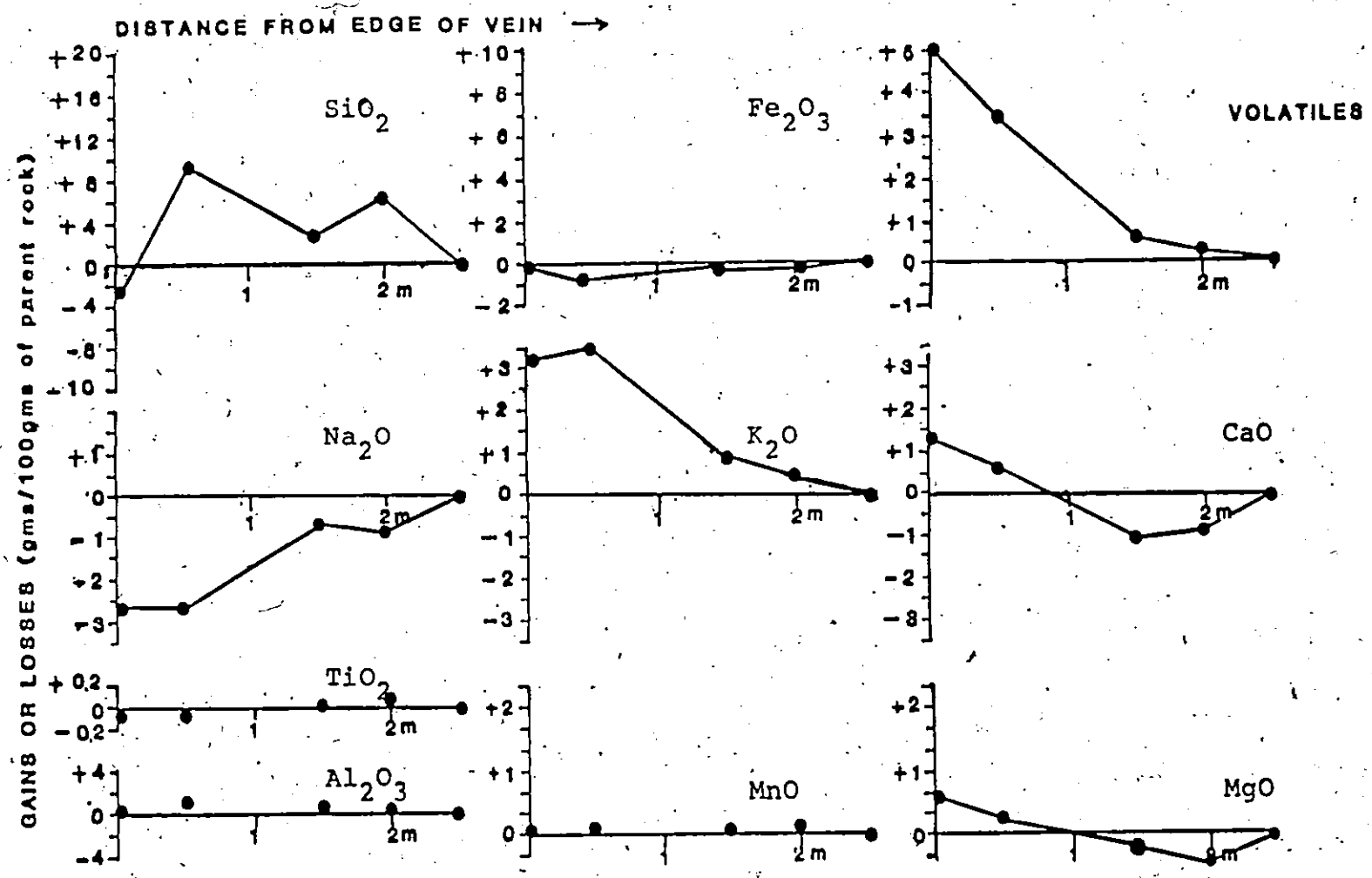

Figure 15B : Changes in minor element abundances in wallrocks about the Renabie gold-bearing quartz-muscoyite-carbonate vein in the eastern section of the "C" zone, Renabie mine. ( Traverse suite : 16 25 ).

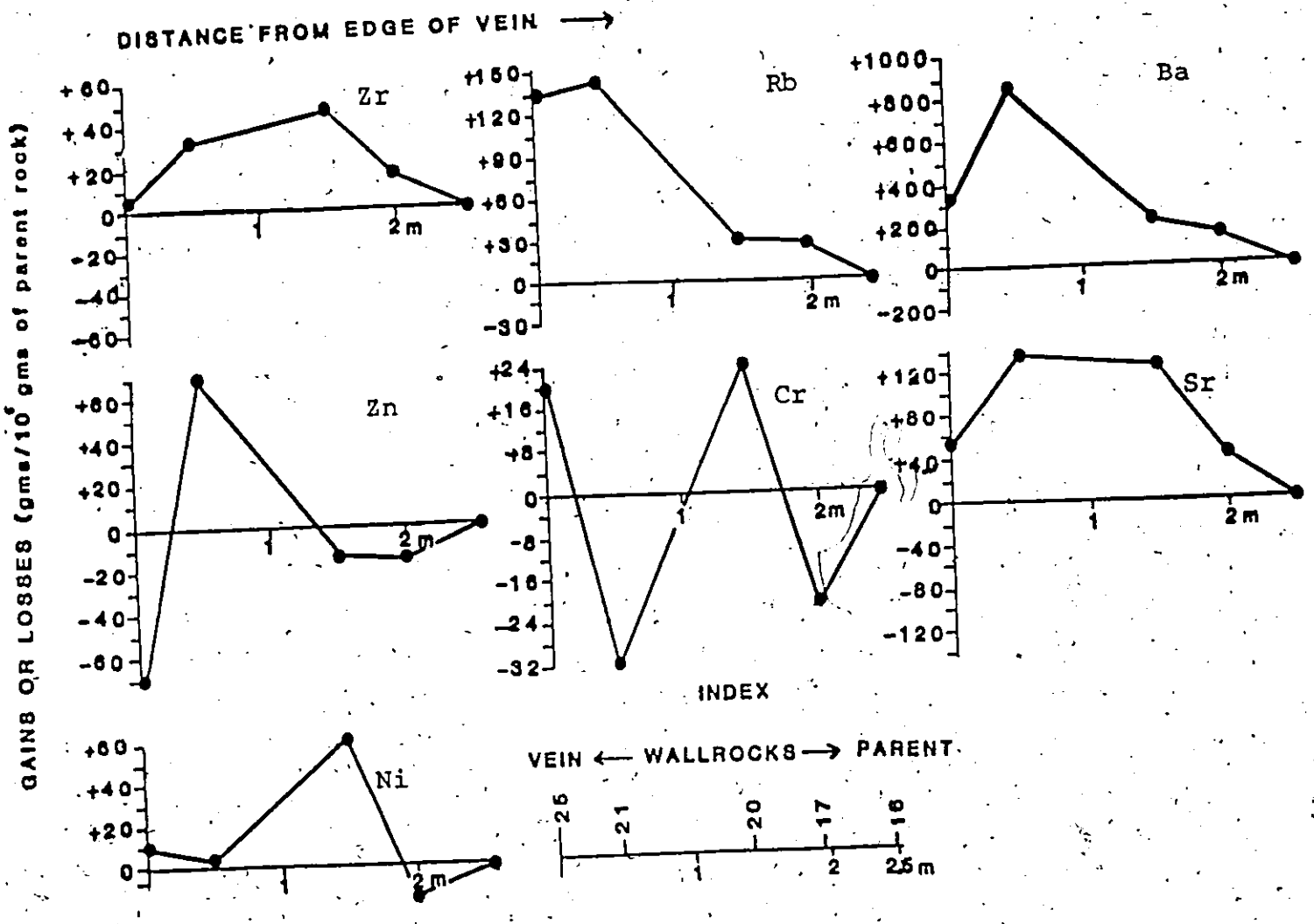

Figure 16A : Changes in major element abundances in wallrocks about the Renabie Gold-bearing quartz-muscovite-carbonate vein at the 914m (3100ft) level workings, Renabie mine. ( Traverse suite : 125 → 129 ).

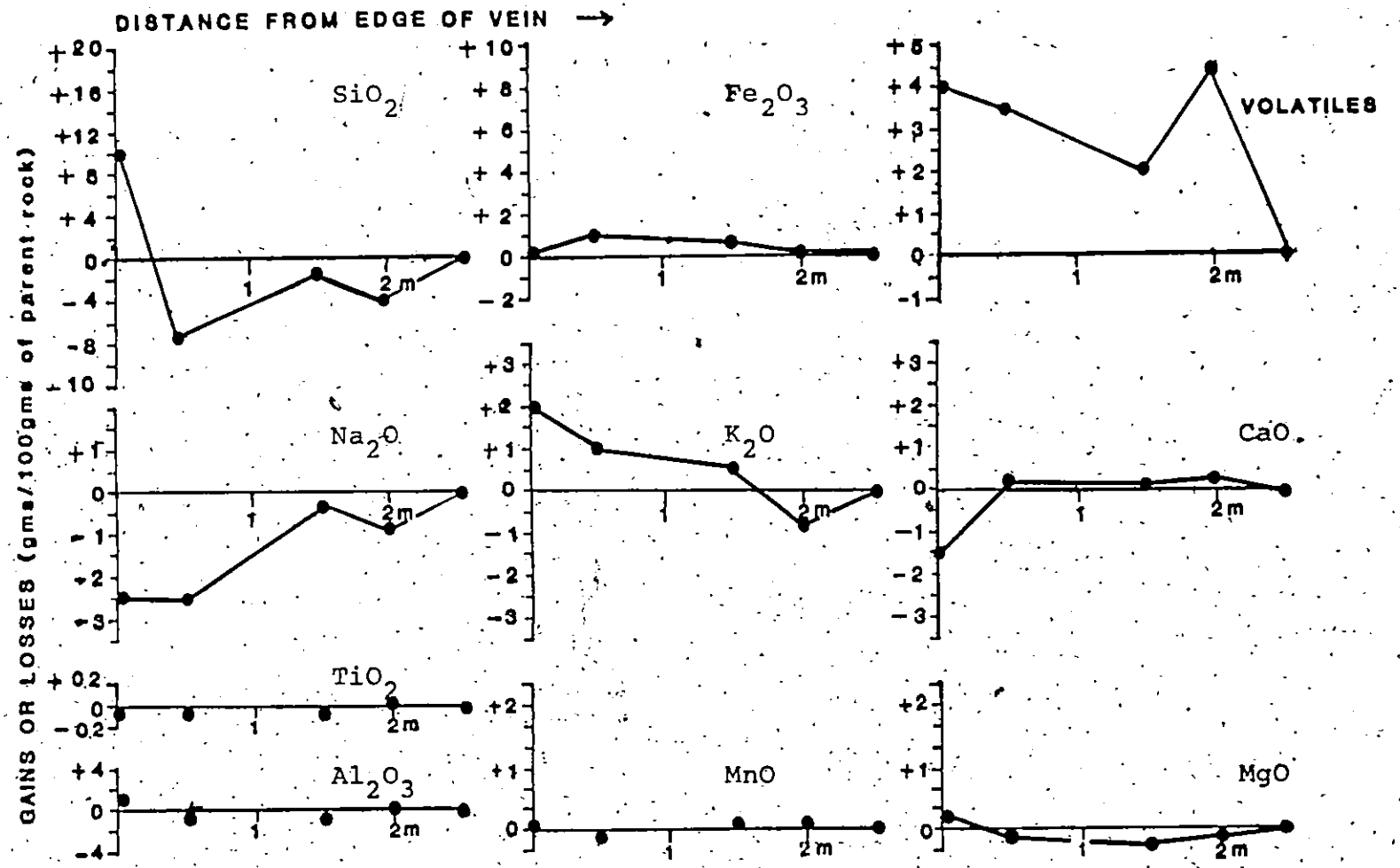

Figure 16B : Changes in minor element abundances in wallrocks about the Renabie gold-bearing quartz-muscovite-carbonate vein at the 914m (3100ft) level workings, Renabie mine. ( Traverse suite : 125→129 ).

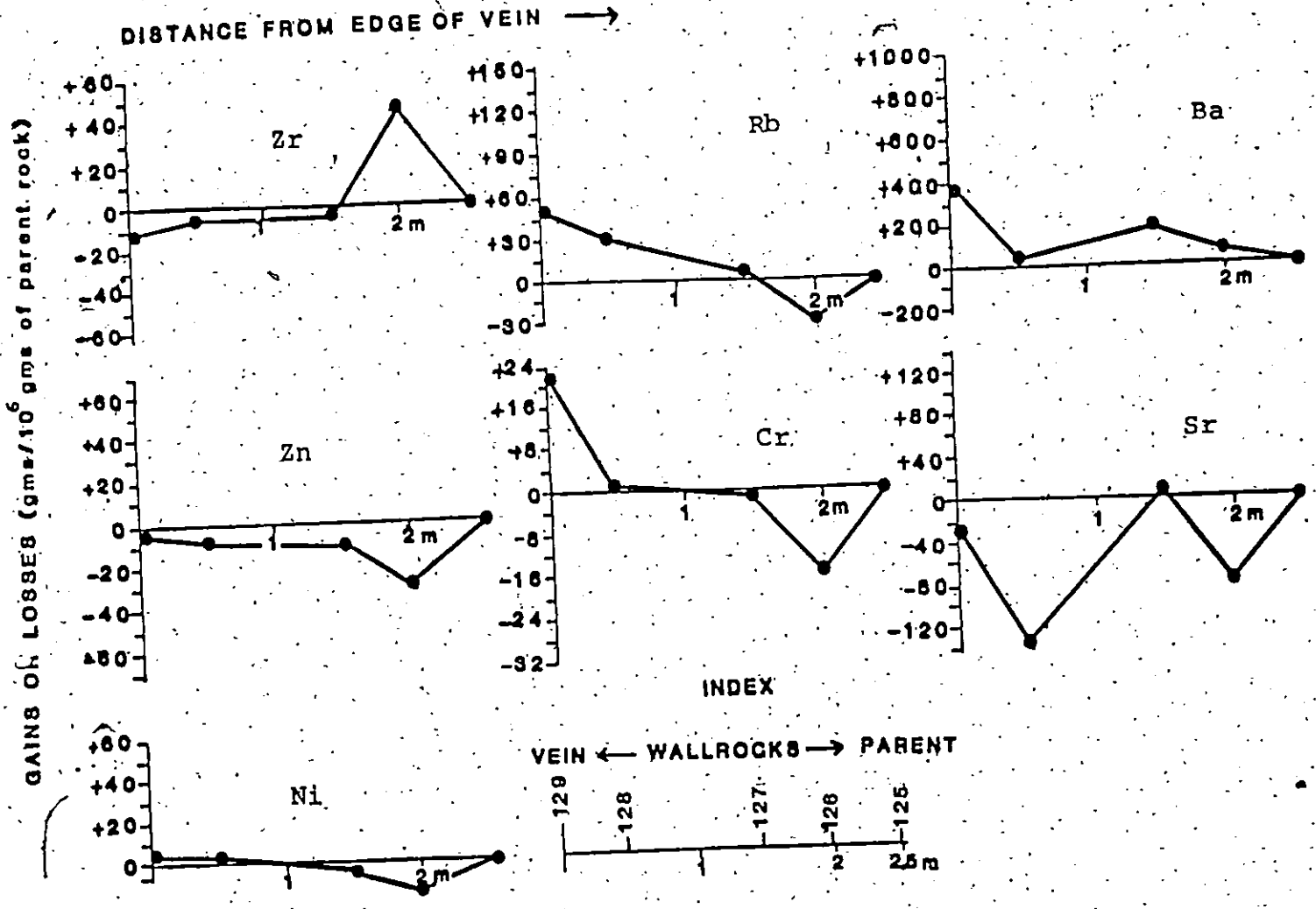

Figure 17A : Changes in major element abundances in wallrocks about the Braminco No. 21 gold-bearing quartz-muscovite-carbonate vein, Braminco gold prospects, southeast of the Renabie mine. ( Traverse suite : 59→69 ).

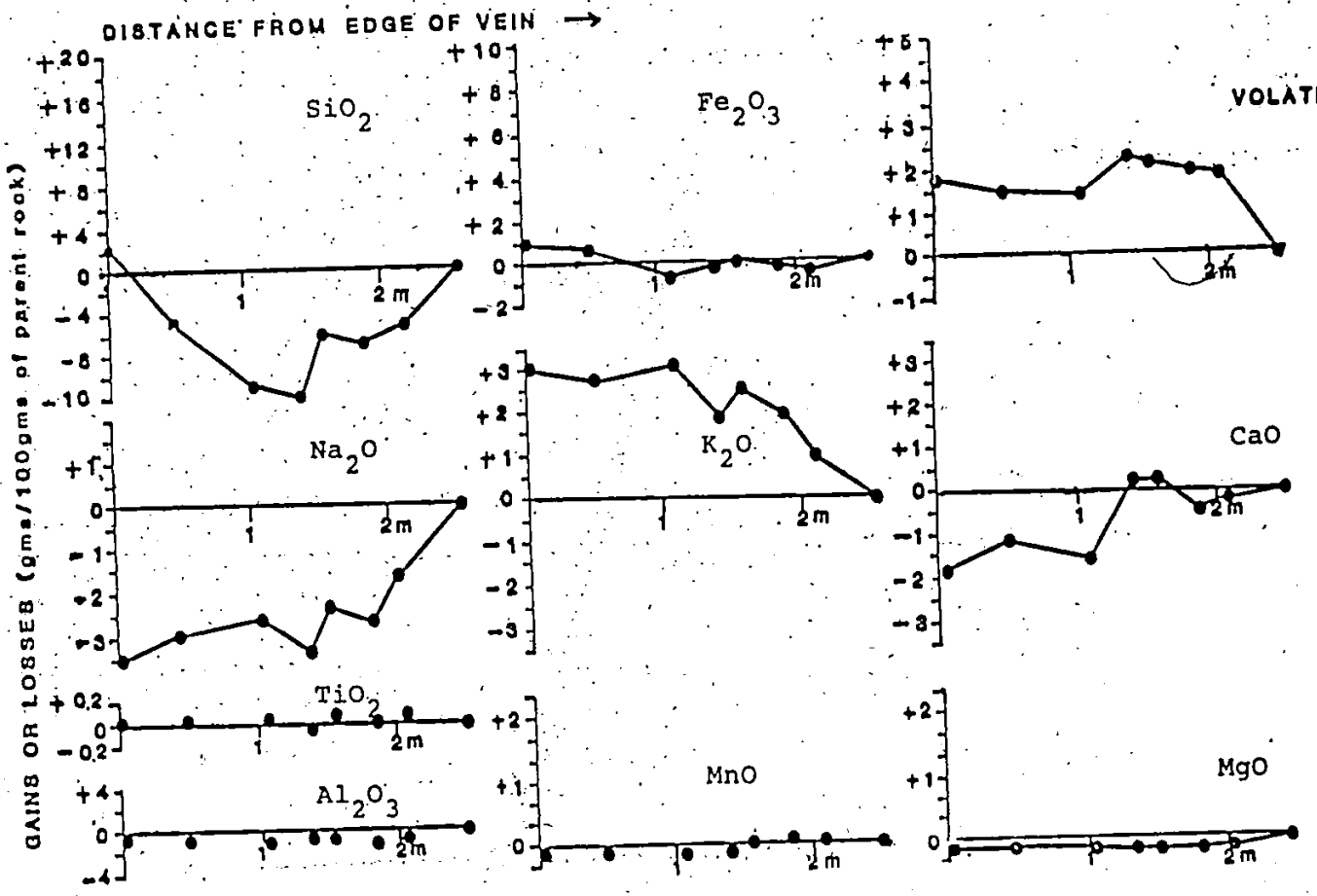

Figure 17B : Changes in minor element abundances in wallrocks about the Braminco No. 21 gold-bearing quartz-muscovite-carbonate vein, Braminco gold prospects, southeast of the Renabie mine. ( Traverse suite : 59→69 ).

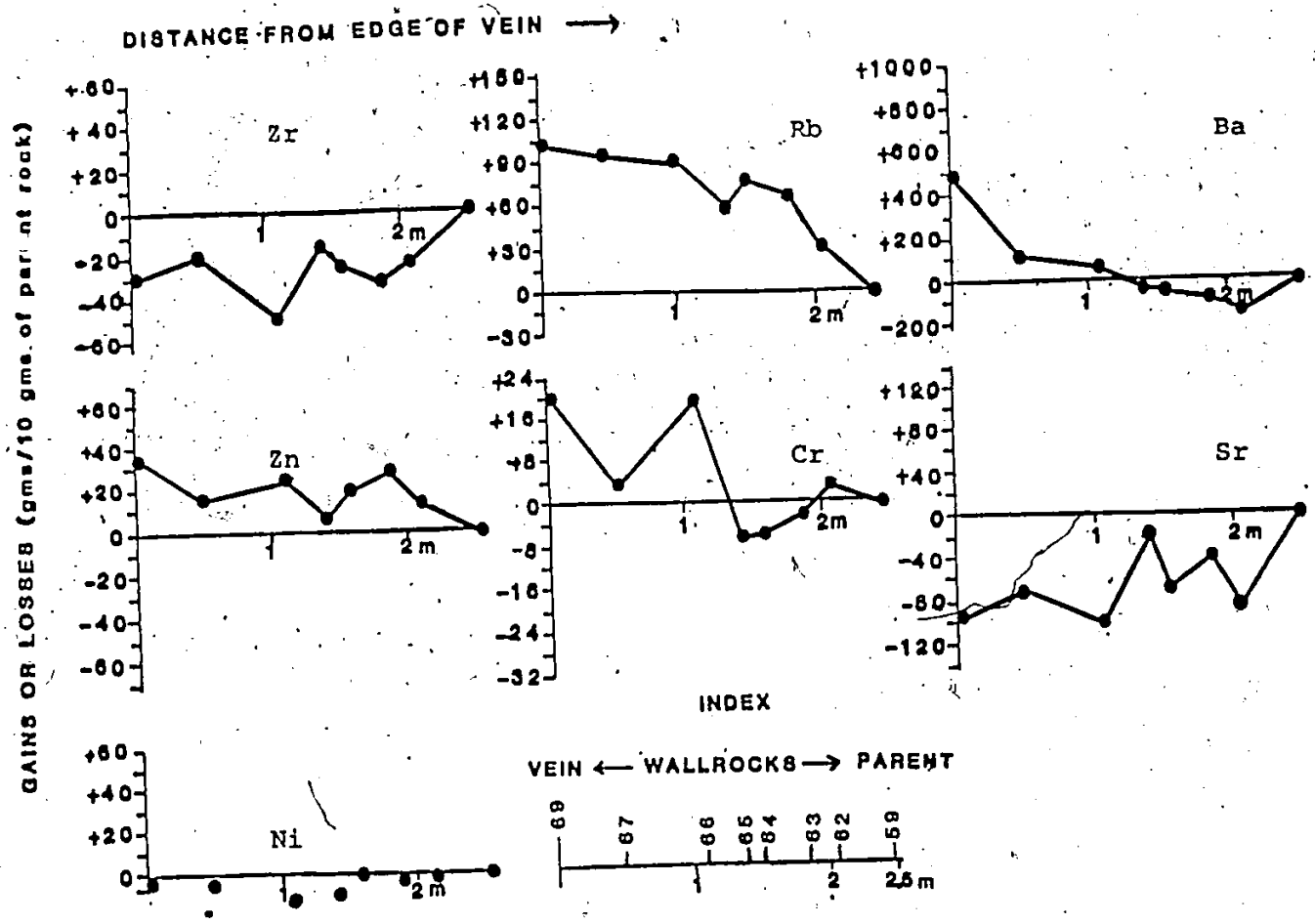

In some wallrock sections Ca is quantitatively leached, whereas in others this element is added, suggesting local leaching and then precipitation elsewhere as carbonate minerals.

The trends for most other elements are not consistent between suites, suggesting that changes in these elements are locally controlled.

The significant changes in composition of amphibolitic wallrocks (Figure 18 a,b) are:

1. Major gains in Si, K, Mg and volatiles.

2. Major loss in Na; Fe appears to have been leached from the outer zone of the alteration envelope and precipitated adjacent to the vein.

Changes in the abundance of other elements are insignificant.

The redox state of iron was determined for mineral fractions of "granitic" wallrocks collected in the same manner as for mass balance calculations, using the modified Wilson (1955) cold acid decomposition method (APPENDIX 5).

Figure 18A : Change in major element abundances in wallrocks about the Campbell gold-bearing quartz-muscovite-carbonate vein, Braminco gold prospects southwest of the Renabie mine. ( Traverse suite : 78 90 )A

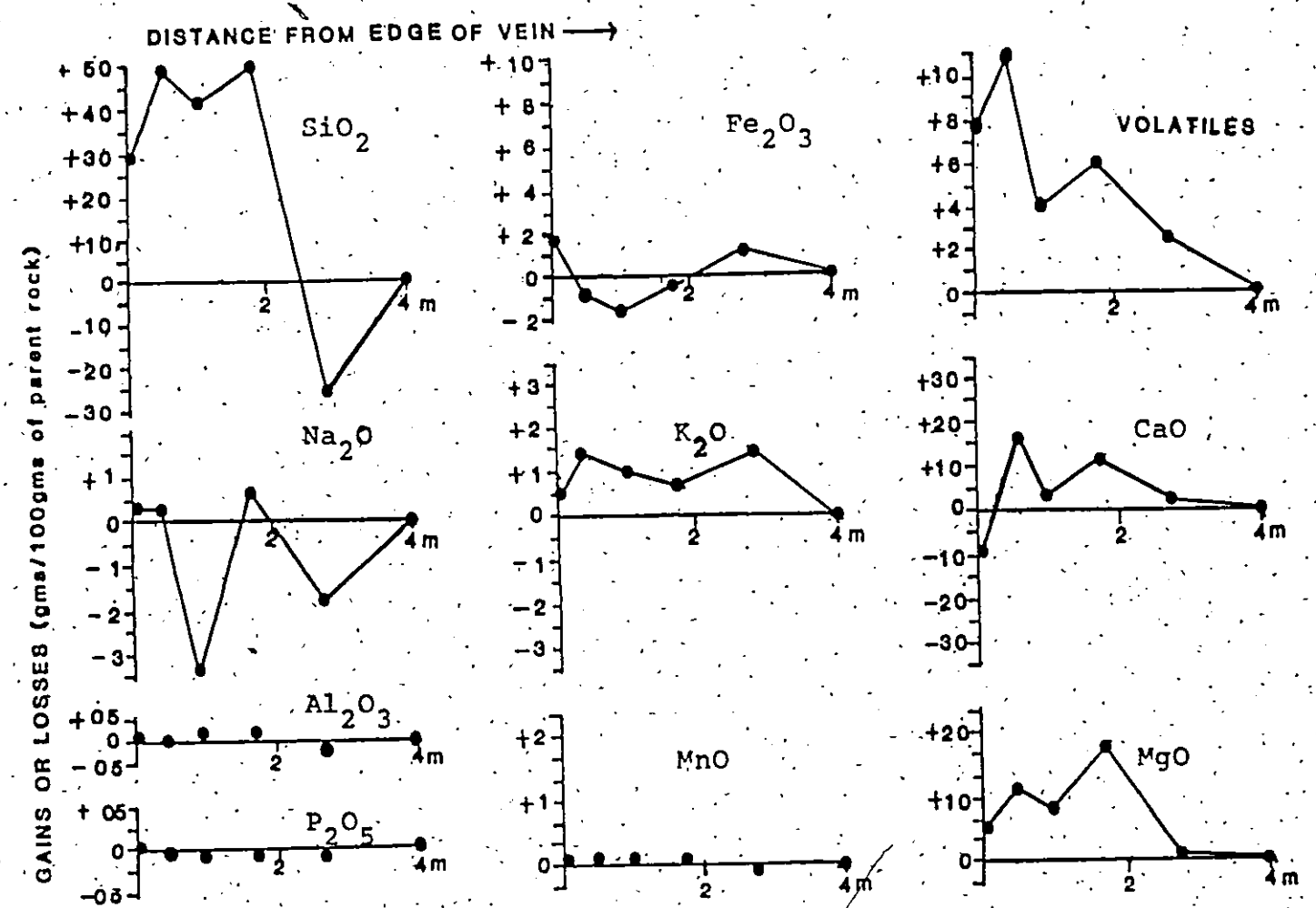

Figure 18B : Changes in minor element abundances in wallrocks about the Campbell gold-bearing quartz-muscovite-carbonate vein, Braminco gold prospects, southwest of the Renabie mine. ( Traverse suite : 78 90 ).

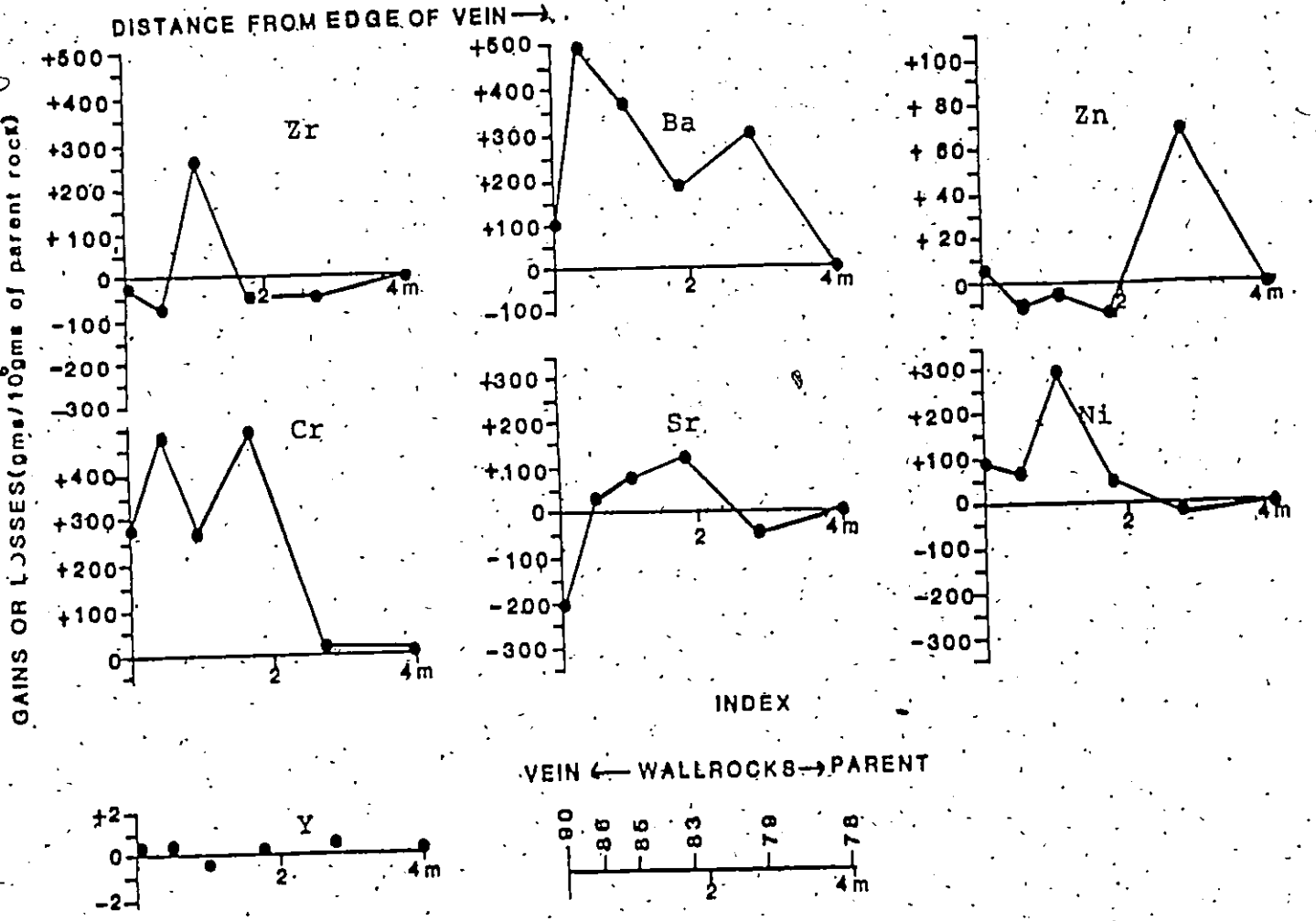

Results of the determinations of the redox state of iron are plotted against distance from the vein (Figures 19,20,21). In all three traverses there is an overall trend towards higher ($Fe^{2+}/Fe_T$) in rocks that have been significantly hydrothermally altered.

Figure 19 : Redox state of iron, ($Fe^{2+}/Fe_T$), in wallrocks about the Renabie gold-bearing quartz-muscovite-carbonate vein in the eastern section of the "C" zone, Renabie mine. ( Traverse suite : 16 - 25 ).

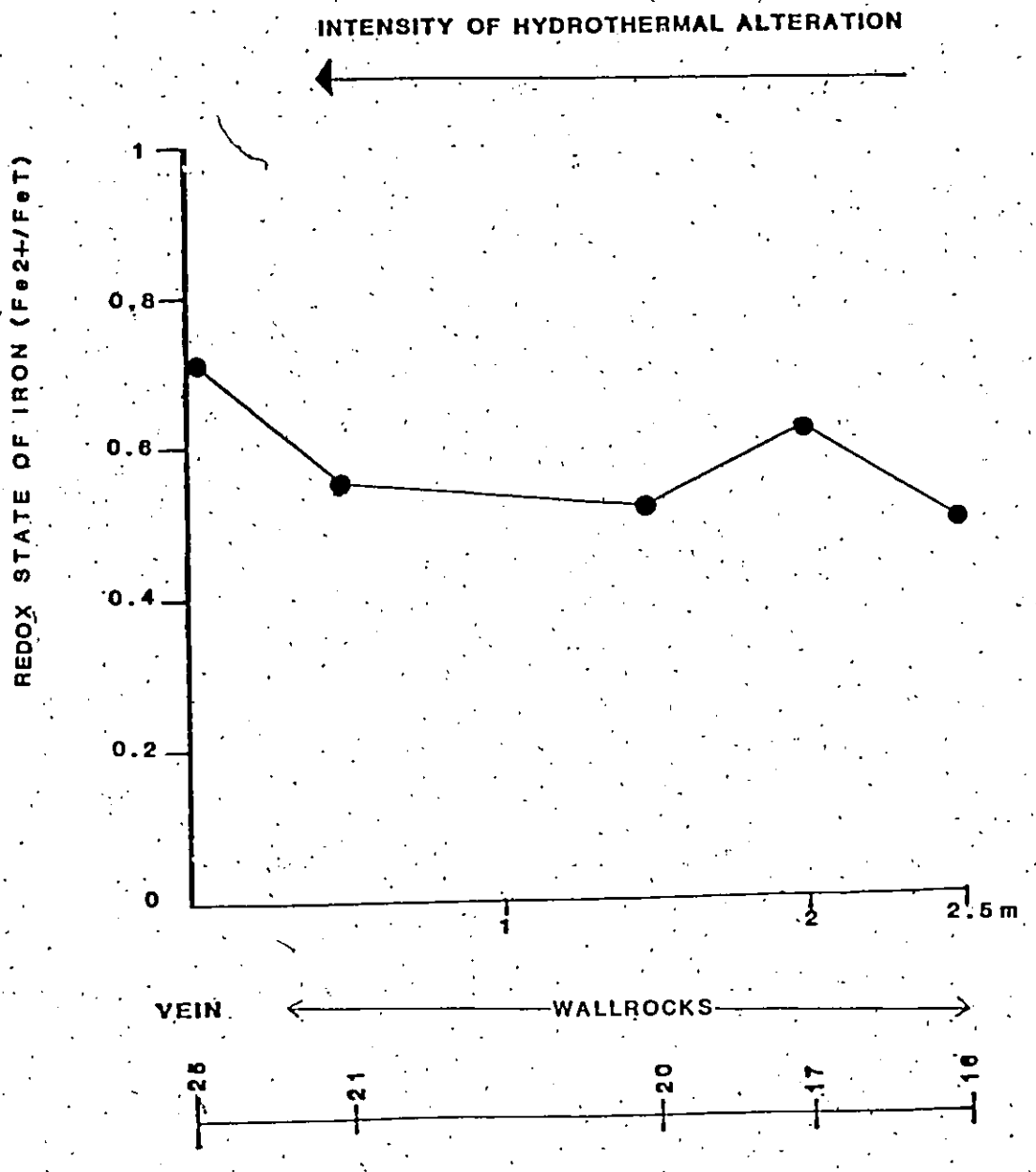

Figure 20 : Redox state of iron, ($Fe^{2+}/Fe_T$), in wallrocks about the Renabie gold-bearing quartz-muscovite-carbonate vein at the 914m (3100ft) level workings, Renabie mine. ( Traverse suite: 125-129 ).

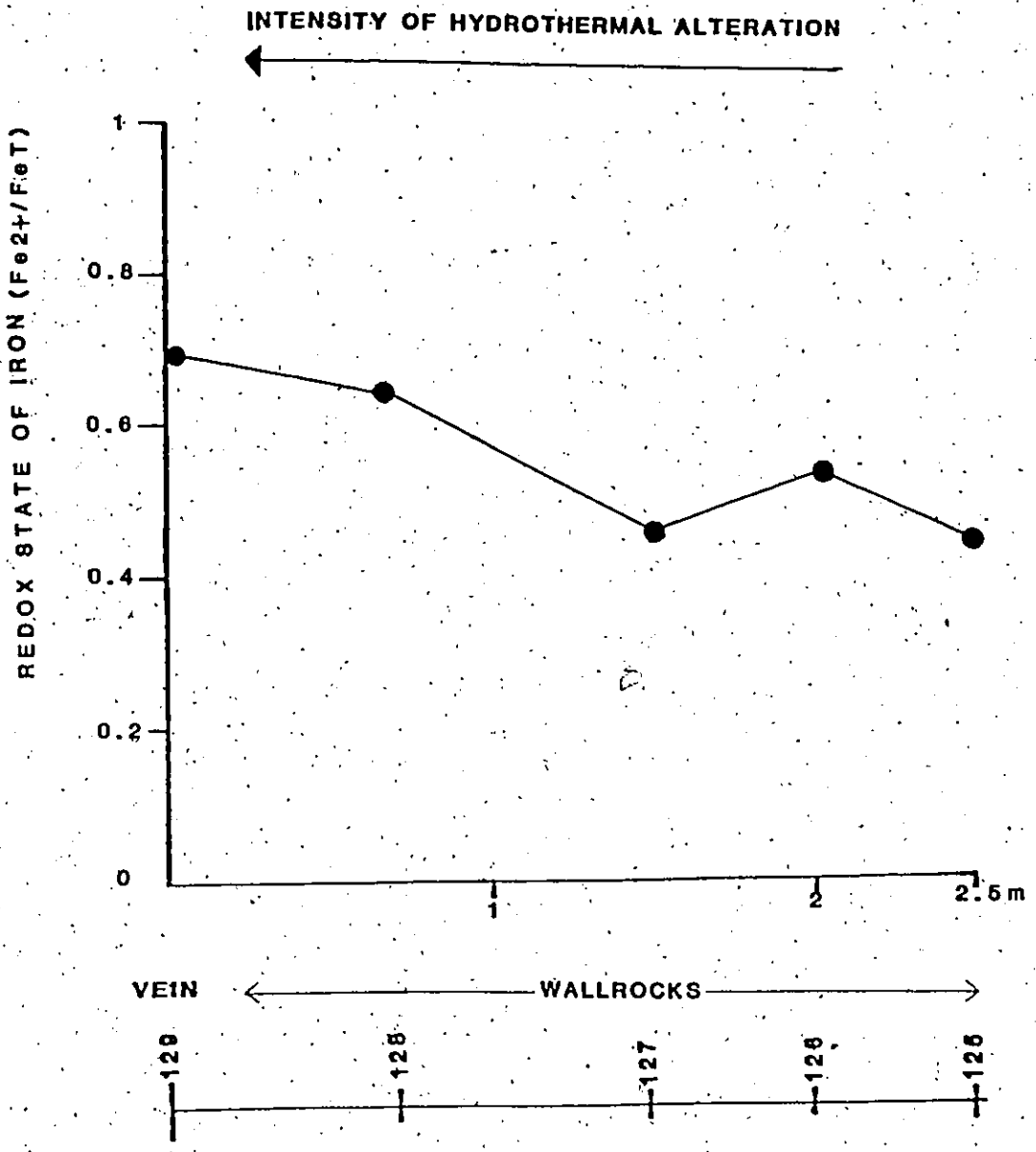

Figure 21 : Redox state of iron in wallrocks about the Braminco No. 21 gold bearing quartz-muscovite-carbonate vein, Braminco gold prospects, southeast of the Renabie mine. ( Traverse suite: 59 - 69 ).

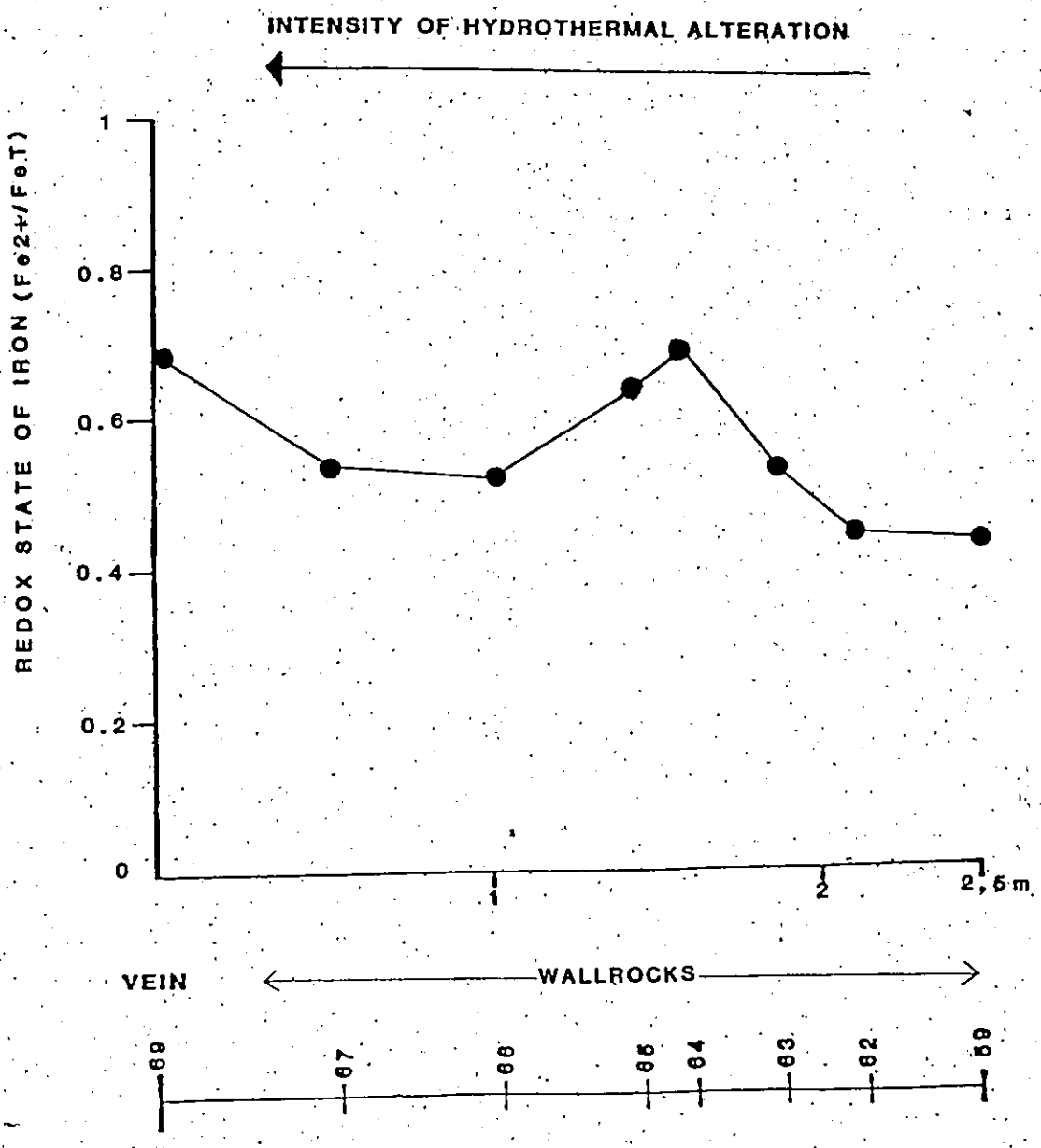

# CHAPTER 5

## 5. FLUID INCLUSION AND OXYGEN ISOTOPIC DATA

### 5.1 General Statement

The purpose of this chapter is to provide estimates of the temperature, density and composition of the hydrothermal fluids responsible for gold deposition and alteration of wallrocks about gold-bearing quartz veins, as well as to provide evidence regarding their source.

### 5.2 Fluid Inclusion Investigation

#### 5.2.1 Background

The application of fluid inclusion investigations to geological problems has been the subject of numerous studies since the middle nineteenth century (Sorby, 1858; Smith, 1953). Fluid inclusion examination began with the search for the composition of ore-forming fluids and the conditions of genesis of mineral deposits. Today fluid inclusion work, excellent reviews of which are given by Roedder ( 1972, 1979, 1981) has become an important tool in geochemical

exploration. Unless otherwise noted the following discussion is based on Roedder's summaries.

When a mineral grows or recrystallizes in a fluid medium, any process that hinders the growth of perfect crystals may result in the trapping of small portions of the fluid within the crystal. If this fluid is trapped during the formation of the enclosing crystal, the result is a primary fluid inclusion. Secondary inclusions form when later and entirely different fluids become trapped in cracks during fracturing or recrystallization. A fluid inclusion which becomes sealed off in a healing fracture before complete formation of the hosting crystal is called pseudosecondary.

Thus, fluid inclusions represent microscopic samples of fluids associated with the geological history of the hosting crystal.

Distinction of types of fluid inclusions is of fundamental importance. This is because the time elapsed between the trapping of primary and secondary inclusions, sometimes millions of years, may result in inclusions of extremely different compositions and P-T histories. Unfortunately, the inclusion's origin

cannot always be inferred with certainty because of lack of genetic information. The most important suggestive criteria for assigning a primary origin is the absence of any planar arrangement. Primary inclusions can be reliably identified if they can be related to growth phenomena. Secondary inclusions usually mark healed fractures, are small in size, on the order of a few microns ($\mu$), and exhibit divergent behaviour during heating or freezing runs, in relation to nearby primary inclusions. Pseudosecondary inclusions are in many cases associated with fractures or dislocation surfaces that can be traced to an abrupt ending within the crystal.

Of importance in the application of fluid inclusion research, is whether necking down or leakage has occurred. Necking down is the process during which large inclusions split into a series of smaller ones.

If several liquid and/or gas phases have been equilibrated in the original inclusion, the resulting inclusions will exhibit varying phase ratios and a spread of microthermometric data. Choosing isolated inclusions to work on would eliminate inclusions that might have necked down. Leakage is the non-isochemical addition or removal of inclusion

material between trapping and experiment. Some inclusions have been shown to have leaked under conditions that do not represent those of nature. The systematic variation of results from fluid inclusion studies of zoned single crystals (Roedder, 1963) and the demonstrated endurance of $CO_2$-rich inclusions to severe internal pressure at high temperatures (Roedder, 1965), constitute the greatest evidence against significance leakage.

The trapped fluid may be homogeneous, carry solid particles in suspension, or be composed of two or more immiscible components or have a gas phase (i.e. "boiling" fluid). Water, with rare exceptions, is the dominant constituent. The total dissolved salt content is usually expressed in terms of "equivalent weight percent NaCl" and is referred to as "salinity".

After trapping, the inclusion follows a cooling and presumably isochoric and isodensity path and it may evolve into a multiphase inclusion. The phase transition or unmixing occurs on the solvus of the corresponding chemical system.

A trapped aqueous brine may evolve a vapour "bubble" because of differential thermal contraction of the

host crystal and the fluid. These "bubbles" should be distinguished from the primary gas trapped from a "boiling" fluid.

If a $H_2O$ - $CO_2$ fluid was trapped at elevated temperature, it may unmix below 300°C, due to $H_2O$, $CO_2$ immiscibility, and separate $CO_2$ into a second fluid phase. If the $CO_2$ concentration is high enough, or if the $CO_2$ partial pressure exceeds 75 bars, gaseous $CO_2$ will separate usually below the critical point for pure $CO_2$, 31°C.

Regularity both of phase volume ratios and microthermometric data provides the best evidence available that the original fluid was homogeneous.

Decreasing solubility during cooling may result in saturation with respect to the solutes and precipitation of daughter minerals.

The composition, density and P-T conditions of the inclusions can be deduced from univariant phase transitions observed during cooling and heating experiments assuming that the inclusions retain constant volumes. The temperature of homogenization of the inclusion ($T_H$) on heating can be used to

estimate the trapping temperature. $T_H$ represents a minimum trapping temperature and a pressure correction must be applied to compensate for the pressure differences between the experiment and the trapping, and for the salinity of the fluid. An independent estimate of pressure or temperature can be used for pressure correction. Pressure may be evaluated from fluid inclusion studies in a limited number of cases (Roedder and Bodnar, 1980). Salinity can be estimated by freezing the inclusion and recording the temperature at which melting of the frozen inclusion occurs. The melting point is related to the composition of the dissolved salts. In $CO_2$ - bearing inclusions, the clathrate compound, carbon dioxide hydrate ($CO_2$ 5.75 $H_2O$) forms upon freezing. When pure, this compound melts at about +10°C (Collins, 1979). Solutes present depress the clathrate melting point, providing an estimate for the salinity, for the case of $CO_2$ - inclusions. However, methane and solutes exert opposed effects on the clathrate melting behaviour: thus melting point data from $CO_2$-bearing liquid inclusions are not easy to interpret without knowledge of the gas species present.

Cooling $CO_2$-rich inclusions to temperatures as low as -80°C causes freezing of the $CO_2$ phase. Melting of solid $CO_2$, upon heating, in equilibrium with liquid and vapour $CO_2$, at a temperature of T = -56.6°C, is the best indication yet available in fluid inclusion research, of the purity of the $CO_2$-phase. The temperature (T = -56.6°C) where three $CO_2$ phases (solid, liquid, vapour) coexist is known as the $CO_2$ triple point (Weast, 1974).

The values obtained for homogenization temperatures and salinity can then be compared to experimental results on fluid phase equilibria systems: $H_2O$ + NaCl (Sourirajan and Kennedy, 1962); $H_2O$ + $CO_2$ (Takenouchi and Kennedy, 1964); $H_2O$ + $CO_2$ + NaCl (Takenouchi and Kennedy, 1965; Gehrig et al., 1979; Hendel and Hollister, 1981) in order to infer trapping conditions (i.e. "boiling" or "immiscibility") or interpret homogenization behaviour.

### 5.2.2 General Microscopic Observations

Numerous inclusions tend to be aligned along microfractures, or in planar arrangements, which could be observed by racking the stage of the microscope up and down. No evidence could be found as to whether

these planes represent original growth planes or healed fractures. Furthermore, the complete lack of zonal arrangement masked any possible chronological implications. However, large and randomly distributed inclusions are commonly considered to be earlier than those exhibiting linear arrangements (Touret, 1981). In most cases of linear arrangements the inclusions vary in size and/or phase proportions, thus supporting a secondary origin. Isolated inclusions, at distances several times their diameter from other inclusions, or for which no evidence of secondary origin was recognized, were considered to be primary or pseudosecondary.

Occasionally inclusions were observed that had partially necked down. Large and sometimes dark inclusions with highly irregular outlines and inconsistent phase ratios mostly exhibited abnormal behaviour during heating and freezing runs. This was interpreted as a sign of leakage.

## 5.2.2a Inclusion Types

The classification scheme employed here is based on phase relations at room temperature. Three main types of inclusions were distinguished:

TYPE I

Three phase $CO_2$ - bearing inclusions (Plate 6.1), containing an outer aqueous liquid phase and inner liquid $CO_2$ phase with associated gaseous $CO_2$ - vapour bubble, constitute the principal type. Cooling induced the nucleation of a $CO_2$ - vapour bubble in some two phase inclusions that are associated with the three phase ones. Thus, these metastable inclusions were also classified as type I.

The inclusions that were studied ranged in size from 9 to 30 $\mu$ in their longer dimension; usually they approach shapes of negative crystals.

The $CO_2$ - phase (liquid and gas) generally fills 10-25% of the inclusion volume, the remainder being occupied by saline water. However, inclusions with higher $CO_2$ contents (30-50% by volume) (Plate 6.2) were also present.

Plate 6.1 : Type I three phase $CO_2$-bearing fluid inclusion containing an outer aqueous liquid phase ($L_{H_2O}$) and inner liquid $CO_2$phase ($L_{CO_2}$) with associated gaseous $CO_2$-vapour bubble ($V_{CO_2}$). Microphotograph under plane polarized light.


5 μ

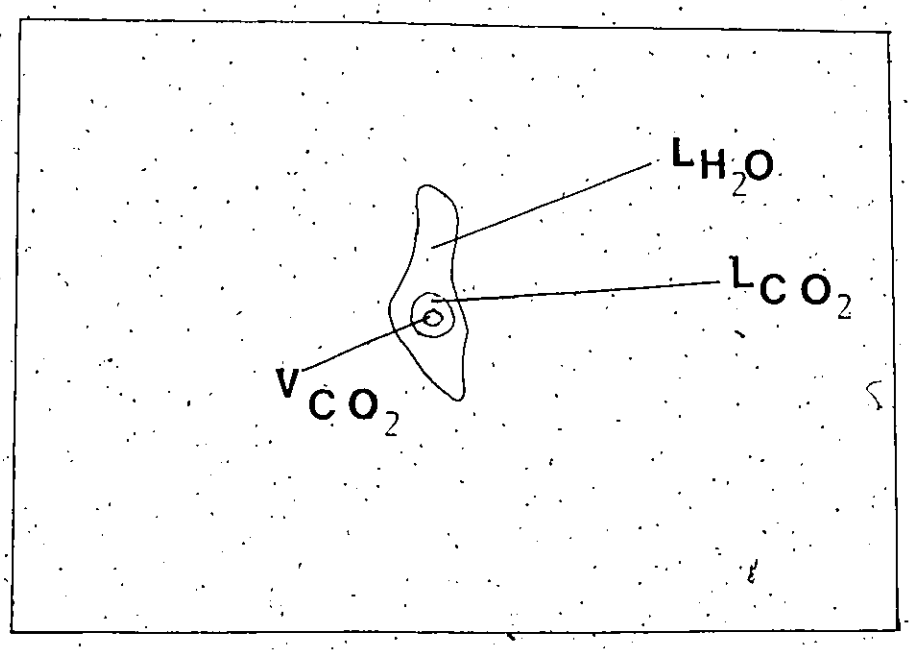
$L_{H_2O}$
$L_{CO_2}$
$V_{CO_2}$

Plate 6.2 : Type I three phase $CO_2$-bearing fluid inclusions containing an outer aqueous liquid phase ($L_{H_2O}$) and inner liquid $CO_2$phase ($L_{CO_2}$) with associated gaseous $CO_2$-vapour bubble ($V_{CO_2}$).
Microphotograph under plane polarized light.

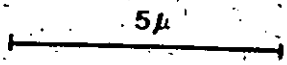
5μ

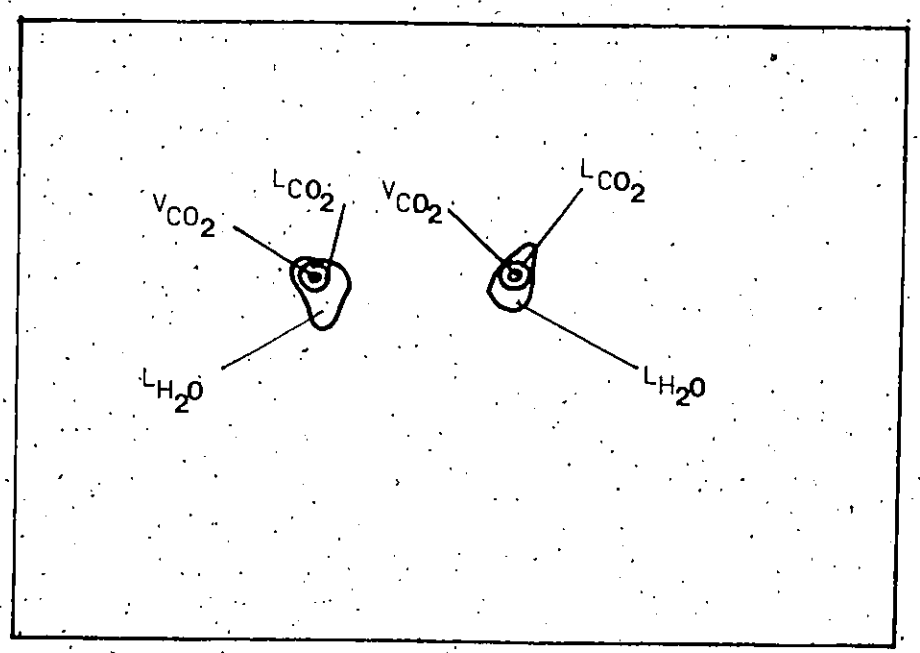
$V_{CO_2}$
$L_{CO_2}$
$L_{H_2O}$
$V_{CO_2}$
$L_{CO_2}$
$L_{H_2O}$

TYPE II

One phase inclusions containing approximately 100 volume percent $CO_2$ with a possible 10 volume percent of undetected water (Plate 6.3 a). These inclusions were intimately associated with type I and they occasionally exhibited negative crystal shapes with their larger dimension ranging from 6 to 25 $\mu$.

Locally and less frequently, dark $CO_2$-rich inclusions (70-90% $CO_2$ by volume) were observed (Plate 6.3 b). The existing water phase adheres as a thin film to the cavity walls and may be easily overlooked. Homogenization and freezing points were difficult to impossible to observe and thus no data are available from this class of inclusions.

TYPE III

Two fluid phase inclusions containing liquid saline water plus 10-50% water vapour or water - carbon dioxide vapour (Plate 6.4). No clathrate formation was detected, indicating a very low $CO_2$ concentration, or $CO_2$ could have failed to develop a separate liquid phase because it was initially under low pressure ( $<$ 75 bars). Type III inclusions were

Plate 6.3 a : Type II one phase fluid inclusion containing liquid $CO_2$ ($L_{CO_2}$).
Microphotograph under plane polarized light.
Vertical bar represents 5 $\mu$ .

Plate 6.3 b : Type II $CO_2$-rich fluid inclusions containing liquid $CO_2$ ($L_{CO_2}$) and minor liquid water ($L_{H_2O}$).
Microphotograph under plane polarized light.
Vertical bar represents 5 $\mu$ .

a

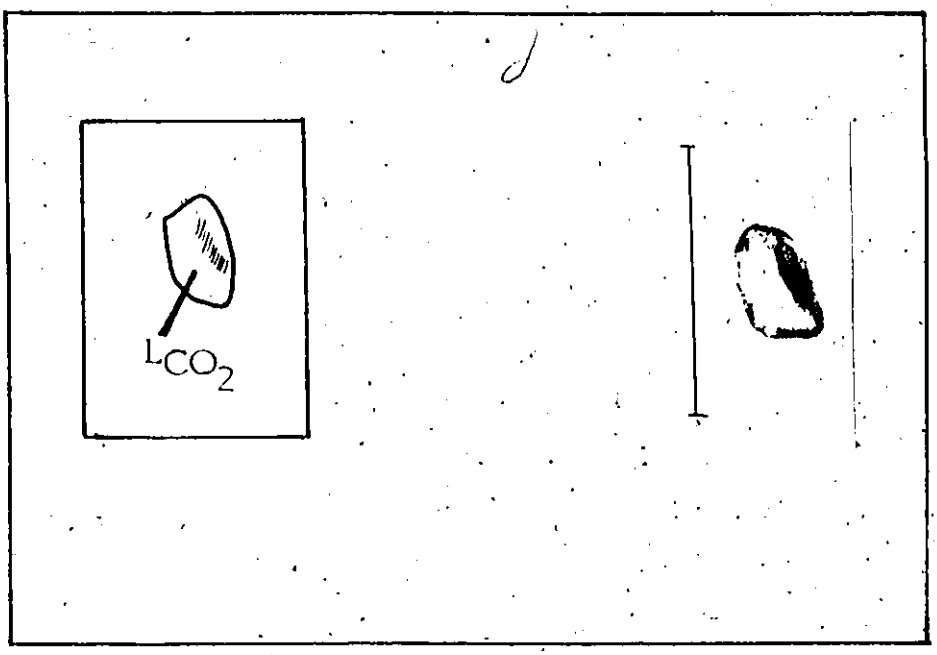


b

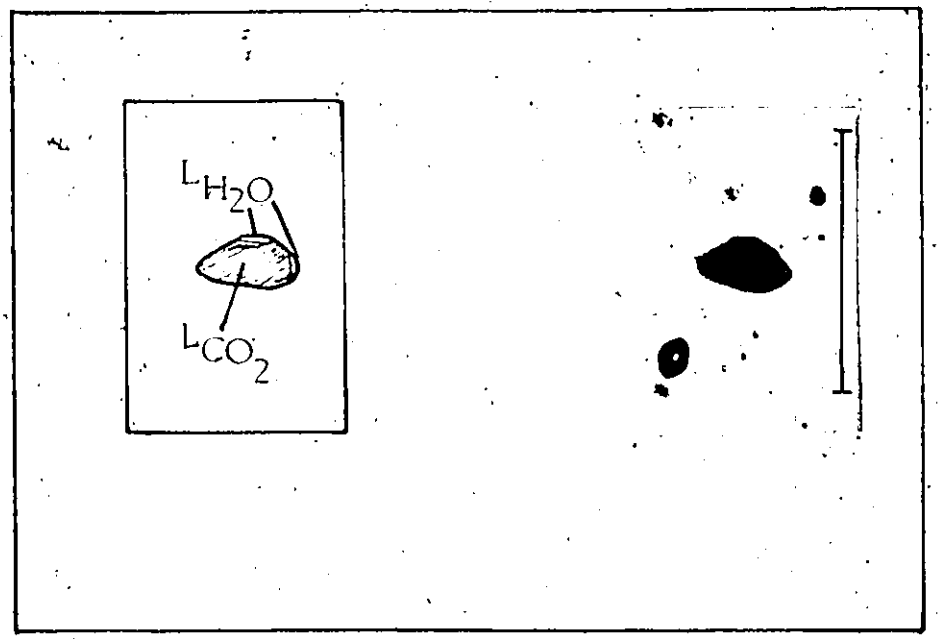

Plate 6.4 : Type III two phase fluid inclusion containing liquid water ($L_{H_2O}$) plus water vapour ($V_{H_2O}$). Microphotograph under plane polarized light.

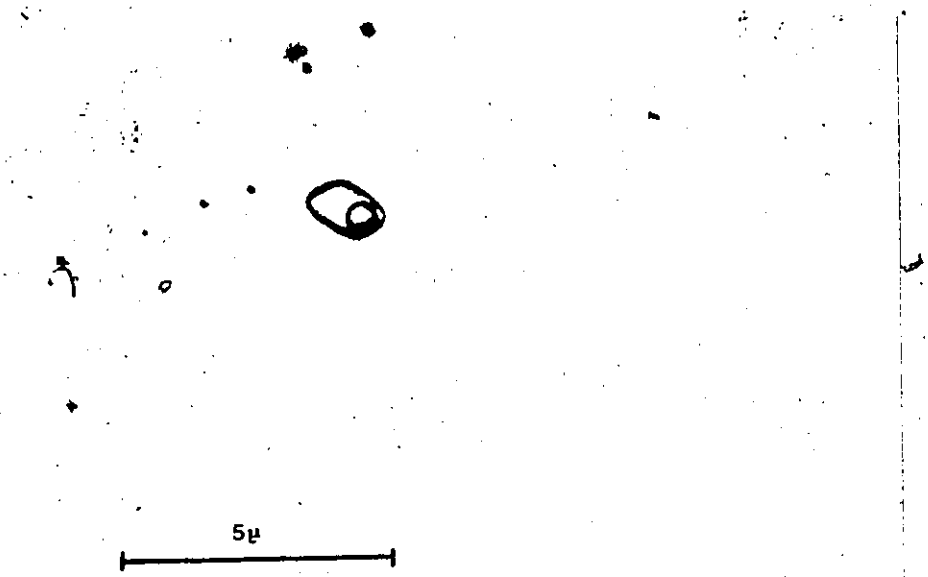
5μ

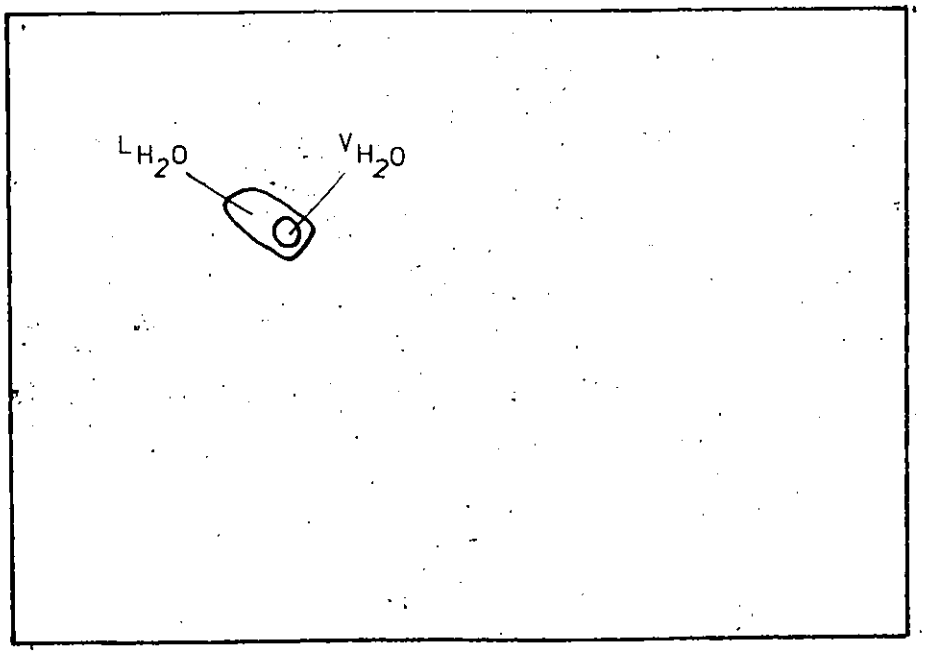
$^{L}H_2O$
$^{V}H_2O$

generally subrounded to cylindrical and those studied ranged in size from 10-30 $\mu$ in the longer dimension.

Rare, two-phase inclusions consisting of large amounts of vapour (60% by volume) accompanied by small amounts of condensed saline water were included in this type.

No systematic distribution of fluid inclusion types in relation to particular veins, or between specific quartz grains within samples was observed. No daughter minerals were observed in any of the types of inclusions, denoting low solute concentration.

**5.2.2b Observation of Homogenization Phenomena.**

When heated, type I inclusions frequently become dark before homogenizing and low index vapour could be observed filling the cavity and/or cracks on the cavity walls. This phenomenon was determined to be non-reproducible, proving that the inclusions had decrepitated. Decrepitation is the result of the isochoric rise of the internal pressure, as the inclusion is heated, to a point exceeding the mineral's strength. It represents a minimum homogenization temperature and provides evidence that the inclusion is at high internal pressure.

The $CO_2$ phases (liquid and gas) homogenized to the liquid at all times, with the central bubble shrinking to disappearance.

On heating to total homogenization, two kinds of behaviour were observed. Most type I inclusions and all type III inclusions homogenized in the outer aqueous liquid phase. The inner $CO_2$ or $H_2O$ - $CO_2$ phase gradually grew smaller until it disappeared. Before disappearing it began moving vigorously and went out of sight, either having homogenized or hidden behind the cavity walls. This was the last that could be seen of the central bubble and it was taken as the homogenization temperature. This point can often only be approximated within 5°C.

A second type of behaviour was noticed in a limited number of type I inclusions, whereby the inner $CO_2$ phase grew larger on initial heating and then maintained a constant volume through much of the heating; the miniscus then became hazy and at a temperature a few degrees higher disappeared without any appreciable change in volume. Roedder (1972) described this as critical behaviour.

## 5.2.2c Observation of Freezing and Melting Phenomena

On cooling type II inclusions below 0°C a second fluid phase, presumably $CO_2$ gas, separated. On further cooling to a temperature as low as -80°C the liquid $CO_2$ froze to an irregular crystal aggregate and the $CO_2$ gas phase became oval shaped. When the inclusion was slowly heated up the temperature at which the frozen $CO_2$ began to melt, and liquid $CO_2$ was observable around the gas bubble, was recorded.

On cooling type I inclusions to about -40°C, the $H_2O$ - $CO_2$ vapour bubble changed to an oval shape, with concomitant reduction in volume. A plate-like crystal formed almost simultaneously, projecting into the outer aqueous phase. After a short time the outline of the distorted bubble became jagged and coarse indicating the formation of $CO_2$ - hydrate (clathrate) (Collins, 1979). On further cooling the aqueous phase turned into a granular mass of ice crystals and the inclusion appeared nearly opaque. For some inclusions this "double freezing" (Collins, 1979) was not completed unless cooling was continued -80°C. No solidification of $CO_2$ could be observed if the temperature was further dropped.

Measuring the temperature of clathrate melting proved very difficult due to the similarity of refractive indices of the $CO_2$ - hydrate and of the aqueous solution. The temperature of disappearance of the jagged interface in the presence of liquid $CO_2$ and $CO_2$ vapour, was recorded as the decomposition temperature of the clathrate.

Formation of translucent aggregates of small ice crystals was easily detected on freezing type III inclusions.

Before final melting, the vapour bubble could be observed adhering to the last ice crystal, which was in motion inside the inclusion. The stopping of this motion combined with the disappearance of the crystal was recorded as the ice melting point.

### 5.2.3 Results

Two groups, A and B, of the $CO_2$ - phase (liquid-vapour) homogenization temperatures, $T_{HCO_2}$, are very well-defined in Figure 22. Group A consists of 41 type I inclusions, most of which homogenized between +15 and +30°C, with a mean $T_{HCO_2}$ of +24°C ($\pm$2.3). Group B is characterized by type II

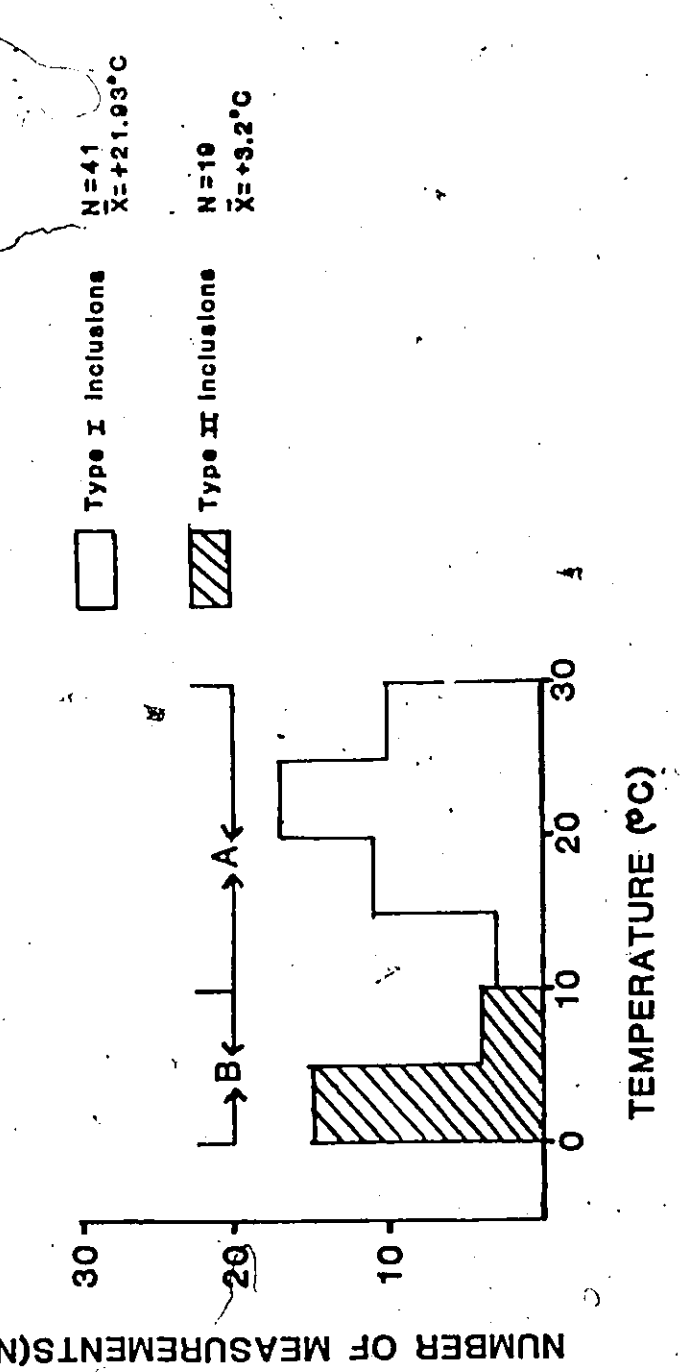


Figure 22 : Histogram of the $CO_2$-phase homogenization temperatures, $T_{HCO_2}$, of type I and type II fluid inclusions.

inclusions with $T_{HCO_2}$ between 0° and +10°C, and a clustering of values around +3.2°C (±0.5).

The molecular proportion of the $CO_2$ phase has been determined to be approximately 10 mole% (21 weight%) for $T_{HCO_2}$ between +15 and +30°C and 20% $CO_2$ phase using a method after Burruss (1981) (APPENDIX 4). For inclusions with a maximum of 50% $CO_2$ phase and $T_{HCO_2}$ ranging between +15 and +30°C, the molecular proportion rises to approximately 20 mole% $CO_2$. In apparently "pure" $CO_2$ inclusions which homogenized between 0° and +10°C, 7-10 mole% $H_2O$ might be present. The largest component of error in determining mole fraction of $CO_2$ using Burruss' (1981) approach is in the visual estimation of volume percent $CO_2$.

Figure 23 summarizes melting temperatures of solid $CO_2$, $T_{MCO_2}$, from type II inclusions. Most of the values are concentrated around a mean value of $T_{MCO_2} = -56.8°C \pm 0.1°C$, indicating that the $CO_2$ phase is pure.

Clathrate melting temperatures presented in the histogram in Figure 24 have a mean $T_{CCO_2}$ value of 7°C. The ice melting temperatures plotted on the

Figure 23 : Histogram of melting temperatures of solid $CO_2$, $T_{MCO_2}$, of type II fluid inclusions.

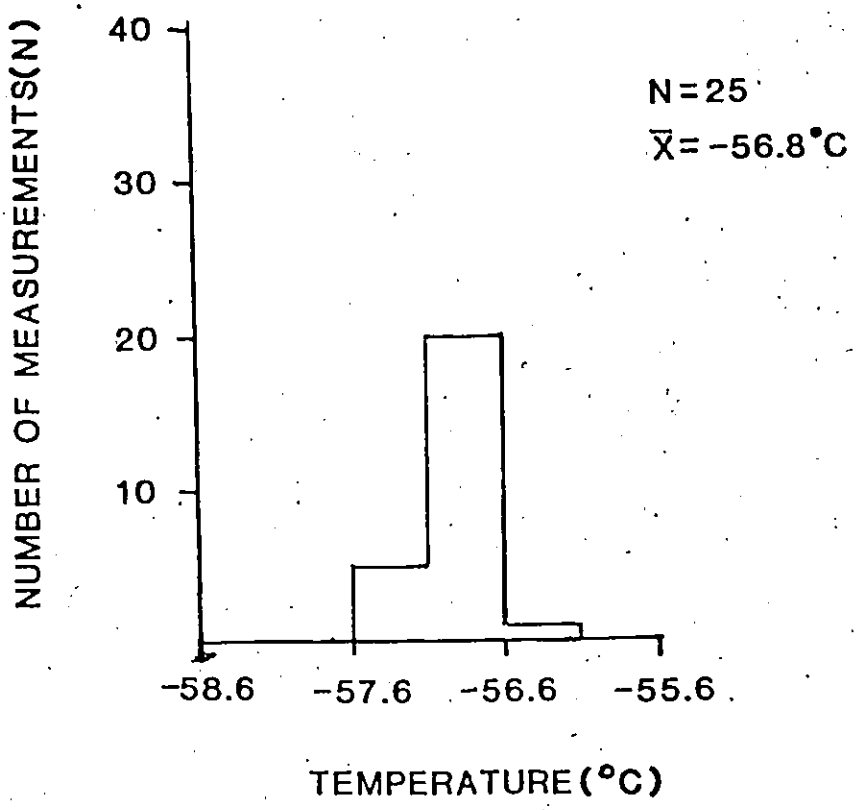

Figure 24 : Histograms of melting temperatures of $CO_2$-hydrate($T_{CCO_2}$) and ice($T_{ICE}$) of type I and type III fluid inclusions.

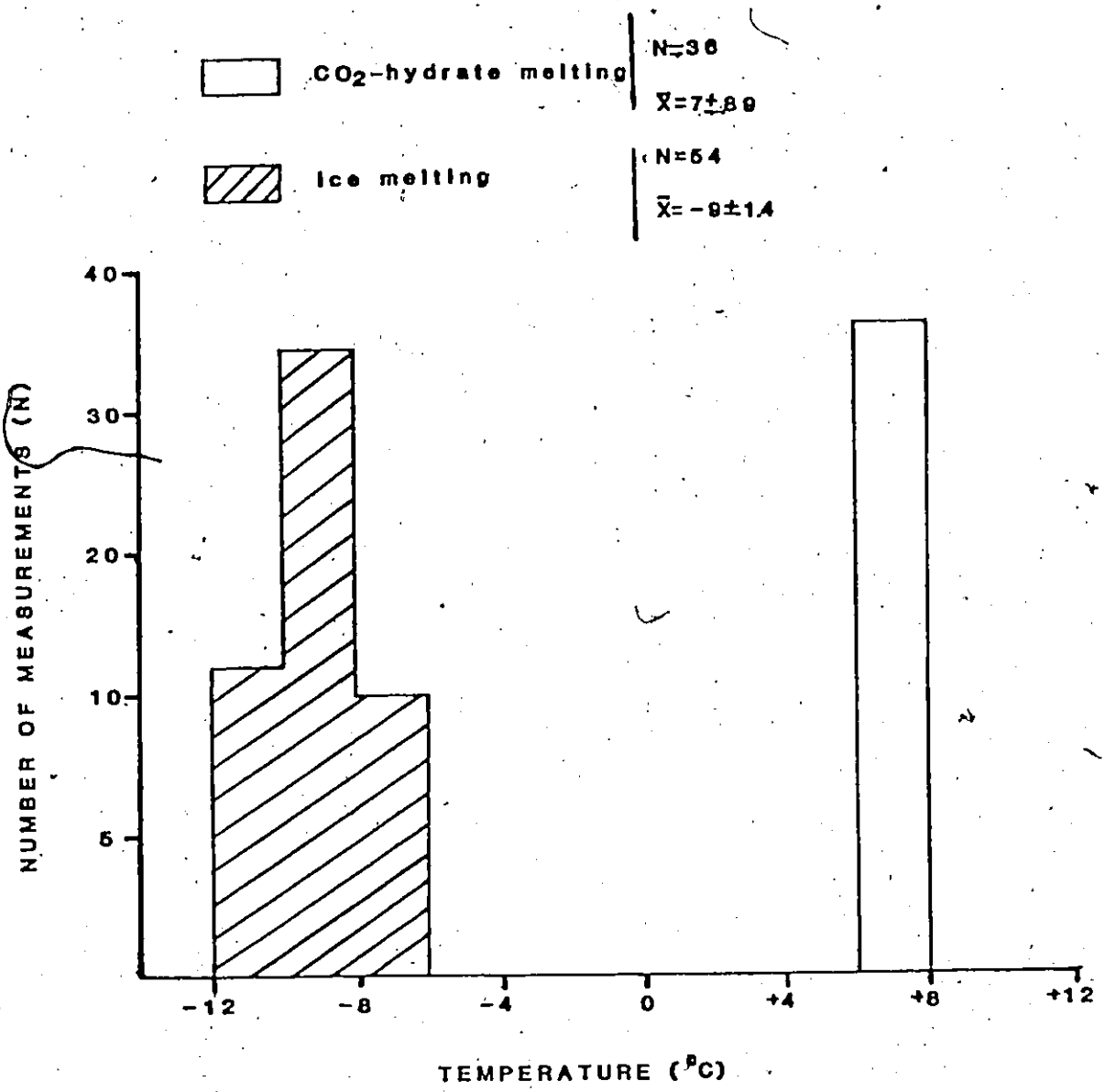

same figure are only from type III inclusions and show a mean $T_{ICE}$ of -9°C. The presence of dissolved salts is evident by the "depression" of the melting temperatures of both clathrate and ice from their "normal" melting temperatures of +10°C and 0°C, respectively. If $CH_4$ was present in substantial amounts in the inclusions it would introduce some ambiguity as it would apply an opposing effect to the clathrate melting point compared to the NaCl effect.

$T_{CCO_2}$ values are in a limited range between +8 and +6, corresponding to salinities of 4 to 6 wt.% NaCl equivalent.

Type III inclusions have salinities between 9 and 16 wt.% NaCl equivalent as suggested by the ice melting temperatures. The melting peak at $-9 \pm 1.4$°C is consistent with the presence of 11 to 13 wt.% NaCl equivalent in the fluids trapped in type III inclusions. The salinities measured in this study have been determined using salt-depressed curves (Figure 25).

Table 10 shows the densities of the $CO_2$ phase for the corresponding $T_{HCO_2}$ (based on Figure 26, after Roedder, 1965). Also shown are the estimated

Figure 25 : Curves for depression of $CO_2$-hydrate (AB; after Bozzo etal., 1975) and for depression of the fusion temperature of ice by NaCl ( CD; after Roedder, 1962 )

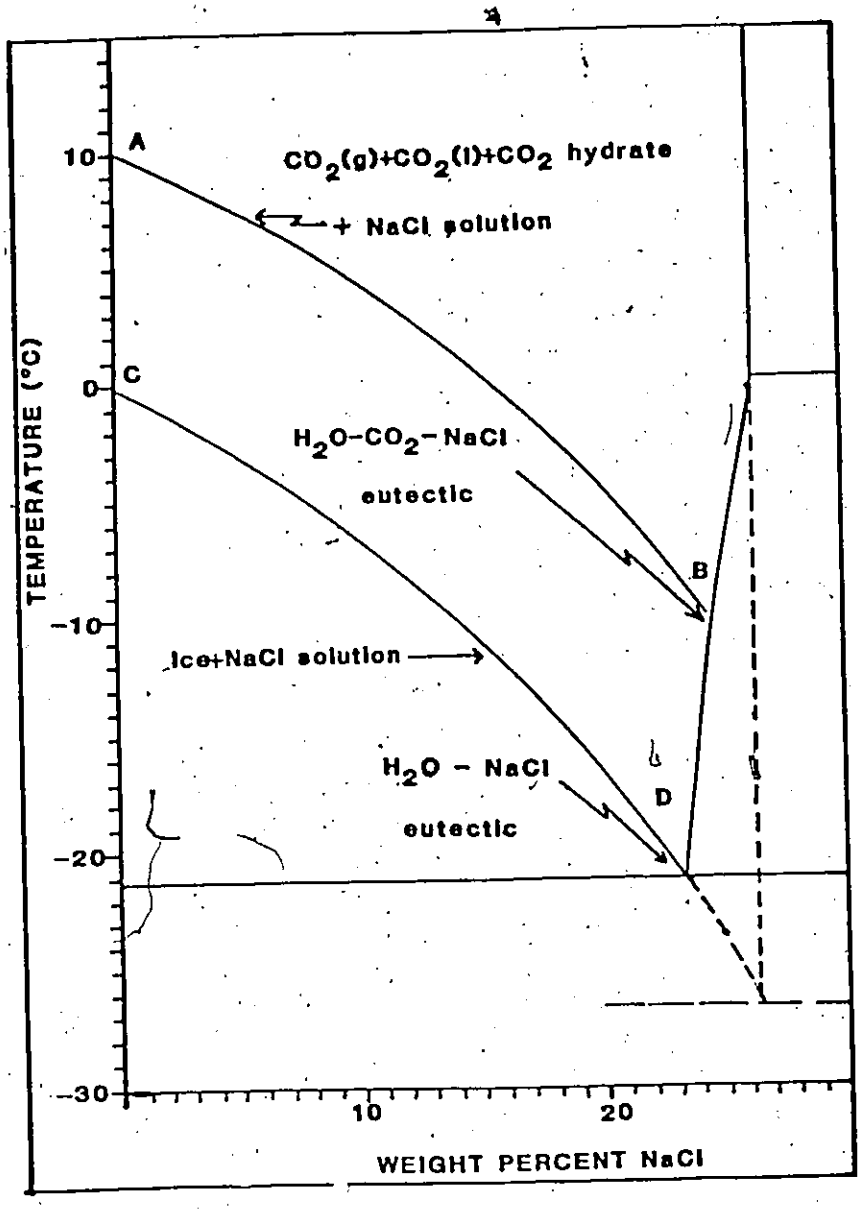

Table 10 : Densities of the $CO_2$-phase present in fluid inclusions and estimated bulk densities of type I and type II fluid inclusions.

| $T_{H_{CO_2}}$ (°C) | D* (g/cm$^3$) | | BULK DENSITY (g/cm$^3$) | | | $CO_2$ DENSITY (g/cm$^3$) |
|---|---|---|---|---|---|---|
| | 5 wt.% | 10 wt.% | 20 vol.% $CO_2$ | 50 vol.% $CO_2$ | 90 vol.% $CO_2$ | |
| +30 | 1.034 | | 0.95 | 0.82 | | 0.60 |
| | | 1.070 | 0.98 | 0.84 | | |
| +24 | 1.034 | | 0.98 | 0.89 | | 0.75 |
| | | 1.070 | 1.00 | 0.91 | | |
| +15 | 1.034 | | 1.00 | 0.94 | | 0.83 |
| | | 1.070 | 1.03 | 0.96 | | |
| +10 | 1.034 | | 1.00 | 0.94 | | 0.86 |
| | | 1.070 | 1.03 | 0.96 | | |
| + 6 | 1.034 | | | | 0.93 | 0.92 |
| | | 1.070 | | | 0.93 | |
| 0 | 1.034 | | | | 0.97 | 0.96 |
| | | 1.070 | | | 0.97 | |

* : relative density of NaCl-$H_2O$ solution at 20°C. (Handbook of Chemistry and Physics 55th edition, 1974-1975)

Figure 26 : Experimental solvus of the pure $CO_2$ system.
( after Roedder, 1965).

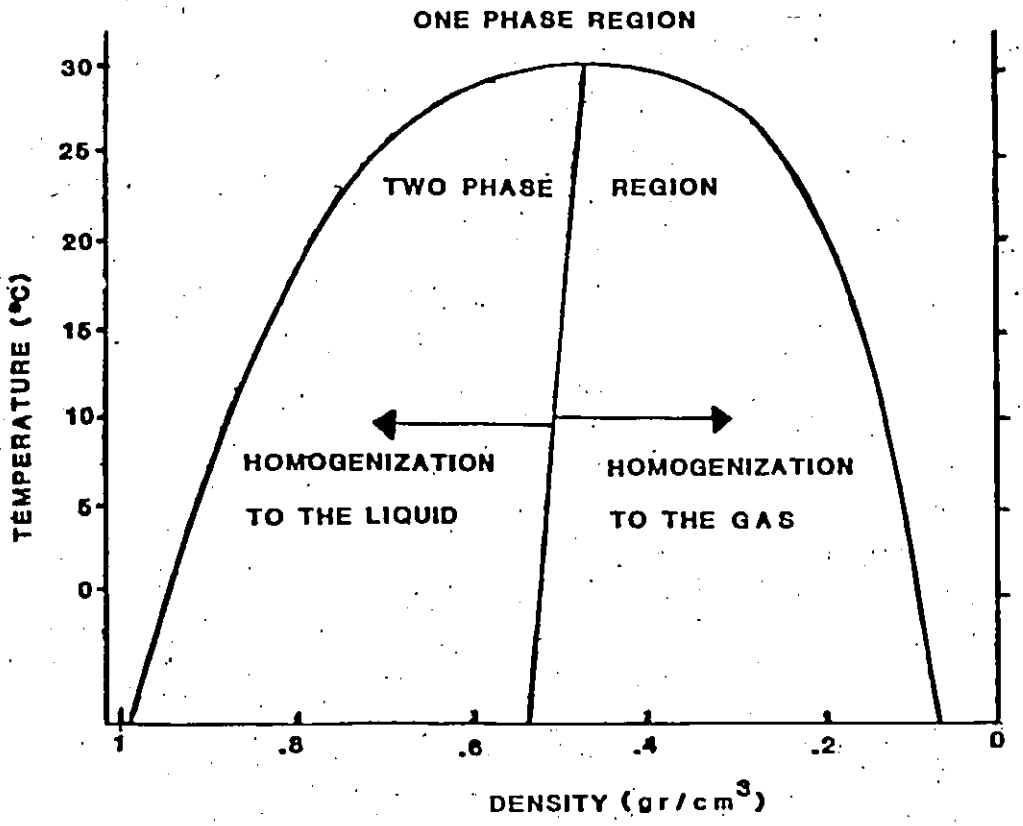

bulk densities of inclusions with the $CO_2/H_2O$ ratios observed in type I and II inclusions. The bulk densities of the inclusions were estimated based on the densities and the relative volumes of the various phases present in the inclusions (estimated visually at room temperature), as suggested by Roedder (1984), considering an inclusion volume of $1cm^3$.

Given a type I inclusion with a volume of $1cm^3$ containing 20% $CO_2$ with a density of $0.75gr/cm^3$, and 80 vol.% $H_2O$-NaCl solution with a density of $1.034gr/cm^3$, the bulk density may be estimated as follows:

Weight of the $CO_2$ phase = $0.2cm^3$ x $0.75gr/cm^3$ = 0.15gr
Weight of the $H_2O$-NaCl phase = $0.8cm^3$ x $1.034gr/cm^3$ = 0.8gr
Density of the inclusion = $0.95gr/cm^3$

Based on the premise that the most common primary inclusions are type I with 20 vol.% $CO_2$ and mean $T_{HCO_2}$ = +24°C, and type II with 90 vol.% $CO_2$ and mean $T_{HCO_2}$ = +3.2°C, the results shown on Table 10 indicates that two different fluids with $CO_2$ densities of 0.75gr/cm and $0.95gr/cm^3$ were trapped in the vein quartz. The possible relation between

these two fluids is discussed in chapter 6.

Figure 27 presents measurements of homogenization and decrepitation temperatures $T_H$ and $T_D$, respectively obtained from type I and type III inclusions. The distribution of $T_H$ values for type III inclusions is somewhat exaggerated as reliable data were easier to collect from simple two phase inclusions. Inclusions rich in carbon dioxide homogenize at temperatures higher than 220°C, to be clearly distinguished from aqueous two-phase inclusions which generally homogenize at temperatures between 220°C and values as low as 120°C.

The $CO_2$ - rich inclusions fall clearly within two groups - group I with mean $T_H = 232 \pm 6.5$°C (n = 17), and group II with mean $T_H = 311 \pm 3.9$°C (n = 13). The rest of the values show a wide scatter but tend to be dispersed about group II.

Decrepitation temperatures $T_D$ show two narrow maximums. One is below the group II peak ($T_D = 271 \pm 4.5$°C), n = 10) and the second coincides with the group I peak ($T_D = 229 \pm 3.8$°C, n = 8). This is a good illustration of the fact that many inclusions decrepitated before homogenizing.

Figure 27 : Histograms of homogenization and decrepitation temperatures ($T_H$, $T_D$) of fluid inclusions in gold-bearing vein quartz from the Renabie mine area.

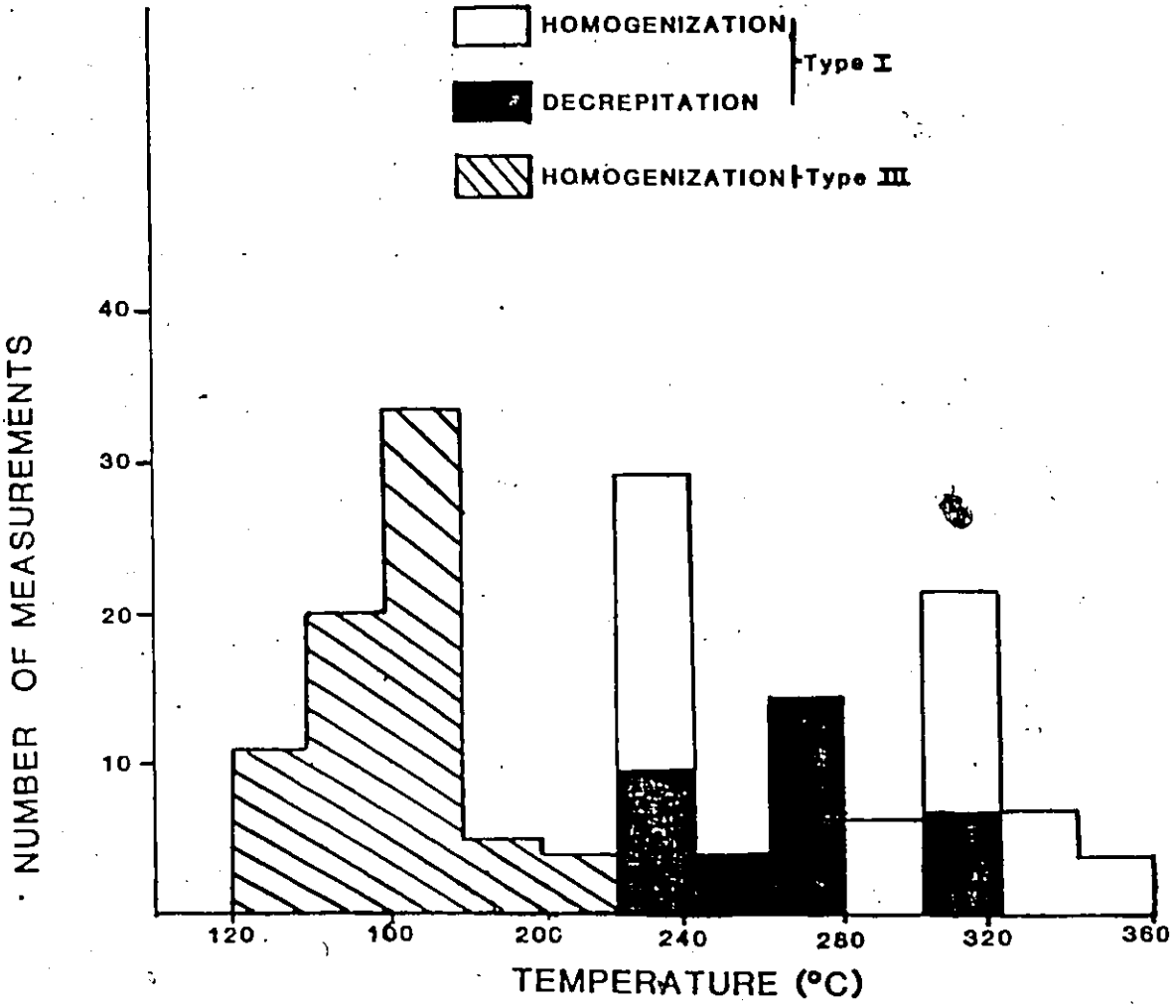

Homogenization temperatures for type III inclusions show a wide spread (mean $T_H$ = 161 $\pm$25.7, n = 78). These results suggest that the type III inclusions constitute a large group of secondary inclusions.

## 5.3 Oxygen Isotope Abundances

Stable hydrogen and oxygen isotope examination of natural waters, along with fluid inclusion work, have illuminated the various sources of $H_2O$ involved in ore deposition and hydrothermal alteration (Taylor, 1974, 1979). Genetic terms for different kinds of water are meteoric, seawater, connate, metamorphic, magmatic and juvenile water (White, 1974). Each of these types of water have characteristic hydrogen and oxygen isotope compositions.

The oxygen isotope compositions are reported as:

$R = \delta^{18}O$ where

$$R_{sample} = \left[\frac{R_{sample}}{R_{standard}}\right] - 1 \quad \times 1000 \ (0/00)$$

and R sample is $^{18}O/^{16}O$ in the sample and R standard is the appropriate ratio in a set of ocean water values, named Standard Mean Ocean Water (SMOW)

by Craig (1961).

If the temperature of equilibration can be independently estimated, the $\delta^{18}O$ value for water in equilibrium with a particular mineral can be calculated. The fractionation factor or isotopic partition coefficient is solely temperature controlled and follows a $1/T^2$ dependence (Taylor, 1979).

Clayton et al. (1972) experimentally determined the oxygen isotope partitioning between quartz and water. The quartz-water fractionation equation in the 200°C to 500°C temperature interval is as follows:

$$10^3 \ln\alpha_{Qtz\text{-}H_2O} = \Delta_{Qtz\text{-}H_2O} = \delta^{18}O_{Qtz} - \delta^{18}O = 3.38\ (10^6 T^{-2}) - 3.40 \text{ where}$$

$\alpha$ = fractionation factor for quartz and water.

$\Delta_{Qtz\text{-}H_2O}$ = the difference in $\delta^{18}O$ between quartz and water in equilibrium.

T = temperature of equilibrium, °K.

The oxygen isotope abundances $\delta^{18}O_{Qtz}$ of quartz separates from gold-bearing quartz - muscovite - carbonate veins (six analyses) from the Renabie area

(Table 11), as well as a barren vein (one analysis) from the same area, were analyzed in an attempt to decipher the origin of the fluid responsible for vein formation and alteration of wallrocks about veins. The $\delta^{18}O_{Qtz}$ values are between +9.4°/oo and +11.2°/oo.

The temperature during the formation of the quartz veins was between 300°C and 470°C as attested by homogenization temperatures of fluid inclusions and a hydrothermal alteration mineral assemblage that corresponds to lower greenschist-facies metamorphic conditions. Substituting $\delta^{18}O_{Qtz}$ = 9.4°/oo to 11.2°/oo and T = 400°C into the quartz-water fractionation equation of Clayton et al. (1972), the $\delta^{18}O_{H2O}$ is between 5‰ and 7‰. Using 350°C as the formation temperature slightly decreases the $\delta^{18}O_{H2O}$ values, to between 4‰ and 6‰.

Table 11: Oxygen isotope composition of quartz, $\delta^{18}O_{Qtz}$, from gold-bearing and barren veins in the Renabie area.

| PROSPECT | SAMPLE No. | $\delta^{18}O_{Qtz}$ |
|---|---|---|
| 1) Renabie Gold mine | | |
| Renabie Vein: | | |
| "C" Zone | RN-22 | +10.2 |
| 458m (1250ft) level | RN-31 | +10.7 |
| | RN-36 | + 9.4 |
| 914m (3100ft) level | RN-122 | +10.9 |
| | RN-125 | +10.6 |
| 2) Braminco Gold Prospects | | |
| No. 21 Vein: | RN-71 | +11.2 |
| 3) Renabie Mines Gold Prospects | | |
| Barren quartz vein: | RN-42 | + 9.9 |

Analyst: Geochron Laboratories, Cambridge, MA.

# CHAPTER 6

## 6. DISCUSSION

### 6.1 Grade of Regional Metamorphism

The batholithic rocks at the Renabie mine area are characterized by an epidote - carbonate - muscovite - chlorite - biotite - hornblende - quartz - albite - oligoclase - andesine assemblage. This assemblage appears to be in textural and chemical disequilibrium, as suggested by the following criteria:

1. Subhedral plagioclase laths are mottled with fine grained sericite, epidote, carbonate and quartz (Plate 2). Compositionally zoned plagioclase has a mottled oligoclase interior and a rim of albite (An5) (Plate 2).

2. The biotite and hornblende are partly replaced by chlorite with or without quartz (Plate 2).

3. Fractures filled with carbonate and muscovite, with or without quartz, transect trondhjemitic and tonalitic rocks.

The chlorite - carbonate - muscovite - albite - quartz assemblage, that appears to overprint a pre-existing biotite - hornblende - quartz - plagioclase assemblage, is typical of the chlorite subfacies of the greenschist facies (Turner, 1981). Therefore, the aforementioned criteria suggest that regional greenschist metamorphism retrograded the batholith. The degree of metamorphism ranges from incipient to intense and the alteration mineralogy suggests the involvement of a carbon-dioxide-bearing fluid.

The mafic volcanic rocks up to 1000 m from the batholith also consist of a mineral assemblage that appears to be characterized by replacement textures, reaction rims around minerals, compositionally zoned minerals, and generally a lack of intimate intergrowth. Textural and compositional disequilibrium is suggested by the following criteria:

1. Poikiloblastic hornblende that commonly has serrated margins and a surrounding halo of carbonate, or carbonate, chlorite and quartz (Plate 1). Hornblende prisms that have a preferred orientation parallel to the general foliation are characteristically crosscut by chlorite flakes (Plate 1).

2. Amphibole is zoned (hornblende core, actinolite rim) (Plate 1).

3. Hornblende is cross cut by fractures filled with epidote or carbonate and with or without chlorite (Plate 1).

4. The composition of plagioclase is variable ranging from andesine ($An_{32}$) to albite ($An_5$).

These criteria suggest the overprinting of a chlorite - carbonate - actinolite - albite - quartz assemblage on a pre-existing hornblende - epidote - oligoclase to andesine plagioclase - quartz assemblage. The association of hornblende with plagioclase of oligoclase to andesine composition and with epidote is diagnostic of medium-grade amphibolites (Winkler, 1976) (epidote - amphibolite facies according to Miyashiro, 1973). Actinolite coexisting with chlorite, epidote, albite and quartz characterizes low temperature low-grade greenschists (Winkler, 1976). Therefore, the aforementioned criteria indicate that medium grade amphibolites were retrograded to low-grade greenschists, during regional greenschist metamorphism. The resultant mineralogy is similar to that within the batholith that was ascribed above to retrogressive metamorphism.

## 6.2 Chemical Composition of the Ore Fluid

The association of gold with tellurides and metal sulphides in the Renabie and Braminco 21 quartz - muscovite - carbonate veins provides evidence that gold was transported in solution together with other rare elements such as Ag, Bi, Te, and also Pb, Cu, Zn, and S. In general, precious metal deposits of Archean age in greenstone belts are characterized by major enrichment of Au, Te, Bi, As, Sb, B, W, and Ag in the $10^3$ to $10^4$ and $10^1$ to $10^2$ range respectively, coupled with slight enrichment of the abundant base metals Cu, Pb, and Zn ($10^1$ to $10^{-1}$), relative to their crustal abundance (Fyfe and Kerrich, 1984).

Fluid inclusion investigation indicates that $CO_2$ was present in the ore-fluid. An almost pure $CO_2$ phase, containing little water, was trapped in the vein quartz, but whether or not this phase is a sample of the actual gold-transporting fluid, is generally debatable, inasmuch that experimental and theoretical studies of gold solubility in the system $H_2O$-NaCl-$CO_2$ are lacking. Such inclusions can result from trapping of an immiscible mixture of $H_2O$-rich and $CO_2$-rich fluids, evolved through unmixing of an earlier homogeneous $CO_2$-$H_2O$ phase (Roedder and Bodnar, 1980). In the present situation

this is unlikely because there is no evidence for widespread immiscibility. Such inclusions can also result from trapping of a distinct "primary" $CO_2$-rich fluid not related to the rest of the fluids present in inclusions of the vein quartz (Hollister and Burruss, 1976).

The $CO_2$-phase homogenization data indicate that the almost pure $CO_2$ type II inclusions have higher $CO_2$ densities ( $0.93 gr/cm^3$) than type I inclusions ($0.80-0.63 gr/cm^3$). It is known (Touret, 1981) that in the case of $CO_2$ inclusions, those denser in $CO_2$ form earlier than the least dense in the case of evolving metamorphic fluids under conditions of decreasing pressure. Furthermore, loss of $CO_2$ from the hydrothermal fluid which was trapped in type II inclusions would reduce the partial pressure of $CO_2$, thus lowering the total fluid pressure. In the light of this discussion it can be suggested in the present study that an early, almost pure $CO_2$ fluid, with little water, was depleted in $CO_2$ through its fixation in altered wallrock and vein filling carbonates, probably during their coprecipitation with gold and quartz. However, a combination of all the above mentioned fluid phase relations can not be excluded.

A fluid composed of water with also approximately 21 wt.% $CO_2$, 4-6 wt.% dissolved salts and a density of 0.95 to

0.96 gr/cm$^3$ was primarily involved in the gold concentration processes. Fluid inclusions in other Archean precious metal deposits also indicate rather dilute solutions of < 10 wt.% NaCl equivalent (Guha et al., 1982).

A salient feature of both the wallrock alteration envelopes and the vein fillings is the presence of abundant carbonate minerals. Fluid inclusion data, as previously discussed, and chemical mass balance calculations support the interpretation by Kerrich and Fyfe (1981) that carbonate minerals were formed via hydrolysis of Fe, Mg, Ca, - silicates such as biotite, hornblende, epidote and chlorite, with the carbon dioxide being introduced by the mineralizing fluids and the bivalent metal cations being provided by the wallrocks. This interpretation is also supported by empirical evidence that changes in wallrock composition along the length of individual gold-bearing veins in Ontario are paralleled by corresponding changes in alteration carbonate mineral composition (Bain, 1933).

Another salient feature of the hydrothermally altered wallrocks and the vein fillings is the extensive development of muscovite. Chemical mass balance calculations clearly demonstrate $K_2O$ addition to the wallrocks, with concomitant $Na_2O$ leaching, suggesting that muscovite was formed consuming hydrothermal potassium

possibly in hydrolysis reaction of sodic plagioclase, releasing sodium into the fluids. This interpretation is also supported by mineralogical evidence such as muscovite replacing plagioclase in the wallrock alteration envelopes. Thus, widespread potassic alteration may imply an initially high K/Na ratio of the fluid. Some of the albite present in the wallrocks could have been stabilized instead of muscovite due to fluid evolution to higher Na/K ratios, via potassium fixation and sodium stripping, coupled with temperature decrease under reducing conditions (Fyfe and Kerrich, 1984). Ba and Rb abundances clearly increase as shown by chemical mass balance calculations, following $K_2O$ in the muscovite rich wallrocks, attributed to similarities in ionic size (Krauskopf, 1967) implying that the two trace elements were also carried in solution by the mineralizing fluids.

Hydrolysis of plagioclase to form muscovite involves loss of $H^+$ from the solution as exemplified by the reaction (Kerrich and Fyfe, 1981):

$$3NaAlSi_3O_8 + K^+ + 2H^+ \longrightarrow KAl_3Si_3O_{10}(OH_2) + 6SiO_2 + 3Na^+$$

The ubiquitous develpment of muscovite in the hydrothermal halo to the veins may indicate a solution of low pH (Kerrich and Hodder, 1982). Furthermore, such a reduction

in the $H^+$ concentration may lead to the precipitation of carbonate minerals by increasing the $CO_3^{2-}$ concentration of the hydrothermal fluid (Holland and Malinin, 1979).

The ore-fluid was apparently saturated with respect to silica carried in solution, probably dominantly as $Si(OH)_4$, and precipitation appears to have been simply due to cooling, and pressure drop, based on silica solubility constraints (Holland and Malinin, 1979). The chemical distribution trends across alteration envelopes in the wallrocks depicted in the Figures 15,16,17, and 18 seem to be conflicting in the case of $SiO_2$. For instance, one traverse adjacent to the Renabie vein suggests that silica was quantitatively added to wallrocks whereas other traverses across different sections of the same vein, and across another vein, suggest that silica was leached from wallrocks. One interpretation is that silica was locally liberated by the circulating fluids during wallrock alteration (Golding and Wilson, 1983), only to be transported and subsequently precipitated in alterated rock along different sections of the vein or in the vein itself.

Chemical mass balance calculations across the wallrocks to the Campbell vein suggest silica addition, which agrees with most trends in hydrothermal veins precipitated from

ascending fluids (Kerrich and Fyfe, 1981), and alteration patterns of Archean lode gold deposits (Kerrich and Hodder, 1982).

Reduced hydrogen species may also have been contained in the ore-forming solutions as attested by the reduction of primary ferric iron immediately adjacent to the veins compared to iron in relatively unaltered wallrocks. Reduction of ferric iron in the wallrocks also implies interaction with ascending fluids (Kerrich et al., 1977; Studemeister, 1983).

The chemical composition of the ore fluid is reflected in the following reactions (Studemeister, 1983), which represent fluid and trondhjemitic and metabasaltic wallrock interaction:

$$20(0.9NaAlSiO_8 \cdot 0.1CaAl_2Si_2O_8) \quad \text{(plagioclase)}$$

$$+ 2K_2(Mg,Fe)_5Al_4Si_5O_{20}(OH)_4 \quad \text{(biotite)}$$

$$+ 2K_2O + 12H_2O + 2CO_2 \longrightarrow 4K_2Al_6Si_6O_{20}(OH)_4 + 32SiO_2$$
$$\text{(fluid)} \quad \text{(fluid)} \quad \text{(fluid)} \quad \text{(muscovite)} \quad \text{(quartz)}$$

$$+ (Mg,Fe)_{10}Al_4Si_6O_{20}(OH)_{16} + 2CaCO_3$$
$$\text{(chlorite)} \quad \text{(calcite)}$$

$$+ NaAlSi_3O_8 + 8Na_2O \quad \text{(fluid)}$$

$$Ca_2(Mg,Fe)_5AlSi_7O_{22}(OH)_2 + 2Ca_2Al_3Si_3O_{12}(OH)$$
$$\text{(Hornblende)} \quad \text{(Epidote)}$$

$$+ \underset{\text{plagioclase}}{NaAlSi_3O_8} + \underset{\text{fluid}}{K_2O} + \underset{\text{fluid}}{6CO_2} + \underset{\text{fluid}}{4H_2O} \longrightarrow$$

$$\underset{\text{chlorite}}{(Mg,Fe)_5Al_3Si_2O_{10}(OH)_8} + \underset{\text{muscovite}}{K_2Al_6Si_6O_{20}(OH)4}$$

$$+ \underset{\text{calcite}}{6CaCO_3} + \underset{\text{quartz}}{11SiO_2} + \underset{\text{fluid}}{Na_2O}$$

## 6.3 Temperature and Pressure of Deposition

Fluid inclusion data indicate that the ore fluid was not "boiling" at the time of trapping. Thus, fluid pressure at the time of trapping was greater than the lithostatic pressure, otherwise the fluid would have been "boiling" (Roedder and Bodnar, 1980). The homogenization temperature is therefore a minimum estimate of the trapping temperature. To obtain the trapping temperature of inclusions a pressure correction must be made. Trapping pressures can often be ascertained on the basis of stratigraphic reconstruction or independent mineralogical methods such as sphalerite geobarometry (Hutchinson and Scott, 1981), permitting introduction of the necessary pressure correction. Conversely, if the homogenization temperature and an independent specific temperature are known, fluid inclusion data can be used to estimate trapping pressures. Roedder (1984) believes that trapping pressure determinations based on inclusions containing liquid $CO_2$ and $H_2O$, either as separate or as composite inclusions, bear high levels of uncertainty and error as a

result of both theoretical and practical considerations.

Fluid inclusion homogenization data allow estimation of a minimum temperature for vein formation. The majority of homogenization temperatures from primary inclusions in vein quartz are in the range of 230° to 330°C. Corrections to these homogenization temperatures would be of the order of +100°C and +170°C for fluid pressures of 1 Kbar (100 MPa) and 2 Kbar (200 MPa), respectively, given a 1-5 wt.% NaCl aqueous solution (Figures 28,29) (Potter, 1977). However, the effect of $CO_2$ is to reduce the corrections to be applied to homogenization temperatures. In light of this discussion, fluid inclusion homogenization temperatures suggest a minimum temperature for vein formation of 300°C.

The temperature regime of vein mineralization can also be estimated on the basis of thermal stability fields for minerals of the wallrock alteration envelopes. The gold-bearing veins are enveloped by halos of alteration assemblages, indistinguishable from those produced by greenschist facies metamorphism. A greenschist wallrock alteration assemblage may imply that gold was concentrated under conditions of greenschist metamorphism. The coexistence of abundant chlorite, actinolite and epidote with albite in mafic metavolcanic rocks adjacent to the veins provides an upper limit for temperature of vein

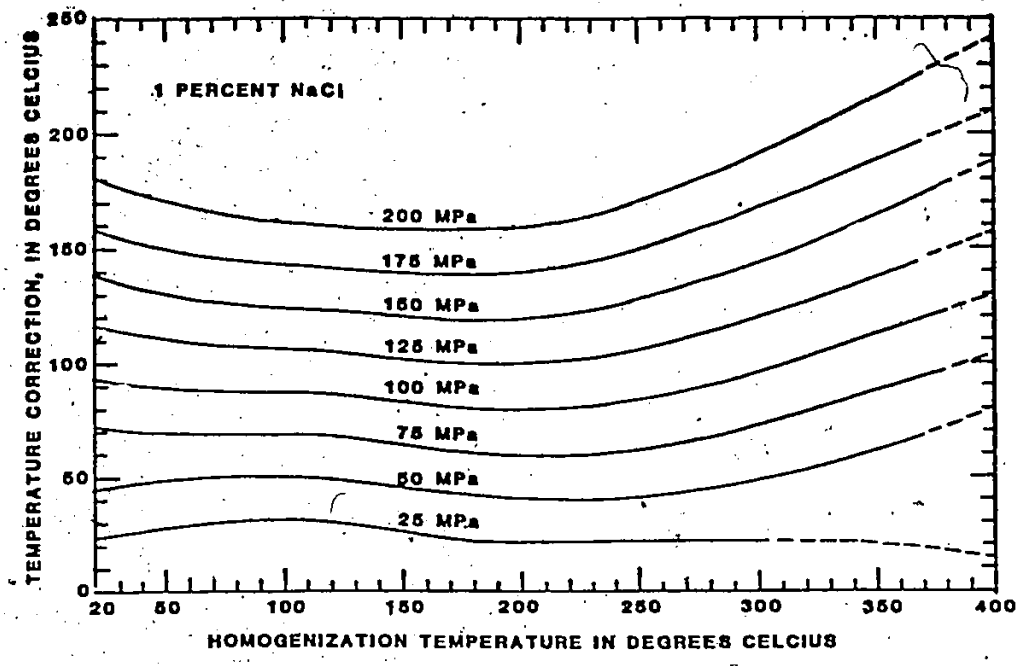


Figure 28 : Temperature correction for a 1-percent NaCl solution as a function of homogenization temperature and pressure (after Potter, 1977).

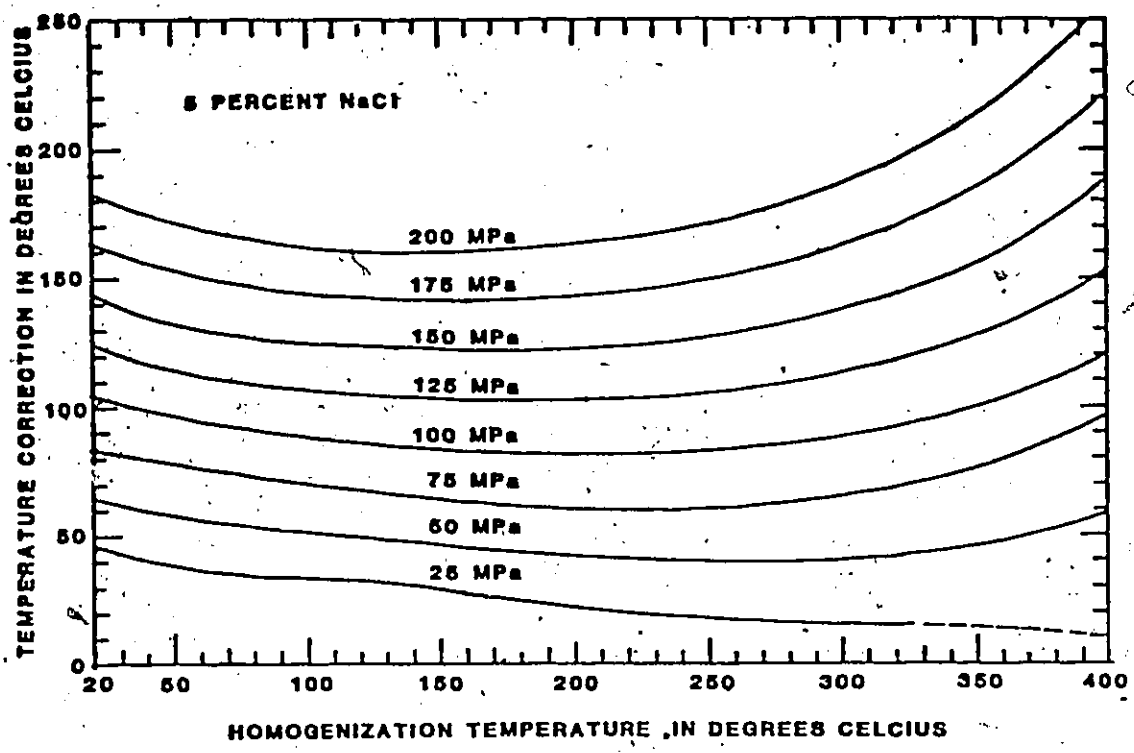


Figure 29 : Temperature correction for a 5-percent NaCl solution as a function of homogenization temperature and pressure (after Potter, 1977).

formation of approximately 470°C at P = 2 Kbar (Liou et al., 1974).

The greenschist envelopes around the gold-bearing veins are products of hydrothermal alteration that was concomitant with vein filling and most likely with gold precipitation. This alteration is thought to follow the emplacement of the batholith inasmuch that it is also superimposed on the batholithic rocks. The similarity of these wallrock alteration assemblages to the assemblage that was superimposed on the mafic metavolcanic rocks and the batholith possibly suggests that hydrothermal alteration about gold-bearing veins and gold concentration were coeval with regional greenschist metamorphism (Studemeister, 1983), which partly retrograded the batholith and the adjacent amphibolites. In this context the gold-bearing quartz - muscovite - carbonate veins about the margin of the batholith are local manifestations of intense retrogression of trondhjemite (tonalite) and amphibolite inasmuch as fracture systems and geological contact areas are zones readily accessible to circulating fluids.

Unconditional direct evidence on pressure or crustal depth at which the gold-bearing veins formed is lacking. However, based on the premise that the veins formed under greenschist facies conditions and considering a temperature

of 500°C for the greenschist-amphibolitic transition (Liou et al., 1974; Turner, 1981), maximum pressures of 2.5 to 3 Kb and depths of 8 to 10 km are indicated, in light of a steeper Archean geothermal gradient (Figure 30).

## 6.4 Possible Source of the Ore-Fluid

The oxygen isotope compositions of quartz from different sections of the Renabie vein, and from the Braminco No. 21 vein, have a restricted range of $\delta^{18}O$ values from +9.4 to +11.2°/oo, implying some common characteristics in the ore- forming process. These values are relatively lower compared to $\delta^{18}O$ from gold-bearing veins in the Yellowknife, Timmins and Val d'Or districts which range from +11.29 to +15.77 (Fyfe and Kerrich, 1984). The reason for low $\delta^{18}O$ values in the present situation is most likely to be due to later reaction of the quartz with a fluid containing light oxygen (i.e. modified meteoric water, seawater, or evolved ground water). This is in agreement with the fluid inclusion data that indicate the presence of a $CO_2$-poor, low to moderate salinity, and low temperature fluid that was trapped in type III inclusions.

The lowered oxygen isotope composition of the Renabie area vein quartz might also be due to $CO_2$ separation from the hydrothermal fluid. Fluid inclusion evidence suggest that

Figure 30 : An estimated Archean geotherm(after Lambert, 1976) compared with the present-day intraplate geotherm (after Clark and Ringwood, 1964).

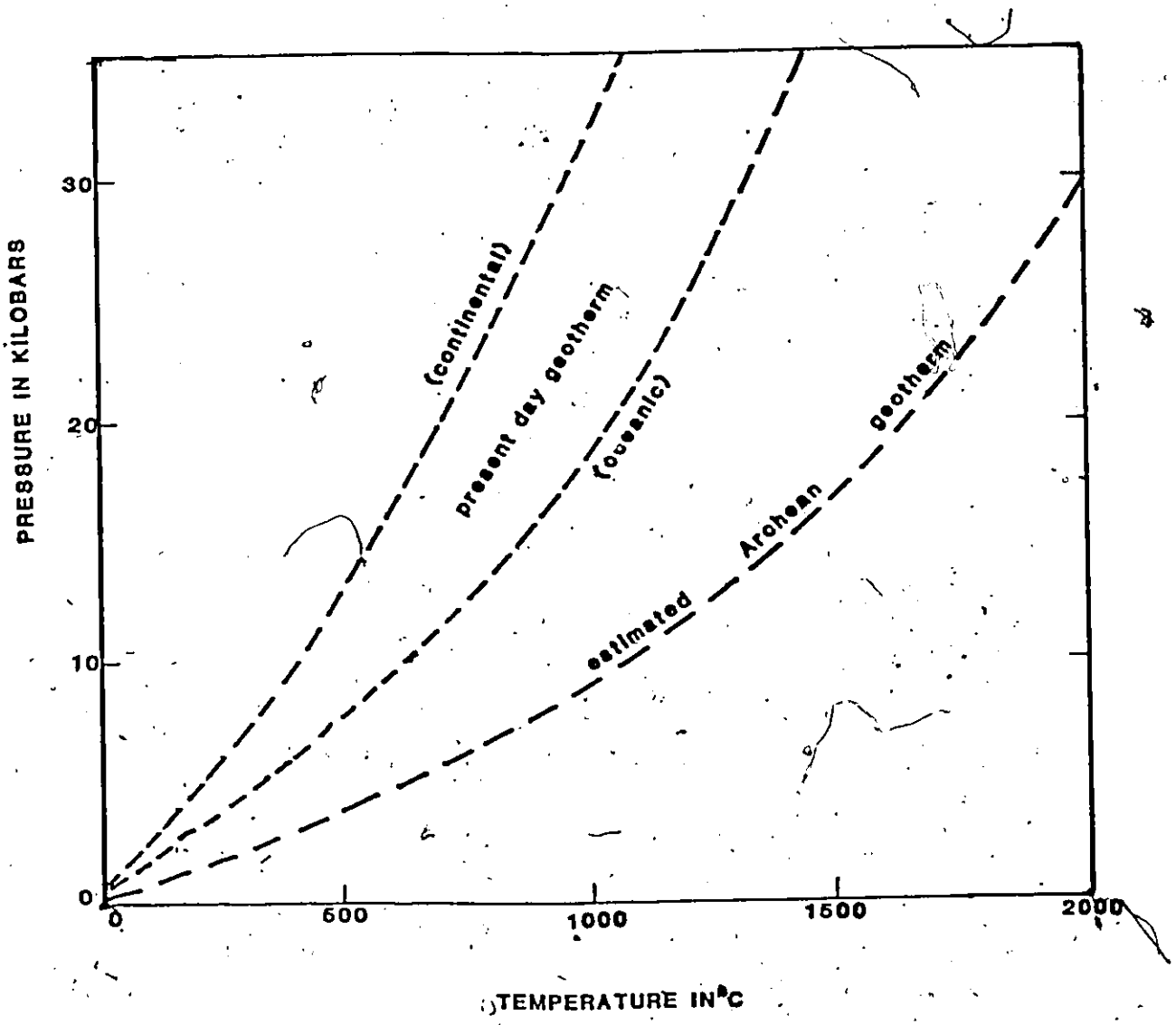

the hydrothermal fluid that precipitated quartz, and probably gold, in the Renabie area was depleted in $CO_2$, most likely through its fixation in altered wallrock carbonates. Such a chemical change would lower the oxygen isotope composition of the residual fluid and the quartz precipitated from it, inasmuch that $CO_2$ is preferentially enriched in $^{18}O$ relative to $H_2O$ (Higgins and Kerrich, 1982). According to the same authors a depletion of up to 7°/oo in $^{18}O$ may occur as a result of a 40 mol.% $CO_2$ loss from hydrothermal fluid.

The calculated $\delta^{18}O$ values for the ore-fluid range from +4°/oo to +7°/oo, for apparent temperatures of 350°C-400°C, and they are consistent with the range of most fluids implicated in metamorphism (Taylor, 1974). These values are isotopically heavy compared to seawater that has undergone high-temperature exchange with the oceanic crust (Kerrich and Hodder, 1982), but they fall in the field of magmatic waters (Taylor, 1974). A metamorphic origin is consistent with the greenschist facies mineralogy of alteration halos to the veins. A magmatic origin is less likely because the veins demonstrably transect and postdate the batholith and the metavolcanic rocks and are broadly contemporaneous with an Archean metamorphic and deformation event that affected the Wawa greenstone belt. For Yellowknife gold-bearing veins where the estimated $\delta^{18}O$ of

the fluid falls within the magmatic range, it ccan be shown that they are isotopically distinct from coeval felsic igneous rocks, suggesting that magmatic fluids are not implicated (Kerrich, 1980). The stable isotope compositions of Archean gold-bearing veins in Canada suggest a metamorphic origin (Fyfe and Kerrich, 1984).

A metamorphic origin is also suggested by the inferred temperature, redox and chemical characteristics of the fluids that deposited gold in quartz veins of the Renabie area. These fluids were at temperatures of 300°C to 470°C, possessed overall low salinity, low pH, high initial K/Na; and contained elevated $CO_2$ contents along with reduced gas species, most probably $H_2$. These characteristics are all consistent with a metamorphic fluid reservoir (Fyfe and Kerrich, 1984). Metamorphic fluids of significant volumes can be generated during burial of a hydrated greenstone succession within the greenschist facies or at the greenshist-amphibolite transition through dehydration reactions (Fyfe et al., 1978; Fyfe and Kerrich, 1984).

Archean greenstone successions deposited in submarine environments become hydrated and carbonated via extensive chemical interaction with seawater. Oxygen isotope evidence from Archean terrains in Canada suggest essential conversion of basalt to hydrated phases such as clays plus

zeolites, at low temperature in the presence of marine water (Kerrich, et al., 1981). Furthermore, altered submarine mafic volcanics contain as much as 3% $CO_2$, most likely incorporated through marine carbonate into cooling basalts (Aumento et al., 1976). Rocks of basaltic composition undergoing metamorphism at the greenschist-amphibolite transition which takes place at about 500°C release 5 wt.% structural water and other volatiles including $CO_2$, producing enormous volumes of $H_2O$-$CO_2$ high-temperature fluids (Fyfe and Kerrich, 1984). Such metamorphic fluids will tend to have a relatively low chlorine content, because of the low Cl-abundance of basaltic rocks (Turekian and Wedepohl, 1961).

Thus, a metamorphic reservoir of basaltic composition, under conditions of the greenschist-amphibolite transition, satisfies the observed fluid temperatures; low salinities and $CO_2/H_2O$ ratios. In addition, such a metamorphic reservoir accounts for the requirements of fluids generated under reducing conditions at elevated temperatures and pressures.

The disposition of metamorphic facies in the eastern part of the Wawa greenstone belt reveals that greenschist-grade rocks of basaltic composition predominate (Riley, 1971; Bennett, 1978), whereas rocks at amphibolite facies,

retrograded to greenschist in the case of the Renabie area, are rare and restricted to the vicinity of igneous intrusions. This is similar to metamorphic facies distribution throughout the length of the Wawa belt (Goodwin, 1961; Studemeister, 1983). These observations may suggest that the metamorphic fluids implicated in gold mineralization in the Renabie area were derived from dehydration reactions during greenschist facies metamorphism of the greenstone succession, or at the greenschist- amphibolite transition.

There exists a lot of evidence suggesting that Archean gold was concentrated in quartz veins from metamorphic fluids (Kerrich, in press), rather than from circulation of marine water (Hodgson and MacGeehan, 1982), or from magmatic fluids (Hodgson and MacGeehan, 1981), or through lateral secretion of vein material from the enclosing rocks (Boyle, 1979). The association of the Renabie deposit with a mesozonal felsic batholith is quite unusual in terms of occurrence of Archean vein gold deposits which are mostly hosted by greenstone succesions or by epizonal felsic stocks. This may imply that, alternatively, a magmatic source could possibly account for the gold-bearing fluids which formed the Renabie area gold deposits. However, in light of the overwhelming evidence presented here, and even though a magmatic signature cannot be completely excluded,

these deposits can be comprehensively explained using the metamorphic model.

## 6.5 Mechanism of Precipitation

Many factors operate to control the precipitation and concentration of a solute carried in solution. However, precipitation will occur as a result of a state of disequilibrium. The physical environment changes in an attempt to reach equilibrium with the new conditions and consequently the fluid may precipitate solutes. Under favorable conditions this may involve the precipitation of native gold together with quartz.

A state of disequilibrium may be caused by many factors such as temperature decline. A temperature decline during vein formation can be inferred from fluid inclusion homogenization data for the $CO_2$-bearing inclusions (Figure 32). A drop in temperature will affect the solubility of solutes (e.g. Au) leading to precipitation. Solubility experiments by Henley (1973) revealed that the solubility of gold in 10 wt.% chloride solutions drops dramatically from 1000 ppm or 500 ppm at T = 500°C to about 10 ppm at T = 300°C.

Gold could be carried in solution as a reduced thio-complex

(Seward, 1973). In the case of the studied deposits, a considerable concentration of sulphur is indicated in the hydrothermal fluids, based on the presence of ubiquitous pyrite, both in the wallrocks and in the vein fillings, implying a S species as the complexing reagent for gold. According to Seward (1973) $HS^-$ is likely to be the most important ligand compared to other candidates such as $S^{2-}$ and $H_2S$. If gold was carried in solution as a thio-complex, precipitation could have been induced by the extraction of sulphur from the solution due to wallrock reactions, coupled with a declining temperature and a change in pH. A decrease in the total sulphur in solution could precipitate gold by destabilizing the reduced gold-sulphur complexes, according to the following reaction (Fyfe and Kerrich, 1984):

$$4HAu(HS)_2 + 2H_2O \longrightarrow 4Au + 8H_2S + O_2$$

However, there is but little experimental data for the above reaction at high temperatures (>300°C). Furthermore, a low fluid pH, as it may be indicated by the extensive muscovitic alteration (Kerrich and Hodder, 1982; Fyfe and Kerrich, 1984), typical of the Renabie area gold deposits, is considered to be an incommensurate condition with the stability of bisulphide complexes for transport of gold (Barnes, 1979, p. 408).

Reactions between the fluids and the presence of cool

wallrocks to fluid-bearing fractures can also lead to thermal decay of the fluid and to a disequilibrium state of gold complexes, triggering the precipitation of gold. Fluid/wallrock reactions would be favorised by the anhydrous mineralogy of the amphibolitic and trondhjemitic wallrocks, which are characterized by high susceptibility to hydration and $CO_2$-fixation reactions.

If wallrock reactions lead to precipitation of gold (Fyfe and Kerrich, 1984), in addition to temperature change, then it is possible that gold may be transported in solution as a carbonyl (CO) or carbonyl-chloride complex (COCl) and fluid/wallrock reaction involving $CO_2$ fixation in carbonates would lead to precipitation of gold, by reduction of $PCO_2$ and/or decrease of acidity (Kerrich and Fyfe, 1981). Experiments on carbonate equilibria (Winkler, 1976; Fyfe et al., 1978; Turner, 1981) show that greenschist conditions appear optimum for carbonate formation involving a $CO_2$-bearing metamorphic fluid.

Thus, a drop in temperature and wallrock reactions are considered here to be important in the concentration of gold around intrusive rocks in the Renabie mine area.

## 6.6 Age of Mineralization

The Renabie gold deposit was formed in the late Archean at about 2688 Ma according to a model lead age based on a new lead evolution model for ore leads of the Superior Province (Thorpe, 1982 and personal communication). Another model (Stacey and Kramers, 1975) provides a very similar 2692 Ma model age. The Thorpe's (1982) model was developed from a paleoisochron defined by lead isotope analyses of galena from Superior Province massive sulphide and gold deposits. A metallogenic epoch for gold deposits was defined on the basis of the new Superior Province model at 2656 to 2700 Ma and formation of the Renabie deposit was apparently during this epoch. The period between 2685 and 2700 Ma was a general span of time for regional metamorphism and deformation in the eastern Wawa greenstone belt, as indicated by U-Pb zircon dating (Percival and Krogh, 1983). This geochronological evidence indicates that the Renabie deposit, and apparently the adjacent gold-bearing veins, were broadly coeval with regional greenschist metamorphism that affected the Archean and was dated near Lochalsh (Figure 2).

# CHAPTER 7

## 7. CONCLUSIONS

1. The Archean greenstone sequence ( 2750 - 2740 Ma) near the Renabie mine experienced metamorphism to the lower amphibolite facies, perhaps coeval with emplacement of the Missinaibi Lake Batholith ( 2707 Ma). This was followed by partial retrogression of the batholith and the adjacent amphibolites to the greenschist facies during subsequent regional metamorphism (2700 - 2685 Ma), involving carbon dioxide-bearing hydrothermal fluids.

2. The Renabie Gold Mine and adjacent gold properties have late Archean (2692 - 2688 Ma) gold-bearing quartz - muscovite - carbonate veins that occupy dilation fractures filled with mineral precipitates and minerals produced by reactions between wallrocks and circulating hydrothermal fluids.

3. The alteration envelopes around the gold-bearing veins were products of hydrothermal activity that was concomitant with gold concentration and vein filling under conditions of greenschist metamorphism at

temperatures of T = 300°C to 470°C and maximum pressures of P = 2 - 3 Kb, at depths of 8-10 km.

4. Hydrothermal solutions forming the Renabie deposit and adjacent gold-bearing veins were high temperature ascending aqueous fluids of metamorphic origin that possessed overall low salinities, probably low pH, and high initial K/Na ratios, and contained significant quantities of $CO_2$, along with molecular hydrogen ($H_2$).

5. An early, almost pure $CO_2$ fluid was first to evolve. This fluid was depleted in $CO_2$ through its fixation in altered wallrock and vein-filling carbonates, giving rise to $CO_2$ - $H_2O$ solution with about 20 wt.% $CO_2$.

6. The distribution of gold-bearing veins in the Renabie mine area is partly controlled the anhydrous mineralogical compositions of trondhjemite (tonalite) and amphibolite, which makes them susceptible to hydration and $CO_2$-fixation when exposed to hydrothermal fluids.

7. A temperature decline and wallrock reactions, involving fixation of hydrothermal $CO_2$ in alteration

carbonates, were important in the concentration of gold in quartz - muscovite - carbonate veins in the Renabie mine area.

## REFERENCES


Abbey, S., 1977, Studies in standard samples for use in the general analysis of silicate rocks and minerals. Geological Survey of Canada Paper 77-34.

Armbrust, G.A., 1980, Geology of the Jogran Disseminated Cu-Mo Deposit, Ryan Township, Ontario. pp. 11-15 in Geoscience research grant program, summary of research 1979-1980, ed. E.G. Pye, Ontario Geological Survey, Miscellaneous Paper 93, 263p.

Attoh, K., 1980, Stratigraphic relations of the volcanic sedimentary successions in the Wawa greenstone belt, Ontario. Geological Survey of Canada, Paper 80-1A, pp. 101-106.

Aumento, F., Mitchell, W.S., and Fratta, M., 1976, Interaction between seawater and oceanic layer two as a function of depth and time. I. Field evidence. Canadian Mineralogist, vol. 14, pp. 269-290.

Bain, G.W., 1933, Wallrock mineralization along Ontario gold deposits. Economic Geology, vol. 28, pp. 705-745.

Barker, F., 1979, Trondhjemite: definition, environment and hypotheses of origin. In: Trondhjemites, Dacites and Related Rocks, ed. F. Barker, Elsevier, Amsterdam, 659p.

Barnes, H.L., 1979, Solubilities of ore minerals. In: Geochemistry of hydrothermal ore deposits, 2nd edition, pp. 236-277, ed. H.L. Barnes, Wiley, New York.

Bennett, G., 1978, Geology of the Crooked Lake Area, District of Sudbury. Ontario Geological Survey, Report 172, 46p.

Boyle, R.W., 1979, The geochemistry of gold and its deposits; Geological Survey of Canada, Bulletin 280, 584 p.

Bozzo, A.T., Chen, H.S., Kass, J.R., and Barduhn, A.J., 1975, The properties of the hydrates of chlorine and carbon dioxide. Desalination, vol. 16, pp. 303-320.

Bruce, E.L., 1944, Geology of the Rennie-Leeson area. Ontario Department of Mines, vol. 51, pt. 8, pp. 1-26 (published 1944).

Bruce, E.L., 1948, Renabie Mine. In: Structural Geology of Canadian Ore Deposits, Canadian Institute of Mining and Metallurgy, (Geology Division) Symposium, January 1948, pp. 436-438.

Burruss, R.C., 1981, Analysis of phase equilibria in C-O-H-S fluid inclusions. In: Fluid Inclusions: Applications to Petrology, ed. L.S. Hollister and M.L. Crawford, Mineralogical Association of Canada Short Course Handbook, vol. 6, pp. 39-74.

Burwash, E.M., 1937, Geology of the Lochalsh-Missinaibi area. Ontario Department of Mines, vol. 44, pt. 8, pp. 27-38 (published 1937).

Canadian Mines Handbook, 1984, ed. M.R. Brown, Northern Miner Press Limited, 444p.

Clark, S.P. and Ringwood, A.E., 1964, Density distribution and constitution of the mantle. Rev. Geophys., vol. 2, pp. 35-88.

Clayton, R.N., O'Neil, J.R., and Mayeda, T.K., 1972, Oxygen isotope exchange between quartz and water. Journal of Geophysical Research, vol. 77, pp. 3057-3067.

Collins, P.L.F., 1979, Gas hydrates in $CO_2$-bearing fluid inclusions and the use of freezing data for estimation of salinity. Economic Geology, vol. 74, pp. 1435-1444.

Colvine, A.C., and Marmont, S., 1981, Early Precambrian porphyry deposits. pp. 242-247 in Summary of Field work, 1981 by the Ontario Geological Survey, ed. J. Wood, O.L. White, R.B. Barlow, and A.C. Colvine, O.G.S. Miscellaneous paper 100, 258p.

Craig, H., 1961, Standards for reporting concentrations of deuterium and oxygen $^{18}O$ in natural waters. Science, vol. 133, pp. 1833-1834.

De Jongh, W.K., 1973, XRF analysis applying theoretical matrix corrections (Stainless). X-Ray Spectrometry, vol. 2, pp. 151-158.

Eugster, H.A. and Skippen, G.B., 1967, Igneous and metamorphic reactions involving gas equilibria. In: Researches in Geochemistry, vol. 1, pp. 492-520, ed. P.H. Abelson, Wiley, New York.

Ferguson, S.A., 1968a, Renabie Mines Limited, Nudulama Mines Limited, and Adjoining Properties, Surface Geology, Parts of Rennie, Leeson and Brackin Townships, District of Sudbury. Ontario Department of Mines, Prelim. Geol. Map No. P. 492, scale 1:500.

Ferguson, S.A., 1968b, Renabie Mines Limited, Nudulama Mines Limited, and Adjoining Properties, Cross Sections and Level Plans, Leeson Township, District of Sudbury. Ontario Department of Mines, Prelim. Geol. Map No. P. 493, scale 1:500.

Freeman, E.B., ed., 1979, Geological highway map of northern Ontario. Ontario Geological Survey Map No. 2240.

Frohberg, M.H., 1935, The ore deposits of the Michipicoten area. Ontario Department of Mines, Annual Report, vol. 44, Pt. 8, pp. 39-83.

Frohberg, M.H., 1948, Unpublished Report on the Gold Deposits of the Renabie Mine Area, Ontario. Regional Geologist's Files, Ontario Ministry of Natural Resources, Sault Ste. Marie.

Fyfe, W.S., Price, N.J. and Thompson, A.B., 1978, Fluids in the Earth's Crust. Elsevier, Amsterdam, 383p.

Fyfe, W.S., and Kerrich, R., 1984, Gold: Natural concentration processes. In: "Gold '82": The geology, geochemistry and genesis of gold deposits, ed. R.P. Foster, Special Publication No. 1, Geological Society of Zimbabwe.

Gardiner, M.C., and Low, J.H., 1947, Report of a geological survey of a portion of the Camabie Mines property, Leeson Township, Ontario, November 5, 1947. Ontario Department of Mines, Assessment Work, Toronto File 63A 27.

Gehrig, M., Lentz, H. and Franck, E.U., 1979, Thermodynamic properties of water-carbon dioxide-sodium chloride mixtures at high temperatures and pressures. In: High pressure Science and Technology 1, Physical properties and material synthesis, ed. K.D. Timmerhaus and M.S. Barber, Plenum, New York, pp. 539-542.

Golding, S.D. and Wilson, A.F., 1983, Geochemical and Stable Isotope Studies of the No. 4 Lode, Kalgoorlie, Western Australia. Economic Geology, vol. 78, pp. 438-450.

Goodwin, A.M., 1961, Some aspects of Archean structure and mineralization. Economic Geology, vol. 56, pp. 897-915.

Goodwin, A.M., 1962, Structure, stratigraphy, and origin of iron formations, Michipicoten area, Algoma District, Ontario, Canada. Geological Society of America Bulletin, vol. 73, pp. 561-586.

Gresens, R.I., 1967, Composition - volume relationships of metasomatism. Chemical Geology, vol. 2, pp. 47-65.

Guha, J., Gauthier, A., Vallée, M., Descarreaux, J. and Lange-Brard, F., 1982, Gold mineralization patterns at the Doyon mine (Silverstack), Bousquet, Québec. In: Geology of Canadian Gold Deposits, ed. R.W. Hodder and W. Petruk, Special Volume 24, pp. 50-58.

Harris, D.C., Sinclair, W.D., and Thorpe, R.I., 1983, Telluride minerals from the Ashley Deposit, Bannockburn Township, Ontario. Canadian Mineralogist, vol. 21, pp. 137-143.

Hawkes, H.E., 1980, Geothermal hydrogen. Mining Engineering, vol. 32, No. 6, pp. 671, 675.

Hendel, E.M. and Hollister, L.S., 1981, An empirical solvus for $CO_2 - H_2O - 2.6$ wt.% salt. Geochimica et Cosmochimica Acta, vol. 45, pp. 225-228.

Henley, R.W., 1973, Solubility of gold in hydrothermal chloride solutions. Chemical Geology, vol. 11, p. 37-87.

Higgins, N. and Kerrich, R., 1982, Progressive $^{18}O$ depletion during $CO_2$ separation from a carbon dioxide-rich hydrothermal fluid: evidence from the Grey River tungsten deposit, Newfoundland. Canadian Journal of Earth Sciences, vol. 19, pp. 2247-2257.

Hodgson, C.J. and MacGeehan, P.J., 1981, Gold ore formation at the Campbell and Dickenson Mine, Red Lake Area. Ontario Geological Survey Miscellaneous Paper 98, pp. 132-143.

Hodgson, C.J. and MacGeehan, P.J., 1982, A review of the geological characteristics of 'gold only' deposits in the Superior Province of the Canadian Shield. In: Geology of Canadian Gold Deposits, ed. R.W. Hodder and W. Petruk, Special Volume 24, pp. 211-229.

Holland, H.D. and Malinin, S.D., 1979, The solubility and occurrence of non-ore minerals. In: Geochemistry of Hydrothermal Ore Deposits, pp. 461-508, 2nd edition, ed. H.L. Barnes, Wiley, New York, N.Y.

Hollister, L.S. and Burruss, R.C., 1976, Phase equilibrium in fluid inclusions from the Khtada Lake metamorphic complex. Geochimica et Cosmochimica Acta, vol. 40, pp. 163-175.

Hutchinson, M.N. and Scott, S.D., 1981, Sphalerite geobarometry in the Cu-Fe-Zn-S system. Economic Geology, vol. 76, pp. 143-153.

Kerrich, R., 1980, Archean gold-bearing chemical sediments and veins: a synthesis of stable isotope and geochemical relations. In: Genesis of Archean volcanic - hosted gold-deposits, ed. R.G. Roberts, Symposium, Waterloo, Ontario, March 1980.

Kerrich, R., in press, Geochemistry of Abitibi Belt lode gold deposits. Can. Min. Met. Bull.

Kerrich, R., Fyfe, W.S., and Allison, I., 1977, Iron reduction around gold-quartz veins, Yellowknife District, Northwest Territories. Economic Geology, vol. 72, pp. 657-663.

Kerrich, R., Gorman, B.E., and Fyfe, W.S., 1980, Geochemistry and field relations of lode gold deposits in felsic igneous intrusions. pp. 136-141 in Geoscience research grant program, summary of research 1979-1980, ed. E.G. Pye, Ontario Geological Survey, Miscellaneous Paper 93, 263p.

Kerrich, R., and Fyfe, W.S., 1981, The gold-carbonate association: source of $CO_2$, and $CO_2$ fixation reactions in Archean lode deposits. Chemical Geology, vol. 33, pp. 265-294.

Kerrich, R. and Hodder, R.W., 1982, Archean lode gold and base metal deposits: Chemical evidence for metal separation into independent hydrothermal systems. In: Geology of Canadian Gold Deposits, ed. R.W. Hodder and W. Petruk, Special Volume 24, pp. 144-160.

Kerrich, R., Pryer, B.J., Milner, K., and Pierce, M.G., 1981, The geochemistry of gold-bearing chemical sediments, Dickenson Mine, Red Lake, Ontario: a reconnaissance study. Canadian Journal of Earth Sciences, vol. 18, pp. 624-637.

Krauskopf, K.B., 1967, Introduction to geochemistry. McGraw Hill, Toronto, 721p.

Lambert, R.St.J., 1976, Archean thermal regimes, crustal and upper mantle temperatures, and a progressive evolutionary model for the Earth. In: The Early History of the Earth, ed. B.F. Windlegs, Wiley, New York, pp. 363-376.

Liou, J.G., Kuniyoshi, S., and Ito, K., 1974, Experimental studies of the phase relations between greenschist and amphibolite in a basaltic system. American Journal of Science, vol. 274, pp. 613-632.

MacDonald, A.J., and Spooner, E.T.C., 1981, Calibration of a Lingham TH 600 programmable heating-cooling stage for microthermometric examination of fluid inclusions. Economic Geology, vol. 76, pp. 1248-1258.

Miyashiro, A., 1973, Metamorphism and Metamorphic Belts. George, Allen and Unwin, London, 492p.

Northern Miner, 1978, Refinancing plan for Renabie approved by Rengold, Kilembe. Northern Miner Press, December 14, 1978, vol. 64, No. 40, p. 1,2.

Northern Miner, 1979, Renabie trying to raise $3.5 million to reopen gold mine late next year. Northern Miner Press, July 5, 1979, vol. 65, No. 17, p. 1,6.

Northern Miner, 1983a, Big jump in Renabie reserves and mill expansion is planned. Northern Miner Press, March 10, 1983, vol. 69, No. 1, p. 1,13.

Northern Miner, 1983b, Braminco's Missinaibi gold property slated for full-scale development. Northern Miner press, August 11, 1983, p. 21.

O'Connor, J.T., 1965, A classification for quartz-rich igneous rocks based on feldspar ratios. United States Geological Survey Professional Paper 525-B, pp. 79-84.

Percival, J.A., 1981, Stratigraphic, structural and metamorphic relations between the Wawa and Abitibi subprovinces and the Kapuskasing structural zone near Chapleau, Ontario. In: Current Research, Part A, Geological Survey of Canada, Paper 81-1A, pp. 83-90.

Percival, J.A., and Krogh, T.E., 1983, U-Pb zircon geochronology of the Kapuskasing structural zone and vicinity in the Chapleau-Foleyet area, Ontario. Canadian Journal of Earth Sciences, vol. 20, pp. 830-843.

Potter, R.W., II, 1977, Pressure corrections for fluid-inclusion homogenization temperatures based on the volumetric properties of the system $NaCl-H_2O$. United States Geological Survey Journal Research 5, vol. 5, pp. 603-607.

Reichen, L.E. and Fahey, J.J., 1962, An improved method for the determination of FeO in rocks and minerals including Garnet. U.S.G.S. Geol. Surv. Bulletin 1144-B.

Riley, R.A., 1971, Geology of Glasgow, Meath, and Rennie Townships, Districts of Algoma and Sudbury. Ontario Department of Mines, Report 90, 55p.

Roedder, E., 1962, Studies on fluid inclusions I: Low temperature application of a dual-purpose freezing and heating stage. Economic Geology, vol. 57, pp. 1045-1061.

Roedder, E., 1963, Studies of fluid inclusions II: Freezing data and their interpretation. Economic Geology, vol. 58, pp. 167-211.

Roedder, E., 1965, Liquid $CO_2$ inclusions in olivine bearing nodules and phenocrysts from basalts. American Mineralogist, vol. 50, pp. 1746-1786.

Roedder, E., 1972, The composition of fluid inclusions Chapter JJ. In: Data of Geochemistry, ed. M. Fleischer, 6th edition, United States Geological Survey Professional Paper 440JJ, 164p.

Roedder, E., 1979, Fluid inclusions as samples of ore fluids. In: Geochemistry of Hydrothermal Ore Deposits, pp. 684-737, 2nd edition, ed. H.L. Barnes, Wiley, New York, N.Y.

Roedder, E., 1981, Origin of fluid inclusions and changes that occur after trapping. In: Fluid Inclusions: Applications to Petrology, ed. L.S. Hollister, and M.L. Crawford, Mineralogical Association of Canada Short Course Handbook, vol. 6, pp. 101-137.

Roedder, E., 1984, Fluid inclusion evidence bearing on the environments of gold deposition. In: "Gold '82": The geology, geochemistry and genesis of gold deposits, ed. R.P. Foster, Special Publication No. 1, Geological Society of Zimbabwe.

Roedder, E., and Bodnar, R.J., 1980, Geologic pressure determinations from fluid inclusion studies. Annual Review of Earth and Planetary Science Letters, vol. 8, pp. 263-301.

Rucklidge, J., 1969, Frohbergite, montbrayite, and a new Pb-Bi telluride. Canadian Mineralogist, vol. 9, pp. 709-716.

Seward, T.M., 1973, Thio-complexes of gold and the transport of gold in hydrothermal solutions. Geochimica et Cosmochimica Acta, vol. 37, pp. 370-390.

Shepard, T., 1981, Temperature programmable, heating-freezing stage for microthermometric analysis of fluid inclusions. Economic Geology, vol. 76, pp. 1244-1247.

Smith, F.G., 1953, Historical Development of Inclusion Thermometry. Toronto, Canada. University of Toronto Press, 149p.

Sorby, H.C., 1858, On the microscopic structure of crystals, indicating the origin of minerals and rocks. Quarterly Journal of the Geological Society of London, vol. 14, pt. 1, pp. 453-500.

Sourirajan, S. and Kennedy, G.C., 1962, The system $H_2O$, NaCl at elevated temperature and pressure. American Journal of Science, vol. 260, pp. 115-141.

Spooner, E.T.C., Beckinsale, R.D., England, P.C., and Senior, A., 1977, Hydration $^{18}O$ enrichment , and oxidation during ocean floor hydrothermal metamorphism of ophiolitic metabasic rocks from E. Linguria, Italy. Geochimica et Cosmochimica Acta, vol. 41, pp. 857-871.

Stacey, J.S., and Kramers, J.D., 1975, Approximation of terrestrial lead isotope evolution by a two-stage model. Earth and Planetary Science Letters, vol. 26, pp. 207-221.

Studemeister, P.A., 1983, The greenschist facies of an Archean assemblage near Wawa, Ontario. Canadian Journal of Earth Sciences, vol. 20, pp. 1409-1420.

Takenouchi, S. and Kennedy, G.C., 1964, The binary system $H_2O$-$CO_2$ at high temperatures and pressures. American Journal of Science, vol. 262, pp. 1055-1074.

Takenouchi, S. and Kennedy, G.C., 1965, The solubility of carbon dioxide in NaCl solutions at high temperatures and pressures. American Journal of Science, vol. 263, pp. 445-454.

Taylor, H.P. Jr., 1974, The application of oxygen and hydrogen isotope studies to problems of hydrothermal alteration and ore deposition. Economic Geology, vol. 69, pp. 843-883.

Taylor, H.P. Jr., 1979, Oxygen and hydrogen isotope relationships in hydrothermal mineral deposits. In: Geochemistry of hydrothermal ore deposits, 2nd edition, pp. 236-277, ed. H.L. Barnes, Wiley, New York.

Thorpe, R.I., 1982, Lead isotope evidence regarding Archean and Proterozoic Metallogeny in Canada. Revista Brasileira de Geociecias, vol. 12, No. 1-3, pp. 510-521.

Thorpe, R.I., 1982, Personal communication.

Thurston, D.C., Siragusa, G.M., and Sage, R.D., 1977, Geology of the Chapleau area, Districts of Algoma, Sudbury and Cochrane. Ontario Division of Mines, Geoscience Report 157, 293p.

Touret, J.L.R., 1981, Fluid inclusions in high grade metamorphic rocks. In: Fluid inclusions: Applications to Petrology, ed. L.S. Hollister, and M.L. Crawford, Mineralogical Association of Canada Short Course Handbook, vol. 6, pp. 101-137.

Turek, A., Smith, P.E., and Van Schmus, W.R., 1982, Rb-Sr and U-Pb ages of volcanism and granite emplacement in the Michipicoten belt - Wawa, Ontario. Canadian Journal of Earth Sciences, vol. 19, pp. 1608-1626.

Turekian, K.K., and Wedepohl, K.H., 1961, Distribution of elements in some major units of the Earth's crust. Bulletin of the Geological Society of America, vol. 73, pp. 175-192.

Turner, F.J., 1981, Metamorphic petrology: mineralogical, field, and tectonic aspects. 2nd edition, McGraw-Hill Book Company, New York, 524p.

Wanless, R.K., Stevens, R.D., Lachance, G.R., and Rimsaite, J.Y.H., 1966, Age Determinations and Geological Studies, K-Ar Isotopic Ages. Report 6, Geological Survey of Canada, Paper 65-17, 120p.

Weast, R.C. (ed.), 1974, Handbook of Chemistry and Physics. Chemical Rubber Company Press Inc., Bola Raton, Florida.

White, D.E., 1974, Diverse origins of hydrothermal ore fluids. Economic Geology, vol. 69, pp. 954-973.

Wilson, A.D., 1955, A new method for the determination of ferrous iron in rocks and minerals. Geological Survey of Great Britain Bulletin, vol. 9, pp. 56-68.

Winkler, H.G.F., 1976, Petrogenesis of metamorphic rocks. 2nd edition, Berlin, Springer, 334p.

Zav'yalov, YE.N., and Begizov, V.D., 1977, Rucklidgeite, $(Bi, Pb_3)\ Te_4$, a new mineral from the Zod and Kochkar gold ore deposits. International Geological Review, vol. 19, pp. 1451-1456.

# APPENDIX 1

## SAMPLE LOCATION MAPS

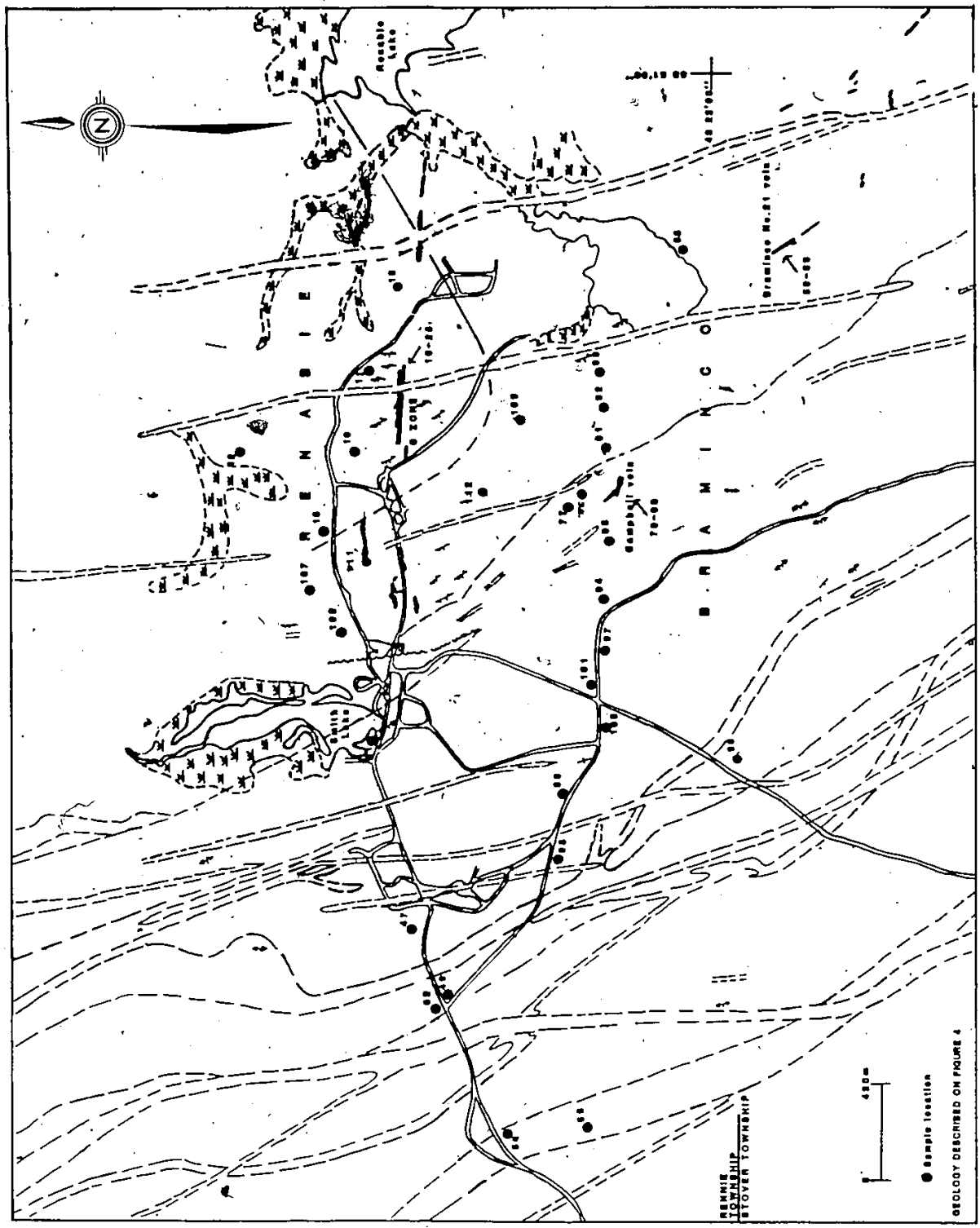
N
RENNIE TOWNSHIP
STOVER TOWNSHIP
Sample location
GEOLOGY DESCRIBED ON FIGURE 4

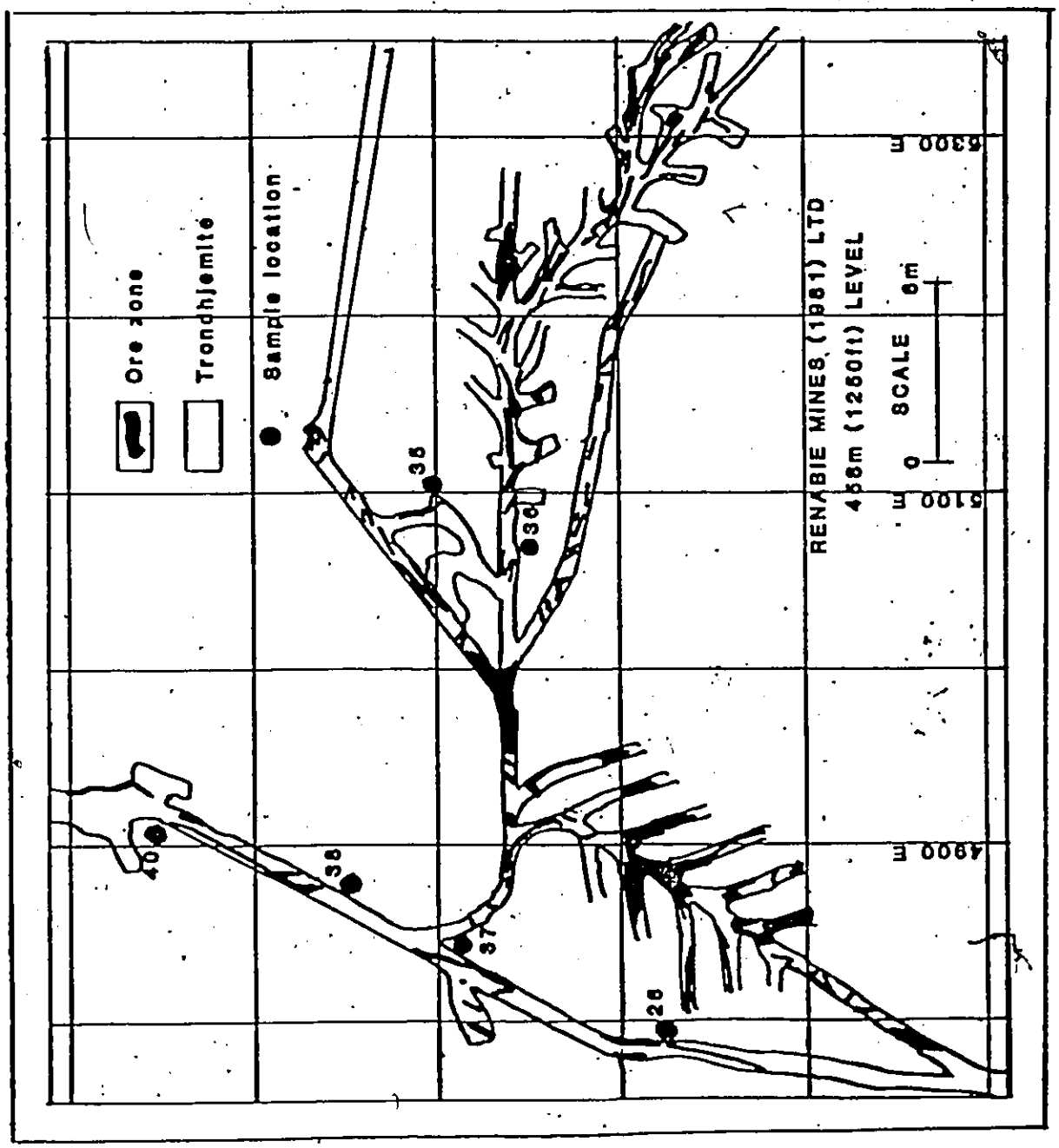
Ore zone
Trondhjemite
Sample location
RENABIE MINES (1981) LTD
458m (1260ft) LEVEL
SCALE
0
8m
5300 E
5100 E
4900 E
40
38
37
35
30
28

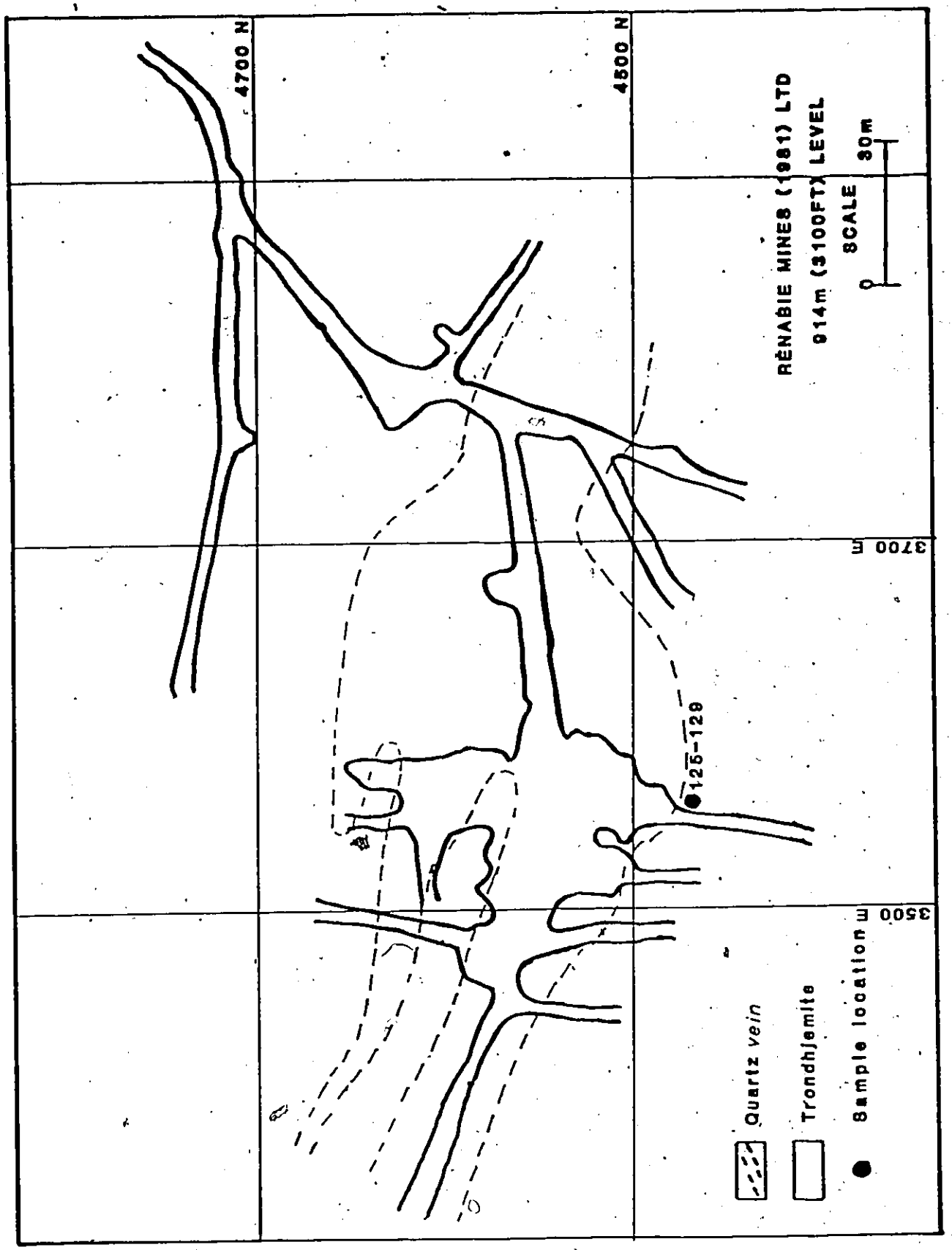
4700 N
4800 N
3700 E
3500 E
RÈNABIE MINES (1981) LTD
914m (3100FT) LEVEL
SCALE
30m
0
125-120
Quartz vein
Trondhjemite
Sample location

# APPENDIX 2

## MAJOR AND MINOR ELEMENT ANALYSES OF TRONDHJEMITE AND TONALITE FROM THE RENABIE AREA

Composition of trondhjemite from the Renabie mine area.

| Sample number | RN-26 | RN-35 | RN-36 | RN-38 | RN-58 |
|---|---|---|---|---|---|
| (wt%) | | | | | |
| $SiO_2$ | 70.88 | 73.88 | 74.09 | 71.57 | 71.83 |
| $Al_2O_3$ | 14.41 | 14.70 | 14.42 | 15.66 | 15.47 |
| $Fe_2O_{3(T)}$ | 2.94 | 2.86 | 1.28 | 2.56 | 1.80 |
| MgO | 1.00 | 0.26 | 0.27 | 0.71 | 0.36 |
| CaO | 3.33 | 2.04 | 1.76 | 2.62 | 1.45 |
| $Na_2O$ | 4.33 | 3.35 | 5.44 | 4.99 | 5.59 |
| $K_2O$ | 1.67 | 0.67 | 1.65 | 1.61 | 1.88 |
| $TiO_2$ | 0.35 | 0.11 | 0.11 | 0.26 | 0.17 |
| $P_2O_5$ | 0.05 | 0.00 | 0.00 | 0.03 | 0.02 |
| MnO | 0.03 | 0.01 | 0.02 | 0.04 | 0.05 |
| S | 0.00 | 0.57 | 0.01 | 0.00 | 0.01 |
| L.O.I | 0.40 | 1.30 | 1.26 | 0.20 | 1.10 |
| TOTAL | 99.29 | 99.71 | 100.41 | 100.37 | 99.85 |
| (ppm) | | | | | |
| Ba | 380 | 333 | 556 | 469 | 506 |
| Cr | 0 | 0 | 0 | 0 | 23 |
| Zr | 135 | 71 | 77 | 119 | 75 |
| Sr | 141 | 194 | 203 | 271 | 225 |
| Rb | 42 | 6 | 25 | 31 | 47 |
| Y | 4 | 2 | 0 | 7 | 7 |
| Zn | 40 | 5 | 15 | 34 | 46 |
| Ni | 0 | 0 | 3 | 0 | 0 |

Composition of trondhjemite from the Renabie mine area.

| Sample number | RN-37 | RN-93 | RN-94 | RN-107 | RN-109 |
|---|---|---|---|---|---|
| (wt%) | | | | | |
| $SiO_2$ | 72.11 | 70.17 | 77.20 | 70.33 | 75.87 |
| $Al_2O_3$ | 14.75 | 16.07 | 12.88 | 14.90 | 13.36 |
| $Fe_2O_{3(T)}$ | 2.43 | 3.25 | 0.71 | 2.15 | 1.44 |
| MgO | 0.49 | 1.00 | 0.04 | 0.50 | 0.19 |
| CaO | 2.67 | 3.30 | 0.92 | 2.44 | 1.87 |
| $Na_2O$ | 5.68 | 5.10 | 5.95 | 4.89 | 5.48 |
| $K_2O$ | 1.00 | 0.94 | 0.40 | 2.00 | 0.81 |
| $TiO_2$ | 0.24 | 0.36 | 0.07 | 0.25 | 0.09 |
| $P_2O_5$ | 0.03 | 0.07 | 0.00 | 0.04 | 0.00 |
| MnO | 0.05 | 0.05 | 0.01 | 0.03 | 0.01 |
| S | 0.00 | 0.00 | 0.01 | 0.01 | 0.01 |
| L.O.I | 0.90 | 0.45 | 1.35 | 2.10 | 0.56 |
| TOTAL | 100.47 | 100.90 | 99.58 | 99.76 | 99.78 |
| (ppm) | | | | | |
| Ba | 405 | 359 | 143 | 469 | 553 |
| Cr | 1 | 2 | 22 | 30 | 9 |
| Zr | 128 | 159 | 34 | 98 | 80 |
| Sr | 298 | 410 | 134 | 378 | 197 |
| Rb | 8 | 12 | 5 | 58 | 0 |
| Y | 0 | 2 | 10 | 8 | 0 |
| Zn | 32 | 46 | 1 | 50 | 2 |
| Ni | 0 | 6 | 0 | 0 | 3 |

Composition of trondhjemite from the Renabie mine area.

| Sample number | RN-40 | RN-91 | RN-92 | RN-108 | RN-111 | RN-112 |
|---|---|---|---|---|---|---|
| (wt%) | | | | | | |
| $SiO_2$ | 73.81 | 74.86 | 74.36 | 71.02 | 71.80 | 71.47 |
| $Al_2O_3$ | 14.85 | 12.60 | 14.28 | 15.97 | 15.64 | 15.64 |
| $Fe_2O_3$(T) | 1.96 | 2.68 | 2.04 | 2.90 | 2.24 | 2.39 |
| MgO | 0.49 | 0.21 | 0.48 | 1.82 | 0.52 | 0.63 |
| CaO | 2.48 | 0.86 | 1.79 | 2.74 | 2.28 | 2.52 |
| $Na_2O$ | 4.86 | 6.21 | 4.33 | 4.24 | 5.37 | 5.07 |
| $K_2O$ | 1.34 | 0.36 | 1.53 | 0.75 | 1.40 | 1.50 |
| $TiO_2$ | 0.19 | 0.07 | 0.24 | 0.47 | 0.22 | 0.25 |
| $P_2O_5$ | 0.02 | 0.00 | 0.00 | 0.05 | 0.01 | 0.01 |
| MnO | 0.03 | 0.00 | 0.03 | 0.08 | 0.04 | 0.04 |
| S | 0.00 | 0.00 | 0.00 | 0.00 | 0.00 | 0.00 |
| L.O.I | 0.94 | 1.47 | 0.71 | 0.89 | 1.00 | 1.07 |
| TOTAL | 100.94 | 100.47 | 99.91 | 101.03 | 100.63 | 100.60 |
| (ppm) | | | | | | |
| Ba | 387 | 113 | 498 | 286 | 510 | 523 |
| Cr | 8 | 12 | 0 | 22 | 2 | 0 |
| Zr | 136 | 47 | 122 | 160 | 120 | 120 |
| Sr | 376 | 122 | 283 | 305 | 272 | 266 |
| Rb | 17 | 0 | 25 | 11 | 19 | 20 |
| Y | 9 | 1 | 1 | 9 | 2 | 6 |
| Zn | 16 | 0 | 13 | 46 | 23 | 30 |
| Ni | 1 | 3 | 0 | 15 | 4 | 0 |

Composition of tonalite from the Renabie mine area.

| Sample number | RN-10 | RN-11 | RN-12 | RN-13 | RN-15 |
|---|---|---|---|---|---|
| (wt%) | | | | | |
| $SiO_2$ | 61.97 | 64.09 | 64.25 | 65.35 | 66.12 |
| $Al_2O_3$ | 16.82 | 14.75 | 15.63 | 15.31 | 15.04 |
| $Fe_2O_{3(T)}$ | 4.88 | 4.04 | 5.94 | 5.22 | 3.66 |
| MgO | 2.51 | 4.08 | 2.69 | 2.26 | 1.70 |
| CaO | 3.23 | 3.97 | 4.87 | 5.19 | 3.80 |
| $Na_2O$ | 5.81 | 4.97 | 4.86 | 3.84 | 3.66 |
| $K_2O$ | 1.93 | 2.33 | 0.87 | 0.86 | 2.92 |
| $TiO_2$ | 0.60 | 0.43 | 0.61 | 0.48 | 0.41 |
| $P_2O_5$ | 0.27 | 0.10 | 0.12 | 0.04 | 0.08 |
| MnO | 0.06 | 0.06 | 0.13 | 0.08 | 0.06 |
| S | 0.02 | 0.01 | 0.01 | 0.00 | 0.00 |
| L.O.I | 1.53 | 0.80 | 0.40 | 1.10 | 2.20 |
| TOTAL | 99.99 | 99.82 | 100.51 | 99.43 | 99.78 |
| (ppm) | | | | | |
| Ba | 1561 | 444 | 342 | 320 | 742 |
| Cr | 24 | 145 | 66 | 29 | 22 |
| Zr | 245 | 145 | 150 | 166 | 133 |
| Sr | 1057 | 575 | 371 | 262 | 108 |
| Rb | 46 | 59 | 15 | 14 | 27 |
| Y | 14 | 5 | 2 | 11 | 1 |
| Zn | 66 | 64 | 68 | 45 | 19 |
| Ni | 44 | 120 | 49 | 18 | 59 |

# APPENDIX 3

## MAJOR AND MINOR ELEMENT ANALYSES OF MAFIC METAVOLCANIC ROCKS FROM THE RENABIE AREA

| Sample number | RN-55 | RN-77 | RN-76 | RN-94 | RN-95 |
|---|---|---|---|---|---|
| (wt%) | | | | | |
| $SiO_2$ | 48.99 | 50.96 | 50.57 | 51.27 | 49.84 |
| $Al_2O_3$ | 14.00 | 12.83 | 13.77 | 12.20 | 15.38 |
| $Fe_2O_{3(T)}$ | 13.00 | 16.21 | 13.03 | 13.74 | 11.74 |
| MgO | 9.23 | 3.86 | 7.60 | 7.92 | 5.02 |
| CaO | 9.27 | 7.42 | 5.09 | 9.68 | 11.88 |
| $Na_2O$ | 2.64 | 3.69 | 4.69 | 1.87 | 1.87 |
| $K_2O$ | 0.51 | 0.08 | 0.68 | 0.17 | 0.19 |
| $TiO_2$ | 0.86 | 1.71 | 1.26 | 0.81 | 0.82 |
| $P_2O_5$ | 0.00 | 0.12 | 0.10 | 0.00 | 0.00 |
| MnO | 0.28 | 0.28 | 0.20 | 0.23 | 0.22 |
| S | 0.00 | 0.00 | 0.00 | 0.00 | 0.01 |
| L.O.I | 1.09 | 2.70 | 2.37 | 1.35 | 3.56 |
| TOTAL | 99.03 | 99.92 | 99.47 | 99.29 | 100.65 |
| (ppm) | | | | | |
| Ba | 152 | 0 | 140 | 36 | 24 |
| Cr | 387 | 63 | 287 | 50 | 356 |
| Zr | 77 | 115 | 101 | 40 | 48 |
| Sr | 175 | 77 | 115 | 78 | 147 |
| Rb | 6 | 0 | 8 | 0 | 0 |
| Y | 13 | 39 | 23 | 9 | 13 |
| Zn | 146 | 129 | 94 | 70 | 57 |
| Ni | 167 | 15 | 100 | 63 | 120 |

| Sample number | RN-41 | RN-47 | RN-49 | RN-52 | RN-54 |
|---|---|---|---|---|---|
| (wt%) | | | | | |
| $SiO_2$ | 50.32 | 50.37 | 53.87 | 48.58 | 49.09 |
| $Al_2O_3$ | 13.52 | 14.39 | 12.48 | 14.25 | 15.34 |
| $Fe_2O_{3(T)}$ | 13.56 | 12.59 | 18.31 | 15.50 | 12.66 |
| MgO | 8.17 | 8.17 | 2.65 | 5.79 | 7.85 |
| CaO | 10.38 | 12.00 | 6.31 | 8.65 | 10.36 |
| $Na_2O$ | 1.98 | 1.40 | 2.88 | 2.30 | 2.89 |
| $K_2O$ | 0.26 | 0.12 | 0.17 | 0.46 | 0.26 |
| $TiO_2$ | 0.87 | 0.77 | 2.25 | 1.42 | 0.77 |
| $P_2O_5$ | 0.00 | 0.00 | 0.10 | 0.03 | 0.00 |
| MnO | 0.22 | 0.20 | 0.26 | 0.23 | 0.18 |
| S | 0.00 | 0.00 | 0.00 | 0.02 | 0.00 |
| L.O.I | 0.63 | 0.72 | 0.19 | 3.61 | 0.81 |
| TOTAL | 99.97 | 100.82 | 99.51 | 100.92 | 100.32 |
| (ppm) | | | | | |
| Ba | 19 | 22 | 0 | 85 | 45 |
| Cr | 110 | 258 | 28 | 138 | 247 |
| Zr | 49 | 47 | 127 | 111 | 58 |
| Sr | 76 | 82 | 45 | 175 | 182 |
| Rb | 0 | 0 | 0 | 8 | 0 |
| Y | 9 | 7 | 43 | 26 | 10 |
| Zn | 63 | 63 | 40 | 108 | 42 |
| Ni | 41 | 90 | 0 | 66 | 153 |

| Sample number | | RN-97 | RN-98 | RN-99 | RN-100 | RN-101 |
|---|---|---|---|---|---|---|
| | (wt%) | | | | | |
| $SiO_2$ | | 49.11 | 48.47 | 50.65 | 49.75 | 52.47 |
| $Al_2O_3$ | | 15.06 | 14.46 | 13.57 | 14.11 | 13.40 |
| $Fe_2O_{3(T)}$ | | 11.04 | 12.53 | 14.98 | 14.62 | 13.21 |
| MgO | | 8.01 | 7.87 | 6.04 | 6.96 | 5.94 |
| CaO | | 11.88 | 12.74 | 9.80 | 9.42 | 9.63 |
| $Na_2O$ | | 1.75 | 1.48 | 2.29 | 2.60 | 2.20 |
| $K_2O$ | | 0.22 | 0.19 | 0.16 | 0.30 | 0.42 |
| $TiO_2$ | | 0.77 | 0.82 | 1.26 | 1.20 | 1.01 |
| $P_2O_5$ | | 0.00 | 0.01 | 0.00 | 0.00 | 0.00 |
| MnO | | 0.21 | 0.25 | 0.24 | 0.27 | 0.23 |
| S | | 0.00 | 0.00 | 0.01 | 0.00 | 0.01 |
| L.O.I | | 1.24 | 1.02 | 0.84 | 1.18 | 1.28 |
| TOTAL | | 99.50 | 99.95 | 99.89 | 100.51 | 99.86 |
| | (ppm) | | | | | |
| Ba | | 82 | 116 | 34 | 97 | 95 |
| Cr | | 375 | 268 | 28 | 182 | 40 |
| Zr | | 51 | 58 | 68 | 71 | 79 |
| Sr | | 125 | 132 | 109 | 102 | 154 |
| Rb | | 0 | 0 | 1 | 0 | 0 |
| Y | | 5 | 17 | 15 | 14 | 15 |
| Zn | | 70 | 104 | 65 | 134 | 91 |
| Ni | | 126 | 123 | 36 | 115 | 26 |

# APPENDIX 4

## FLUID INCLUSION STUDIES

# APPENDIX 4

## 4.1 INSTRUMENTATION, CALIBRATION AND PROCEDURE

### 4.1.1. Instrumentation

Fluid inclusion experiments were conducted using a commercially available TH 600 microthermometric system (Shepard, 1981), manufactured by Linkam Scientific Instruments, 37 Pine Ridge, Carshalton Beeches, Survey SM5 4QQ, England. The apparatus can be programmed to proceed to any temperature between -180 and +600°C at any of 27 different rates of change of temperature between 0.1°C/min. and 90°C/min., and to hold at any temperature. This procedure has the advantages that measurements can be standardized to a known rate of change of temperature and that measurements can be made without continuous manual adjustment. The heating-freezing stage consists of a silver plated thermal block with a sapphire window, and is completely enclosed in a double-walled thermal cell with upper (double) and lower glass window. Thus, thermal gradients are reduced and problems of decomposition products of condensation and frost accumulation at low temperatures, obscuring optical surfaces, are minimized.

The apparatus in this study is mounted on Cooke, Troughton and Simms, Ltd., binocular microscope fitted with long working distance UTK 50/0.63 objective lense.

### 4.1.2 Calibration

The heating-freezing stage was calibrated according to the method described by MacDonald and Spooner (1981). The stage was calibrated between -95°C and +398°C using 13 standard melting point substances. Below room temperature four organic liquids (toluene, chloroform, chlorobenzene, carbon tetrachloride) and distilled water were used. Above room temperature four Merck Sighotherm standards, two solid compounds (napthalene and adipic acid), and three solid inorganic compounds (sodium nitrate, potassium dichromate, barium nitrate) were used. Results of calibration runs are shown on Table A1.

The data obtained from the 13 standards were used to construct the calibration curve which is shown on Figure A2. Error bars are from MacDonald and Spooner (1981). They are estimated on the basis of a combination of standard melting temperature reproducibilities and horizontal thermal gradients. The calibration curve relates a temperature correction factor $\Delta T$, which is the difference between the actual temperature read from the

TABLEA1: Data obtained from 13 selected standards for the calibration of the LINKAM 600 heating-cooling stage.

| SUBSTANCE | MELTING POINT(°C) | $T_{READ}$(°C) | ΔT(°C) |
|---|---|---|---|
| Toluene | -95.0 | -92.7 | -2.3 |
| Chloroform | -63.5 | -61.1 | -2.4 |
| Chlorobenzene | -45.0 | -43.1 | -1.9 |
| Carbon tetra-chloride | -22.8 | -20.8 | -2.0 |
| Distilled water | 0.0 | + 2.0 | -2.0 |
| SK*70 | 70.0 | 71.8 | -1.8 |
| Napthalene | 80.2 | 82.0 | -2.2 |
| SK*100 | 100.0 | 101.3 | -1.3 |
| Adipic acid | 151.4 | 154.5 | -3.1 |
| SK*200 | 200.0 | 198.0 | +2.0 |
| SK*247 | 247.0 | 249.0 | -2.0 |
| Sodium nitrate | 306.8 | 305.6 | +1.2 |
| Potassium di-chromate | 398.0 | 400.0 | -2.0 |

* : Merck Signotherm Standard.

Figure A2 : Calibration curve for a LINCAM TH 600 heating-cooling stage defined by 13 selected standards. Error bars are from MacDonald and Spooner (1981).

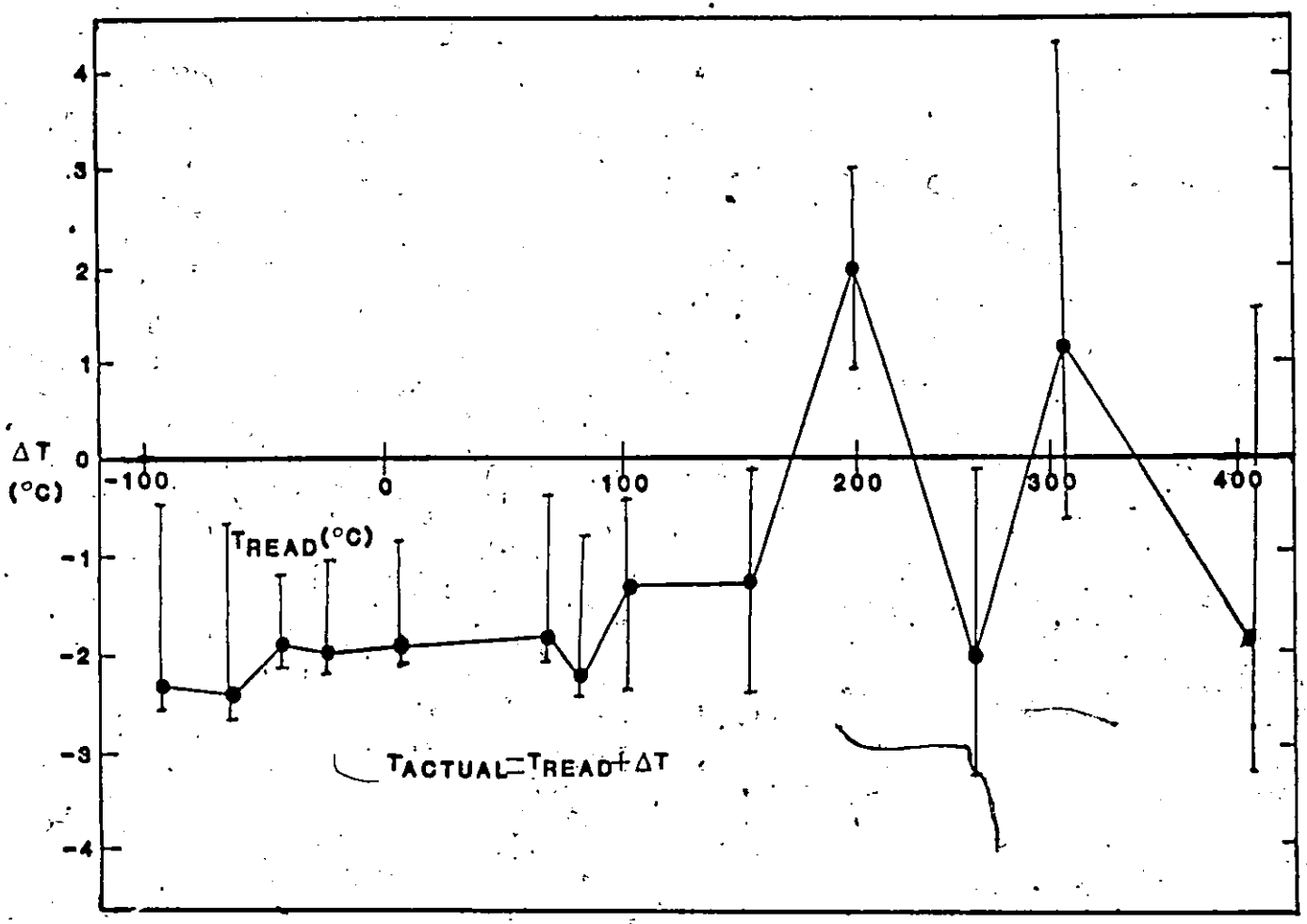

digital read-out of the instrument, to the read temperature. Thus, any read temperature is simply converted to the actual temperature by the addition of the appropriate value for T. Correction factors, $\Delta T$, vary from +2°C to -2°C. Determinations of fluid inclusion are temperatures corrected according to the interpolation between the nearest two calibration points.

### 4.1.3 Procedure

Samples of vein quartz from the 914m and 458m working levels of the Renabie mine and from the surface exposure of the C zone, as well as from the Braminco No. 21 and Campbell veins, were collected and studied in doubly polished 0.15mm to 0.5mm thick plates. Samples from the Renabie and the Braminco No. 21 veins were intimately associated with gold and/or telluride mineralization.

A petrographic examination was initially carried out on the polished slabs and small areas favorable for fluid-inclusion study were identified. Fluid inclusion characteristics, namely morphology (size, shape, etc.) mode of occurence and appearance at room temperature were noted and photographed. Areas containing several usable inclusions (large size, subrounded shape, "flat", distinguishable phases) were broken from the larger slab

and used in heating and freezing stage experiments.

Heating and freezing runs were carried out once per fragment observing 1-3 inclusions each time. Reheating the same chip could destroy internal equilibrium of the inclusions by thermally deforming the host crystal and thus altering the physical and chemical nature of the trapped fluid.

Individual inclusions were first frozen down to -90°C. Subsequently they were heated up until temperatures of 400°C were reached. Over this temperature range the following significant phase transitions could take place depending on the composition of the inclusions: a) melting of frozen $CO_2$, b) melting of ice, c) melting of $CO_2$ clathrate compounds, d) homogenization of the $CO_2$ phase (liquid and gas), e) total homogenization.

## 4.2 A graphical technique for the estimation of the bulk composition (molar percentage) of $CO_2$-$H_2O$ fluid inclusions (after Burruss, 1981).

This method uses the relative volume percentage of the participating $H_2O$ and $CO_2$ phases, estimated visually and it is based on the following:

a) At temperatures slightly greater than the $CO_2$ critical point (i.e. +31 T 50°C) the coexisting phases are pure end members.

b) The bulk molar volume (VB) of an inclusion, which is related to the bulk density ( B) as: $B=1/VB \times 10^3$ is a linear combination of the end member components: in other words:

VB: $X_iV_i + X_2V_2$ where

VB: bulk molar volume

$X_i$: mole fraction of pure phase i

$V_i$: molar volume of pure phase i

c) The $H_2O$ phase is incompressible up to -40°C.

Based on these assumptions the bulk composition (molar percentage) can be estimated as follows: The $CO_2$ liquid-vapour homogenization temperature defines the $CO_2$ density (Figure A3) and the corresponding one-phase $CO_2$ fluid isochore. The observed $CO_2$ phase density fixes the pressure inside a given inclusion at 40°C (Figure A4), and this pressure fixes the bulk density (moles/liter) of the inclusion based on the estimated volume percentage of the $H_2O$ phase in the inclusion (Figure A5). The bulk density, $_B$ recalculated as molar volume Vb ($cm^3$/mole)

Figure A3 : Experimental solvus for the pure $CO_2$ system. (after Roedder, 1965).

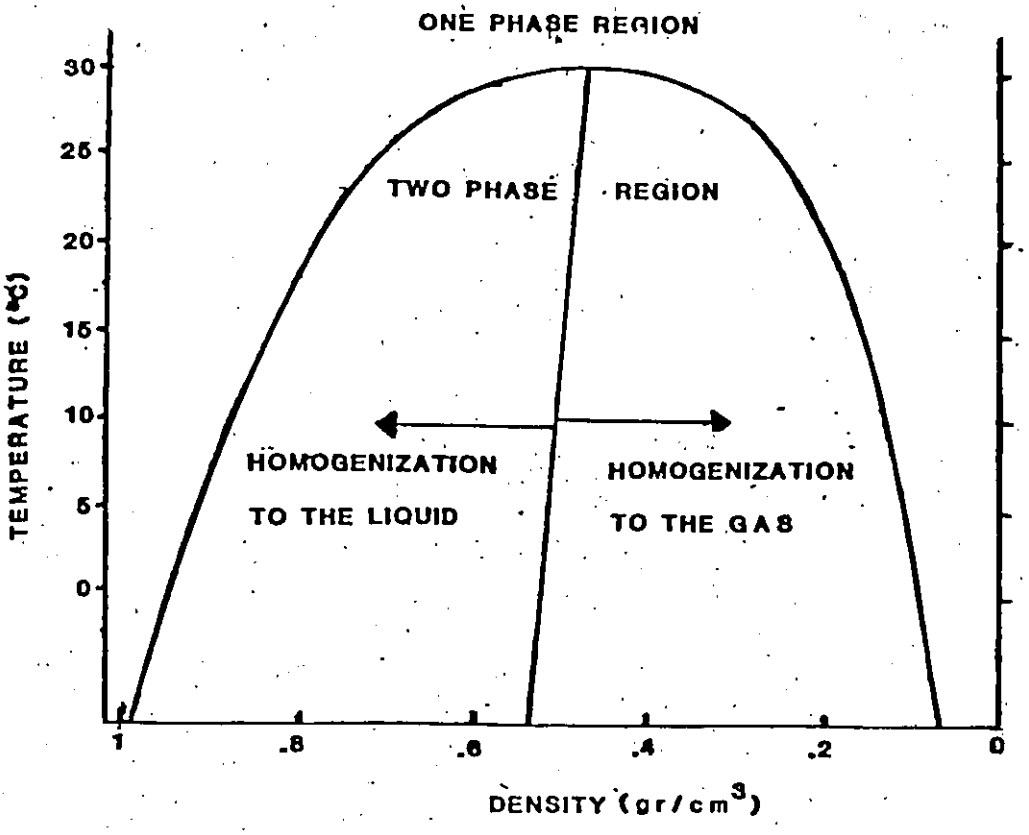

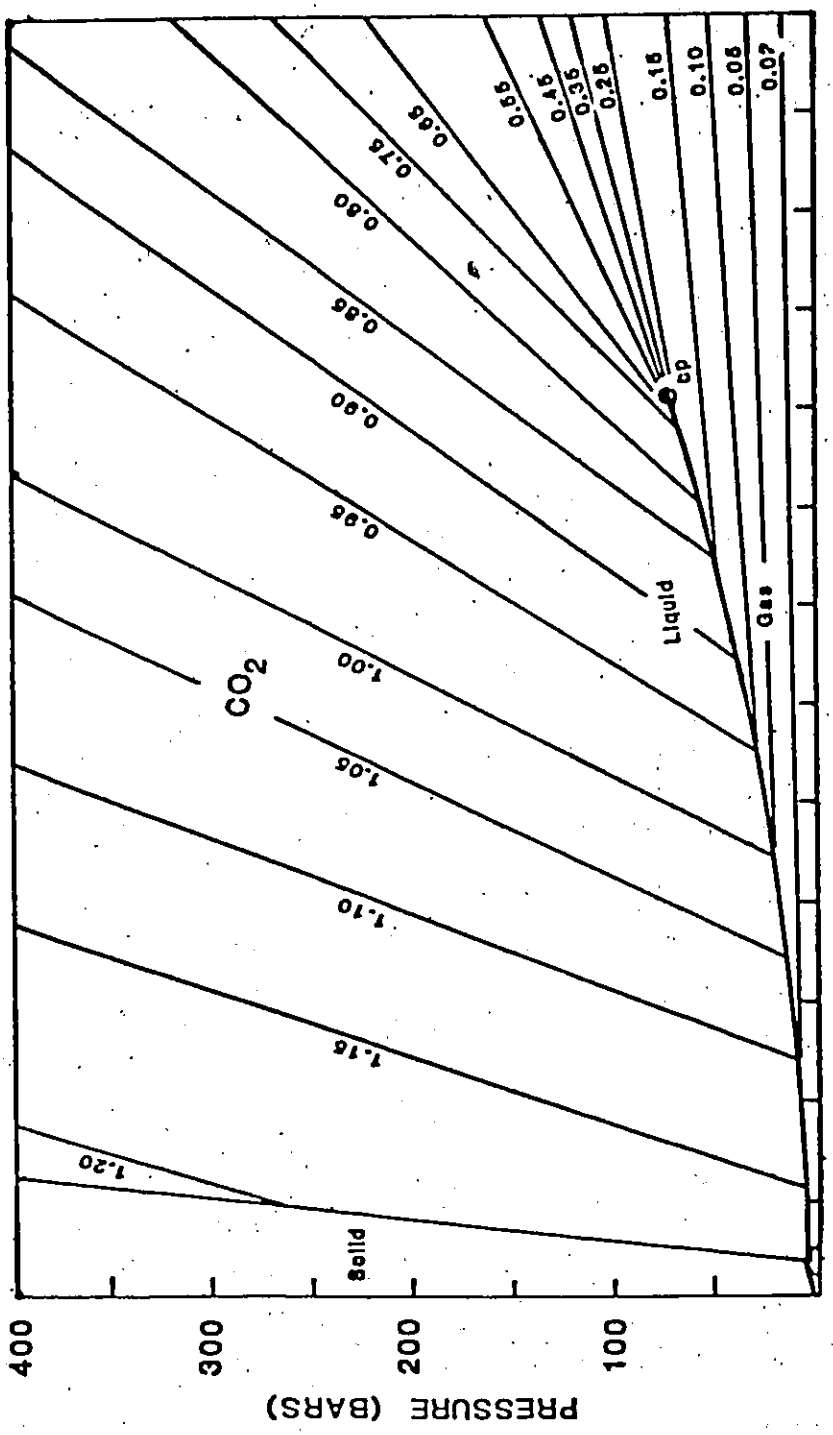


Figure A4 : Phase diagram for $CO_2$, showing densities ($gr/cm^3$) of several isochores.

Figure A5 : A quantitative, isothermal P - P diagram for coexisting $CO_2$ and $H_2O$ fluids at +40°C. The volume % $H_2O$ contours allow estimation of the bulk density of an inclusion for any observed $CO_2$ phase density.

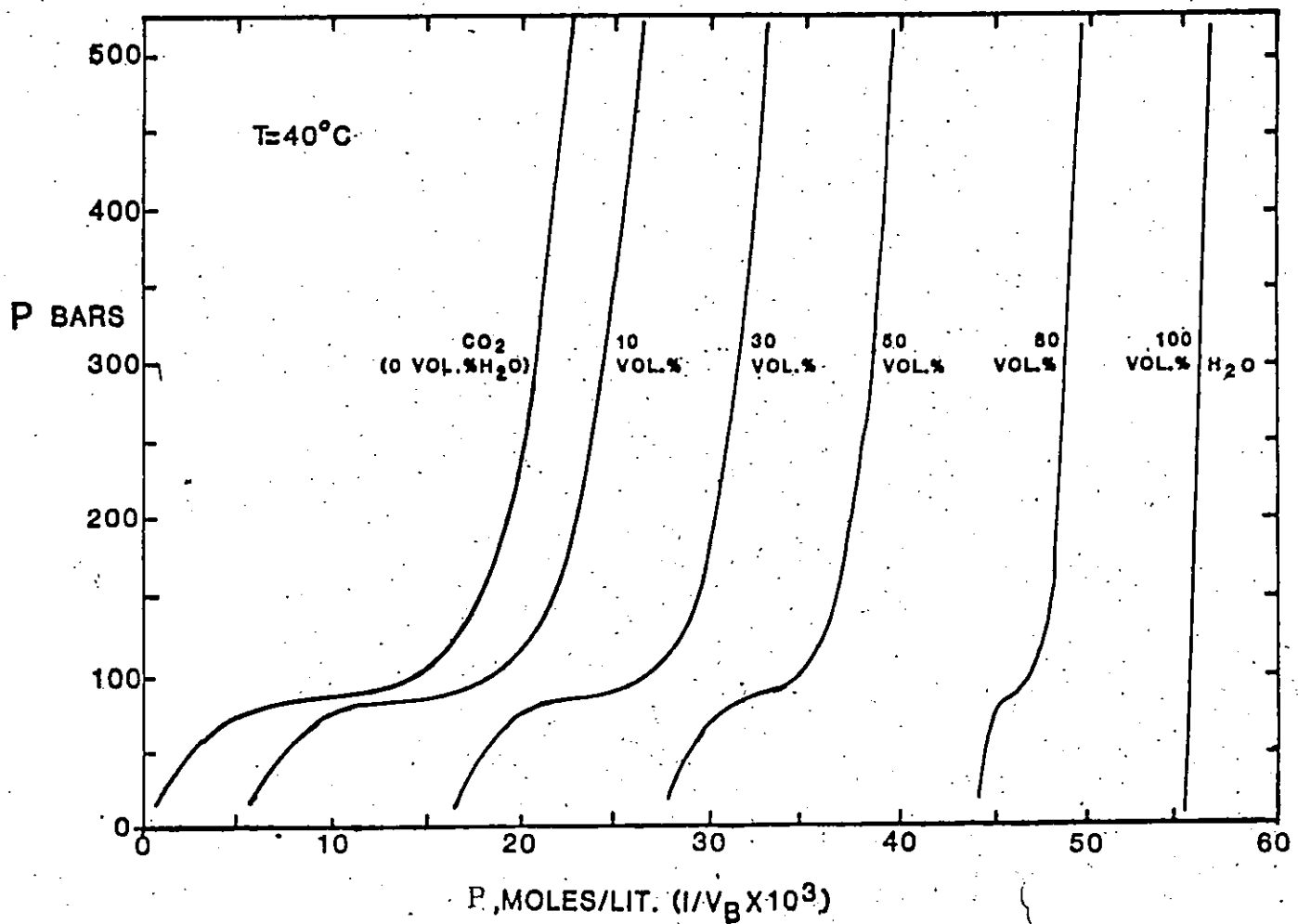

$_B$ $1/Vb \times 10^3$

fixes the molar fraction of the inclusion for the observed $CO_2$ liquid-vapour homogenization temperature (Figure A6). The largest component of error in determining the mole fraction of $CO_2$ (or $H_2O$) using this approach is in the visual estimation of volume percent $CO_2$ (or $H_2O$).

Figure A6 : A polythermal VB-$XH_2O$ diagram with conecting lines for coexisting $CO_2$ fluids and $H_2O$-rich fluid for the designated $CO_2$ liquid-vapour homogenization temperatures ($T_H$, where subscripts L or V indicate homogenization to liquid or vapour).

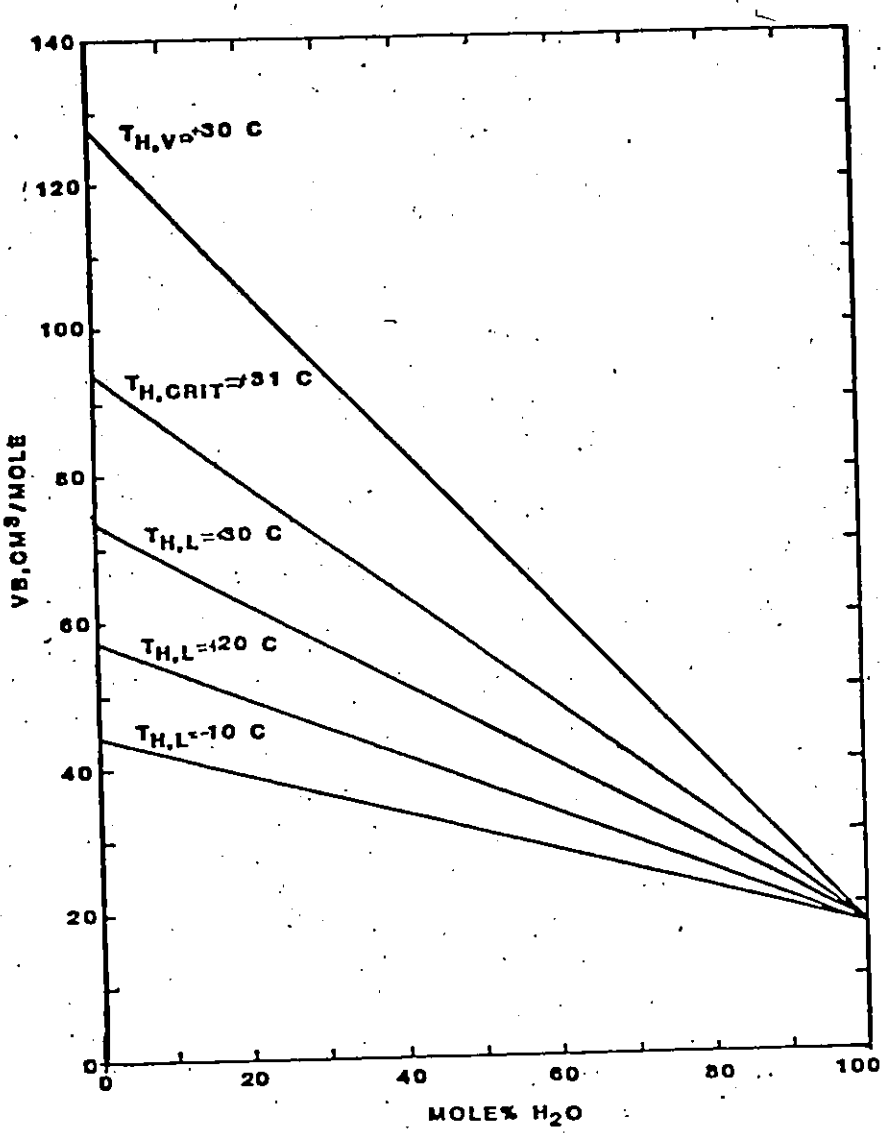

# APPENDIX 5

## TITRIMETRIC DETERMINATION OF FERROUS IRON BY THE MODIFIED WILSON COLD ACID DECOMPOSITION METHOD

# APPENDIX 5

The ferrous iron content in rock powders was determined volumetrically by quantitatively oxidizing the $Fe^{2+}$ in a prepared rock solution with a known volume of ammonium metavanadate solution (0.1N), and then adding a known amount of ferrous ammonium sulphate and determining the excess $Fe^{2+}$ with a standard potassium dichromate titrant (Reichen and Fahey, 1962). In the Wilson (1955) method, after the $Fe^{2+}$ of the rock powder was oxidized by the added ammonium metavanadate, the exces $V^{5+}$ was quantitatively reduced with a standardized ferrous ammonium sulphate titrant.

The modification was applied to prevent the atmospheric oxidation of ferrous iron liberated during decomposition by sulphuric and hydrofluoric acids.

Between 0.10 and 0.20 g of specimen powder was added to 5 ml of ammonium metavanadate solution, and the mixture dissolved for 24 hours in 10 ml of concentrated hydrofluoric acid (HF). Reagent blanks (B) (3 per 10 rock samples) were also prepared similarly but omitting the rock sample. To this solution 10 ml of ferrous ammonium sulphate solution (0.05N) were added; and the

solution was then titrated against potassium dichromate standard solution (0.0125N). The same analytical procedure was applied on one standard rock powder (U.S.G.S. standard G-2).

The amount of ferrous iron in the rock is:

$$Fe^{2+}(Wt\%) = \frac{V_{PDS} - V_B}{1000 \times Ws} \times 0.00125 \times 55.85 \times 100$$

where:

$V_{PDS}$ = volume (ml) of PDS titrant.

$V_B$ = volume (ml) of "reagent blank" solution.

$W_S$ = weight (gr) of sample.

All specimens were run in duplicates; variation in replicate $Fe^{2+}$ determinations was less than 2%. Standard runs were accurate 98% to 100%.

The ferrous iron content refers to the iron locked in hydrofluoric acid soluble silicate and carbonate minerals. Pyrite does not readily dissolve in cold HF and therefore does not contribute to $Fe^{2+}$.

The redox state of iron, $(Fe^{2+}/Fe_T)$ in rocks with negligible sulphide minerals was calculated by

substituting into $Fe_T$ the iron content determined by XRF analyses. For rocks with significant pyrite, $Fe_T$ was determined by Atomic Absorption (A.A) analyses. About 0.20 gms of rock powder was dissolved for 24 hours in cold HF, and then diluted aliquots of this solution were analyzed for total iron with A.A. This method gives total iron present in minerals other than pyrite, which resists dissolution in cold HF.

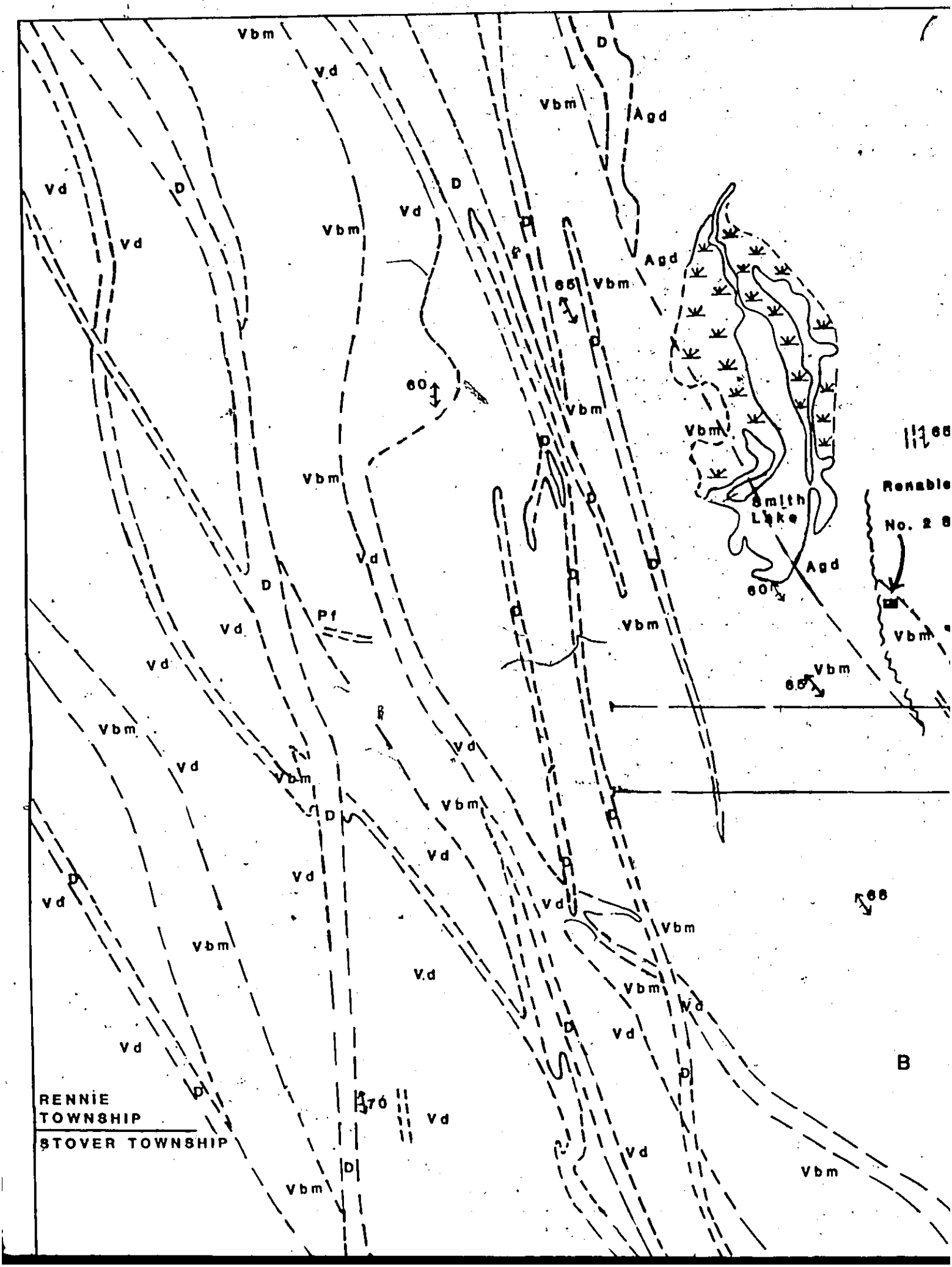
Vbm
Vd
D
Agd
Pf
60
66
Smith Lake
Renable
No. 2 S
B
RENNIE TOWNSHIP
STOVER TOWNSHIP

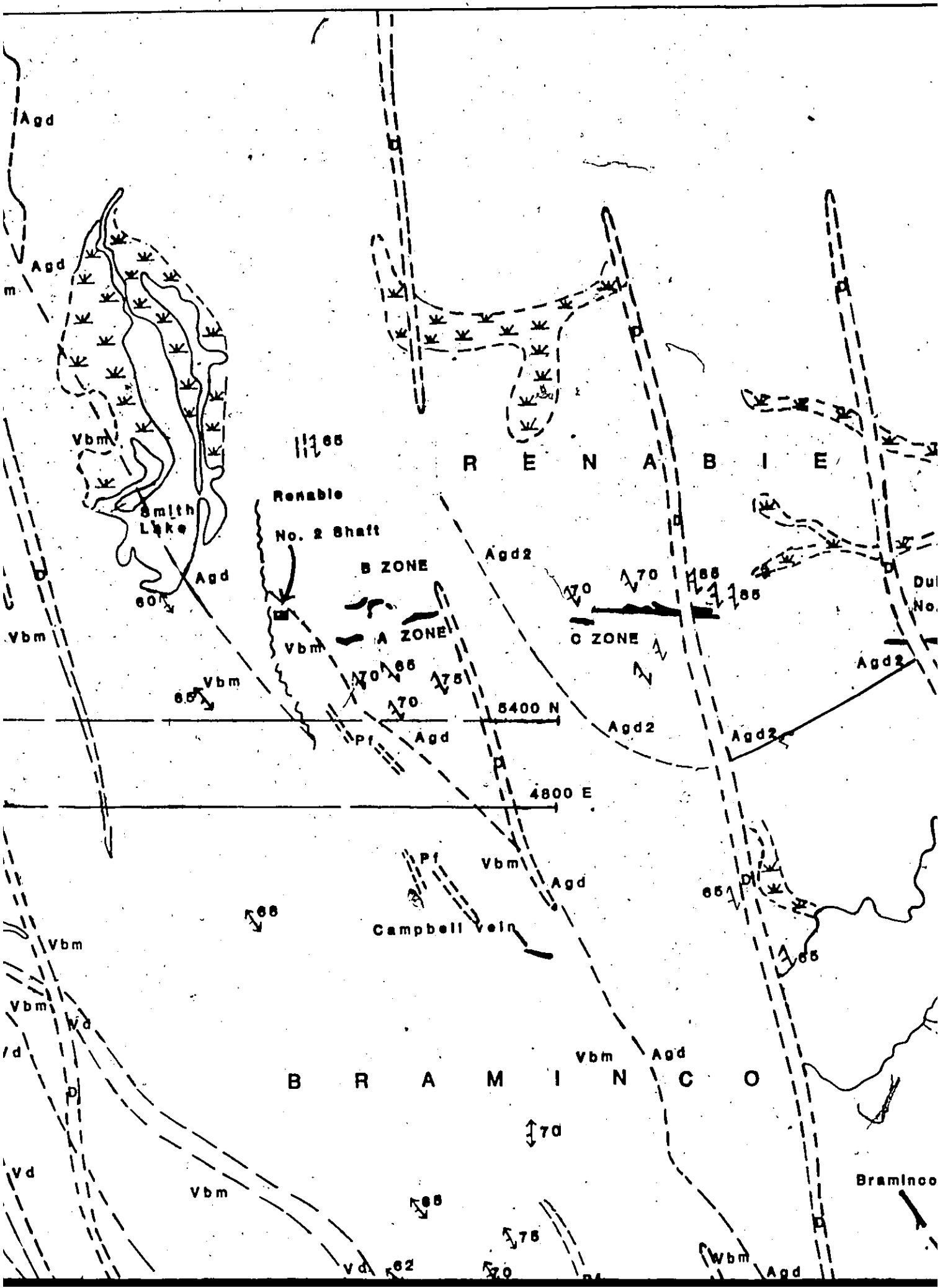
Agd
Agd
Vbm
Smith Lake
Agd
60
Vbm
Vbm
Vbm
65
Renable
No. 2 Shaft
B ZONE
A ZONE
Agd2
70
70
65
65
C ZONE
Agd2
70
65
75
70
5400 N
Pf
Agd
Agd2
Agd2
4800 E
R E N A B I E
Pf
Vbm
Agd
65
Campbell Vein
65
65
Vbm
Vbm
Vd
Vbm
Agd
B R A M I N C O
70
Vd
Vbm
65
75
Vbm
Agd
Braminco
Vd
62
70

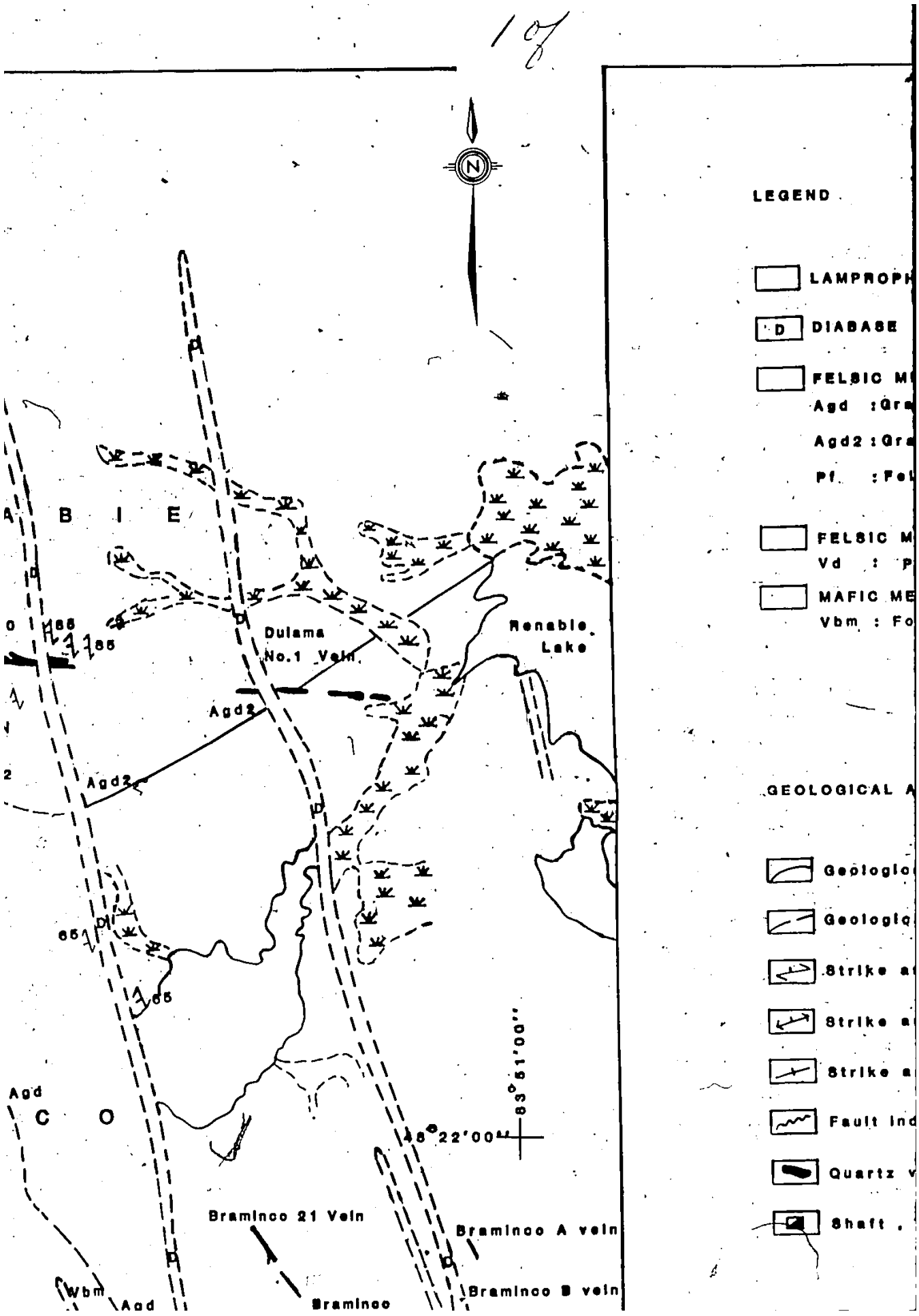
LEGEND
LAMPROPH
D DIABASE
FELSIC M
Agd :Gra
Agd2 :Gra
Pf :Fel
FELSIC M
Vd : P
MAFIC ME
Vbm : Fo
GEOLOGICAL A
Geologic
Geologic
Strike a
Strike a
Strike a
Fault ind
Quartz v
Shaft
Dulama
No.1 Vein
Renable
Lake
Agd2
Agd2
Agd
Braminco 21 Vein
Braminco A vein
Braminco B vein
Braminco
Vbm
Agd
48°22'00"
83°51'00"

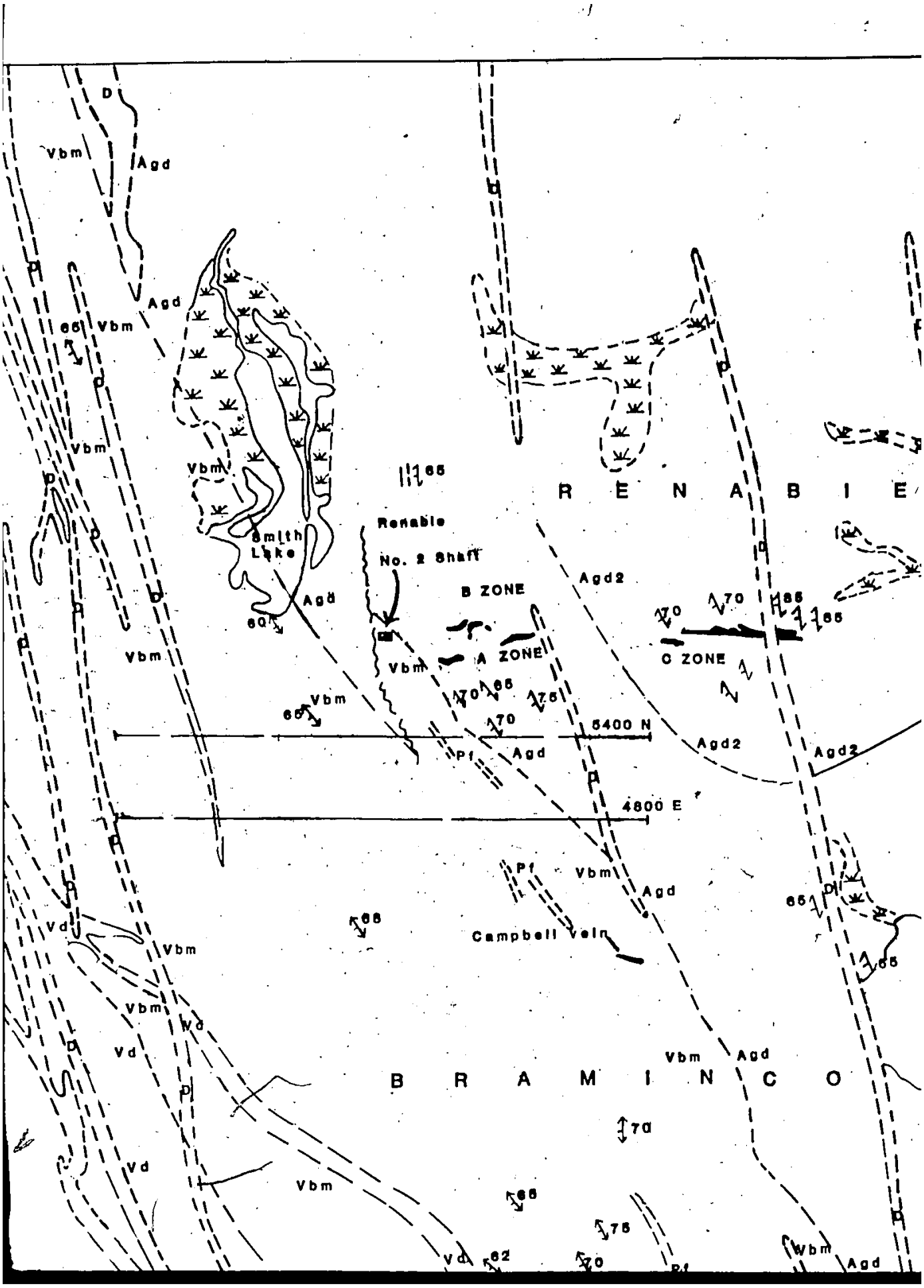
D
Vbm
Agd
Agd
65
Vbm
Vbm
Vbm
Smith Lake
Agd
60
Vbm
Vbm
65
Vbm
Renable
No. 2 Shaft
B ZONE
A ZONE
Agd2
70
70
65
65
C ZONE
70
65
75
5400 N
Agd2
Agd2
Pf
Agd
4800 E
Pf
Vbm
Agd
65
65
Campbell Vein
Vd
Vbm
Vbm
Vd
Vd
Vbm
Agd
70
Vd
Vbm
65
75
Vbm
Vd
62
70
Pf
Vbm
Agd
R E N A B I E
B R A M I N C O

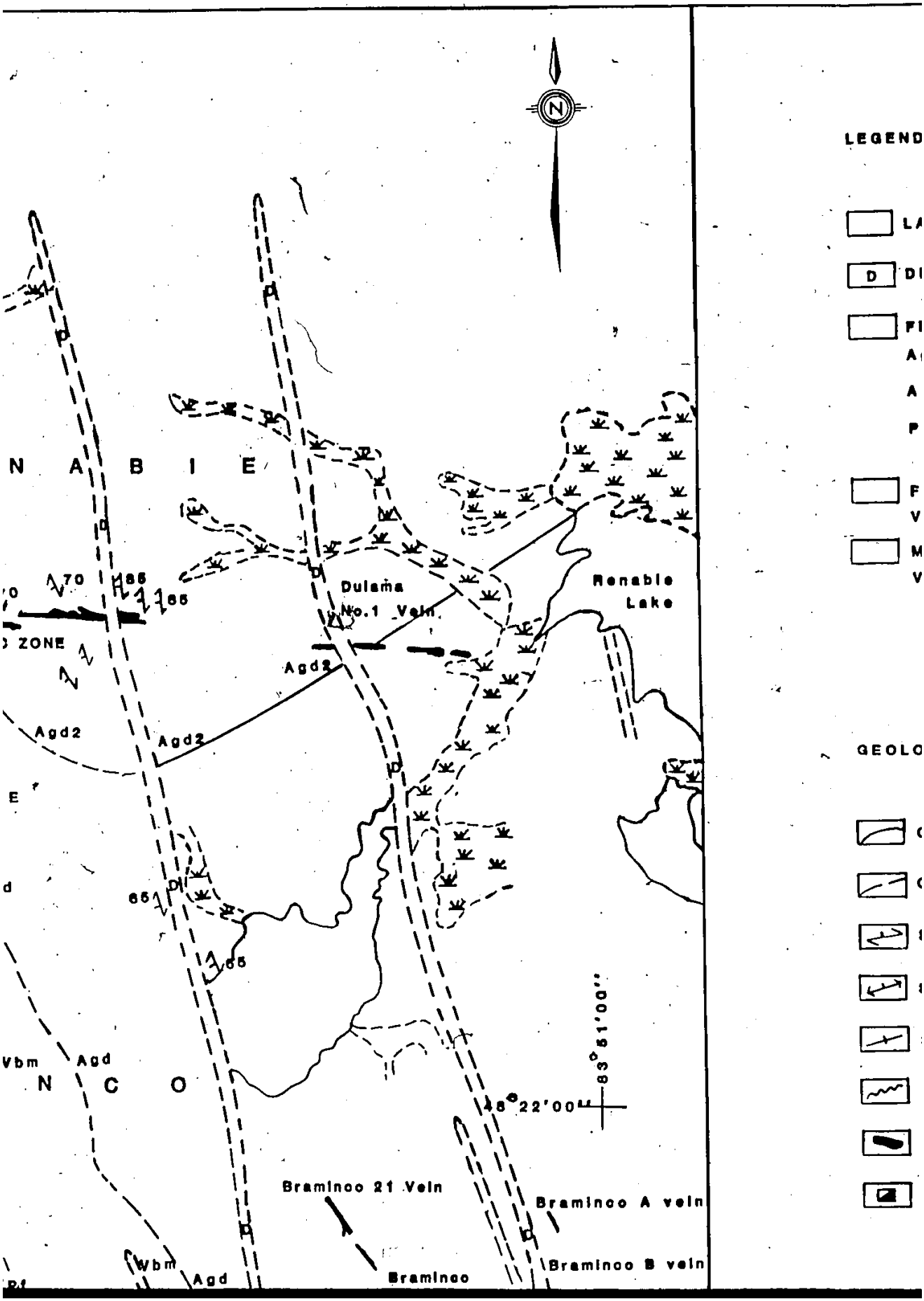
N
LEGEND
N A B I E
70
65
Dulama
No.1 Vein
Renable
Lake
ZONE
Agd2
Agd2
Agd2
65
65
Vbm
Agd
N C O
63°61'00"
48°22'00"
Braminco 21 Vein
Braminco A vein
Braminco B vein
Braminco
Vbm
Agd
GEOLO

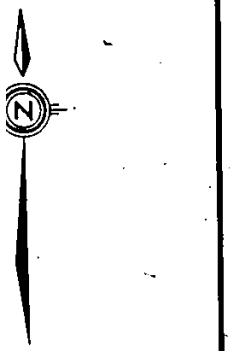

Renable Lake

83°51'00"

'00"

Braminco A vein

Braminco B vein

## LEGEND

LAMPROPHYRE

D DIABASE

FELSIC META-INTRUSIVE ROCKS

Agd : Granitoid to gneissic trondhjemite

Agd2 : Granitoid to gneissic tonalite

Pf : Feldspar porphyry

FELSIC METAVOLCANIC ROCKS

Vd : Porphyritic metadacite

MAFIC METAVOLCANIC ROCKS

Vbm : Foliated fine to medium grained metabasalt

## GEOLOGICAL AND MINING SYMBOLS

Geological boundary, defined

Geological boundary, approximate

Strike and dip of schistosity

Strike and dip of foliation

Strike and vertical dip: direction of top unknown

Fault indicated or assumed

Quartz vein

Shaft, vertical

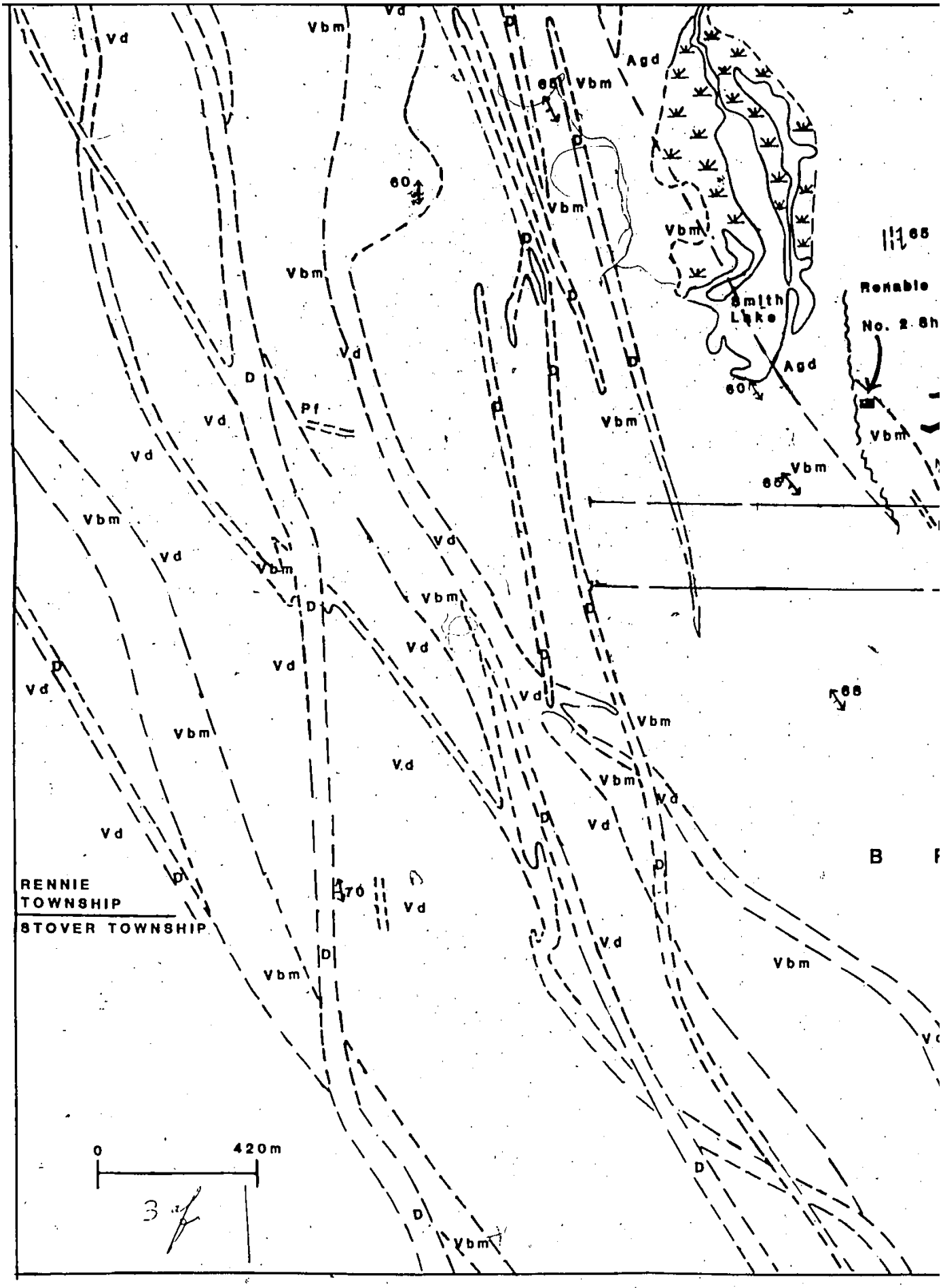
Vd
Vbm
Agd
D
Pf
60
66
Smith Lake
Rennie
No. 2 Sh
RENNIE TOWNSHIP
STOVER TOWNSHIP
0
420m

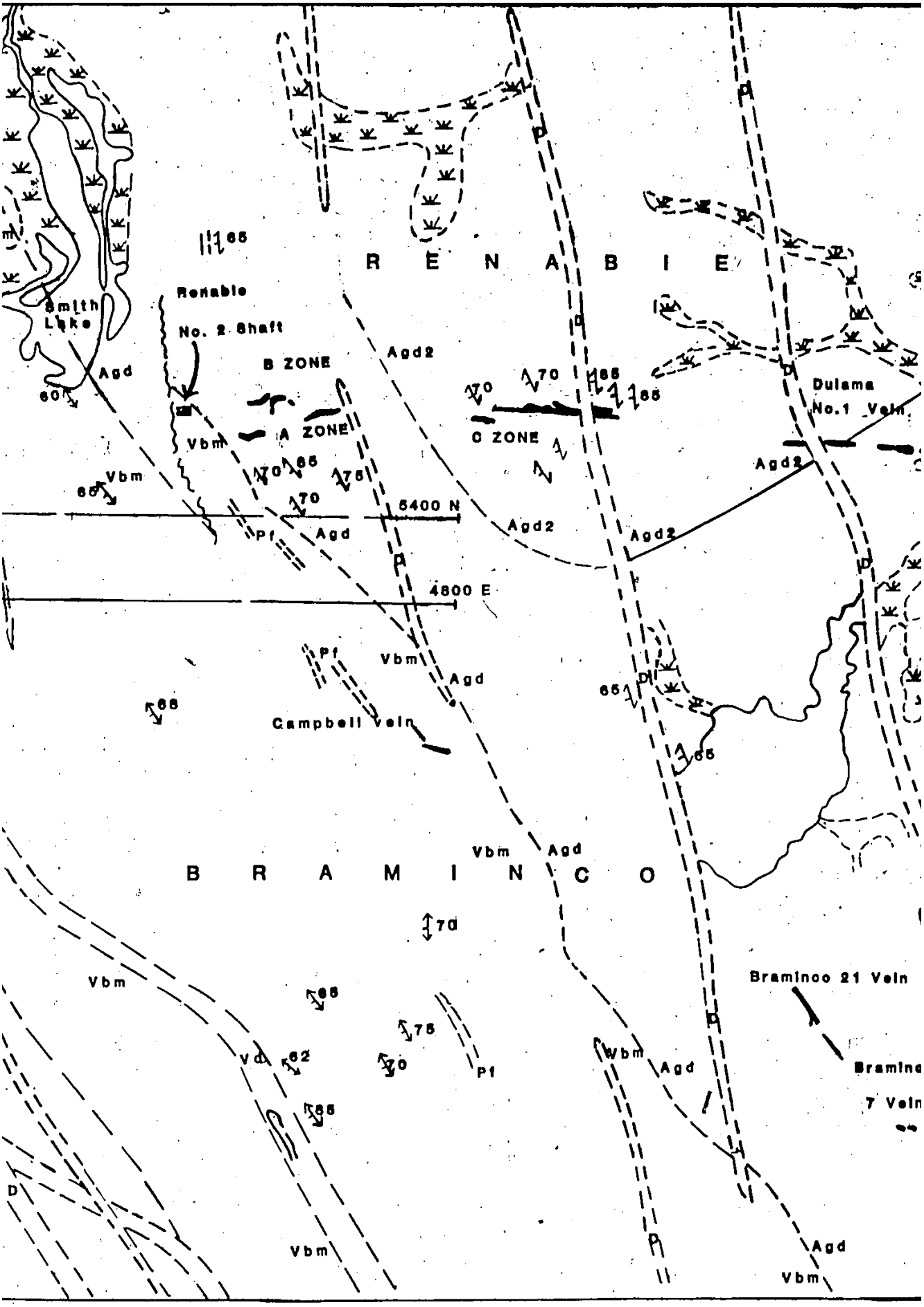
RENABIE
Renable
No. 2 Shaft
Smith Lake
B ZONE
A ZONE
C ZONE
Agd2
Agd
Vbm
Pf
5400 N
4800 E
Campbell Vein
Dulama No.1 Vein
BRAMINCO
Braminco 21 Vein
Bramine 7 Vein

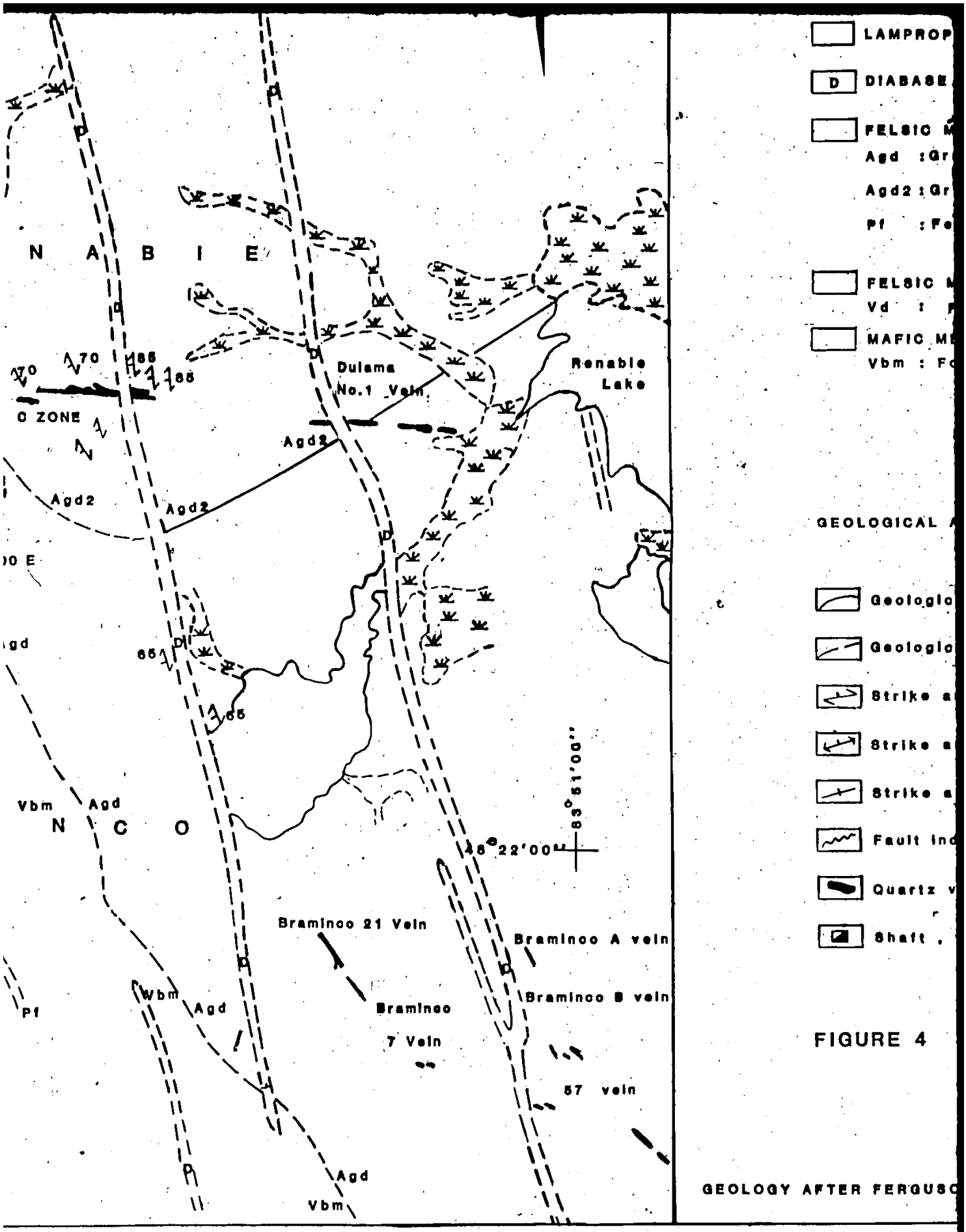
N A B I E
C ZONE
Dulama
No.1 Vein
Renable
Lake
Agd2
Agd2
Agd2
N C O
Vbm
Agd
Pf
Wbm
Agd
Agd
Vbm
83°51'00"
48°22'00"
Braminco 21 Vein
Braminco
7 Vein
Braminco A vein
Braminco B vein
57 vein
LAMPROP
DIABASE
FELSIC M
Agd :Gr
Agd2 :Gr
Pf :Fe
FELSIC M
Vd :
MAFIC MI
Vbm : Fe
GEOLOGICAL
Geologic
Geologic
Strike a
Strike a
Strike a
Fault ind
Quartz v
Shaft
FIGURE 4
GEOLOGY AFTER FERGUSO

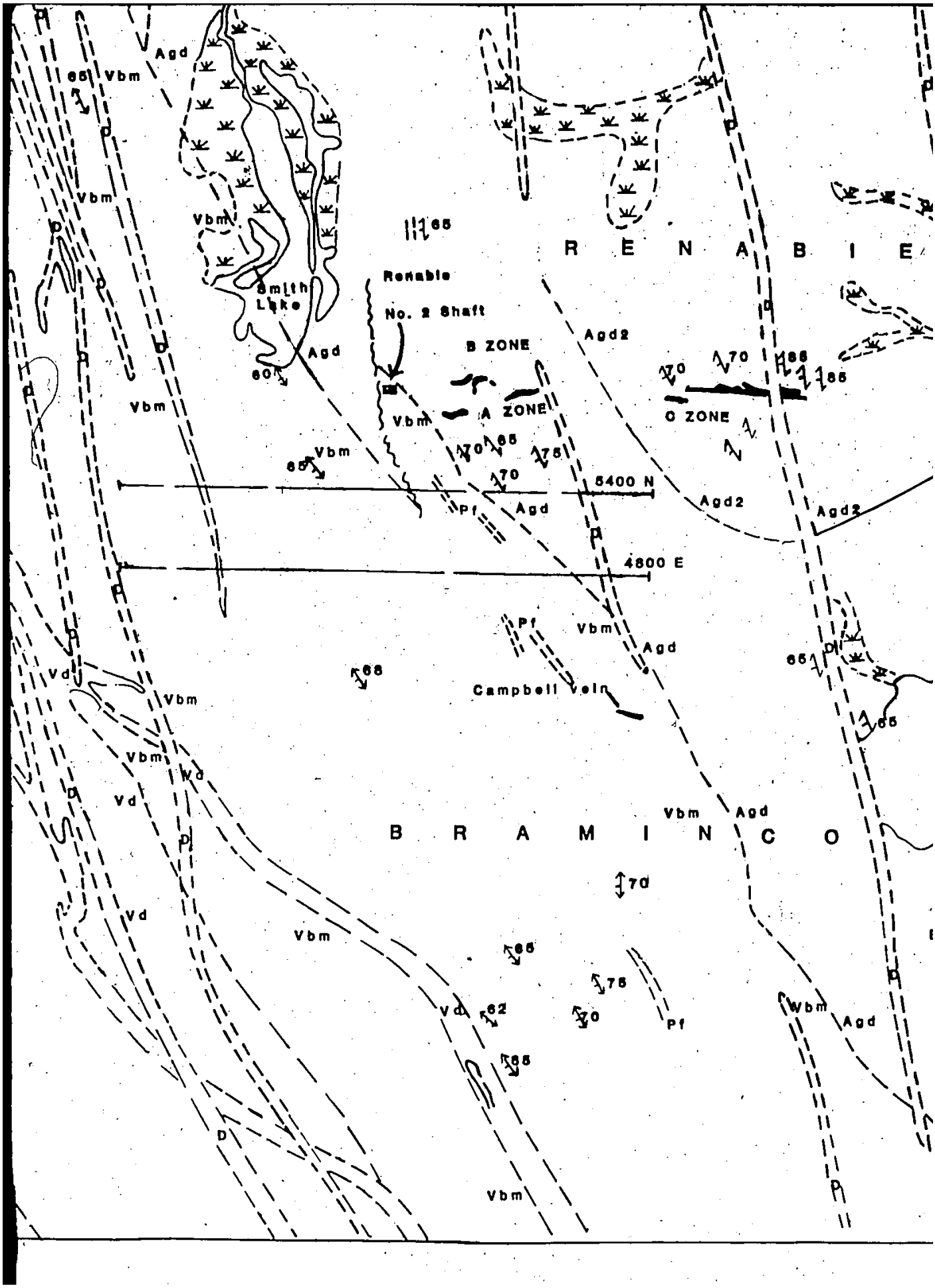
Agd
Vbm
65
Smith Lake
Renable
No. 2 Shaft
B ZONE
A ZONE
C ZONE
Agd2
5400 N
4800 E
Pf
Campbell Vein
R E N A B I E
B R A M I N C O
Vd
70
75
62
60

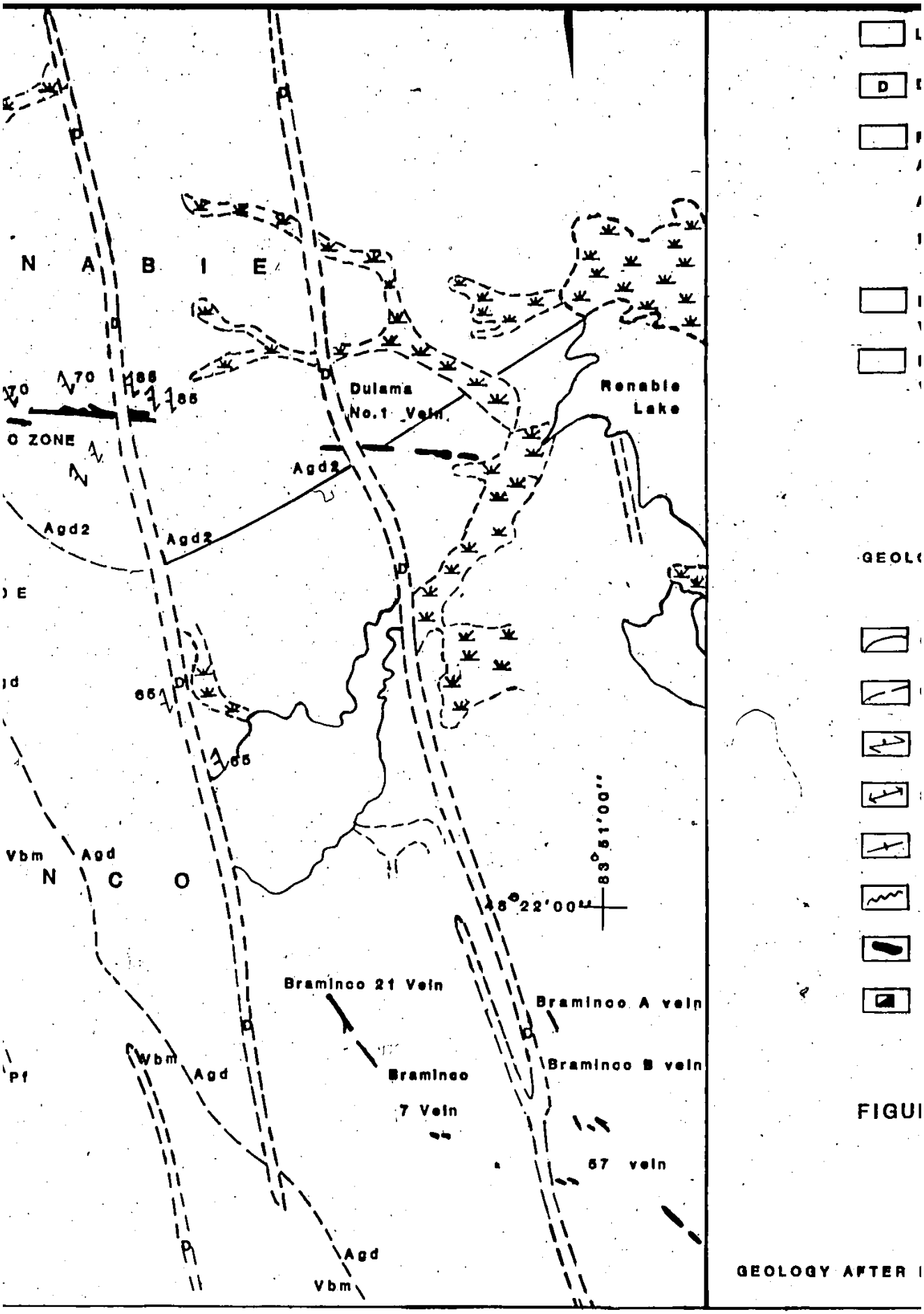
N A B I E
O ZONE
Dulama
No.1 Vein
Renable
Lake
Agd2
Agd2
Agd2
65
65
65
70
70
65
Vbm
Agd
N C O
Pf
Wbm
Agd
Agd
Vbm
83°51'00"
48°22'00"
Braminco 21 Vein
Braminco
7 Vein
Braminco A vein
Braminco B vein
67 vein
GEOL
FIGU
GEOLOGY AFTER


LAMPROPHYRE

D DIABASE

FELSIC META-INTRUSIVE ROCKS

Agd : Granitoid to gneissic trondhjemite

Agd2 : Granitoid to gneissic tonalite

Pf : Feldspar porphyry

FELSIC METAVOLCANIC ROCKS

Vd : Porphyritic metadacite

MAFIC METAVOLCANIC ROCKS

Vbm : Foliated fine to medium grained metabasalt

GEOLOGICAL AND MINING SYMBOLS

Geological boundary, defined

Geological boundary, approximate

Strike and dip of schistosity

Strike and dip of foliation

Strike and vertical dip: direction of top unknown

Fault indicated or assumed

Quartz vein

Shaft, vertical

83°51'00"

inco A vein

minco B vein

67 vein

FIGURE 4

GEOLOGY AFTER FERGUSON (1968a)

4 of 4